

MATHEMATICAL MODELS OF EMERGENT AND
RE-EMERGENT INFECTIOUS DISEASES: ASSESSING
THE EFFECTS OF PUBLIC HEALTH
INTERVENTIONS ON DISEASE SPREAD

A Dissertation
Presented to the Faculty of the Graduate School
of Cornell University
in Partial Fulfillment of the Requirements for the Degree of
Doctor of Philosophy

by
Gerardo Chowell-Puente
January 2005

© 2005 Gerardo Chowell-Puente

ALL RIGHTS RESERVED

MATHEMATICAL MODELS OF EMERGENT AND RE-EMERGENT
INFECTIOUS DISEASES: ASSESSING THE EFFECTS OF PUBLIC HEALTH
INTERVENTIONS ON DISEASE SPREAD

Gerardo Chowell-Puente, Ph.D.

Cornell University 2005

Communicable diseases have long been recognized as a continuous threat to humans. Hence, understanding the underlying mechanisms by which diseases spread and cause epidemics is key for their control. This dissertation is concerned with the development of new mathematical models for the spread of infectious diseases and the effects of Public Health interventions.

In Chapter I, a mathematical model for the 2003 Severe Acute Respiratory Syndrome outbreaks in Toronto, Hong Kong and Singapore is developed. In Toronto, our model predicted control in late April by the identification of the nonexponential dynamics in the rate of increase of the number of cases. The reproductive number is estimated to be approximately 1.2. Our model predicts that 20% of the population in Toronto could have been infected without control interventions. In Chapter II, an uncertainty and sensitivity analysis is performed on the basic reproductive number.

In Chapter III, a novel mathematical model for Ebola spread is developed. Ebola outbreaks have been observed in African regions since 1976. Our model

includes a smooth transition in the transmission rate at the time when interventions are put in place. We evaluate the effects of interventions and estimate the reproductive number.

In Chapter IV, Foot-and-Mouth disease (FMD) epidemics are modeled using spatial deterministic epidemic model. FMD is a highly infectious illness of livestock. Our model is compared to its non-spatial counterpart. We assess the effectiveness of the contingency plan implemented during the epidemic and explore the expected impact of a mass vaccination policy depending on when it is implemented.

In Chapter V, we analyzed from a network point of view the cumulative and aggregated data generated from the simulated movements of 1600,000 individuals generated by TRANSIMS (Transportation Analysis and Simulation System developed at Los Alamos National Laboratories) during a typical day in Portland, Oregon. The node out-degree, the out-traffic, and the total out-traffic follow power law behavior. The resulting weighted graph is a “small world” and has scaling laws consistent with an underlying hierarchical structure. We also explore the time evolution of the largest connected component and the distribution of the component sizes.

BIOGRAPHICAL SKETCH

Gerardo Chowell is a native of Leon, Guanajuato, Mexico. Gerardo became interested in Science at very early stages of his life influenced in part by his father Rafael, an engineer of mines and metallurgics. Gerardo became particularly interested in mathematics with a special emphasis in applications to real world problems. His interests in computers and mathematics took him to complete an engineering in Computer Science and Telecommunications from the Universidad de Colima, Mexico graduating as the top student in the 1997-2001 class. Gerardo was an exchange student at the British Columbia Institute of Technology for the Fall 1998 semester where he received training on fiber optic technology. He has been a visiting student at the Universidad de Cadiz, Spain during the Spring of 2001. Gerardo took part in the Mathematical and Theoretical Biology Institute (MTBI) at Cornell University in the summers of 2000 and 2001. Gerardo's experience in MTBI exposed him to an exciting spectrum of biological problems ready to be tackled through mathematical and computational tools. It was his participation in MTBI that led him to pursue a PhD in Biological Statistics and Computational Biology at Cornell University. Gerardo became interested in the mathematical modeling of infectious diseases with a special emphasis on the role of public health interventions and social structures in disease spread. Gerardo spent the year of 2003 at the Center for Nonlinear Studies of Los Alamos National Laboratory while his PhD advisor, Professor Carlos Castillo-Chavez, was the Ulam Scholar at the same center. His work and collaborations at Los Alamos on the transmission dynamics of Severe Acute Respiratory Syndrome (SARS) and the patterns of pedestrian traffic led him to attain the 2002 National Prize for Youth from Mexican President Vicente Fox. Gerardo will take a postdoctoral po-

sition at the Mathematical Modeling and Analysis group of Los Alamos National Laboratory starting in January of 2005.

To my parents

ACKNOWLEDGEMENTS

I am thankful to my PhD advisor, Professor Carlos Castillo-Chavez, for all his advice, support, and all the hours we have spent thinking and talking about science. I thank my committee members Professors Marty Wells, Carlos Bustamante, and Jon Kleinberg for their time and support. I thank my collaborators at Los Alamos National Laboratories Mac Hyman, Nick Hengartner and Paul Fenimore. This research has been supported by Cornell University, the Mathematical and Theoretical Biology Institute, the Center for Nonlinear Studies and the Mathematical and Analysis group at Los Alamos, the Department of Energy under contracts W-7405-ENG-36, and the National Infrastructure Simulation and Analysis Center (NISAC).

TABLE OF CONTENTS

1 SARS Outbreaks in Ontario, Hong Kong and Singapore: The Role of Diagnosis and Isolation as a Control Mechanism *	1
1.1 SARS epidemiology and related issues	2
1.2 SARS' Transmission Model	5
1.3 Simulation Results	10
1.4 Conclusions	16
1.5 Appendix	19
2 Implications of an Uncertainty and Sensitivity Analysis for SARS' Basic Reproductive Number for General Public Health Measures *	21
2.1 Introduction	21
2.2 Methods	22
2.3 Results	25
2.3.1 Uncertainty analysis	25
2.3.2 Sensitivity analysis	26
2.4 Conclusion	29
2.5 Appendix	32
3 The Basic Reproductive Number of Ebola and the Effects of Public Health Measures: The Cases of Congo and Uganda *	38
3.1 Introduction	38
3.2 Methods	39
3.2.1 Epidemic Models	40
3.2.2 The Transmission Rate and the Impact of Interventions	42
3.2.3 Epidemiological data	43
3.2.4 Parameter Estimation	45
3.2.5 The Reproductive Number	46
3.2.6 The Effective Population Size	48
3.2.7 Uncertainty Analysis on R_0	50
3.3 Results	51
3.4 Discussion	52
4 Modeling the 2001 Foot-and-Mouth Epidemic in Uruguay using Geo-referenced Data	57
4.1 Introduction	57
4.1.1 The 2001 Foot-and-Mouth Epidemic in Uruguay	59
4.2 Materials and Methods	61
4.2.1 Data	62
4.2.2 Non-spatial Epidemic Model	63
4.2.3 Non-spatial Epidemic Model with Interventions	65
4.2.4 Spatial Epidemic Model	66

4.2.5	Spatial Epidemic Model with Interventions	69
4.2.6	Parameter Estimation	70
4.3	Results	71
4.4	Discussion	76
4.5	Conclusions	81
5	Scaling laws for the movement of people between locations in a large city *	82
5.1	Introduction	82
5.1.1	Transportation Analysis Simulation System (TRANSIMS) .	84
5.2	Portland's location-based network	86
5.3	Power law distributions	86
5.4	Correlation between out-degree and total out-traffic	94
5.5	Conclusions	95
	Bibliography	101

LIST OF TABLES

1.1	Parameter definitions and values that fit the cumulative number of cases in class J (“diagnosed”) for Hong Kong. These parameters are used to compute the basic reproductive number R_0	9
1.2	Estimated starting times of the SARS outbreak	11
1.3	Long-time model results for Ontario, Canada, assuming various changes in behavior on March 26th, 2003.	13
2.1	Parameters definitions and baseline values for our model. Baseline values for k , γ_2 , α , ρ , p and δ have been taken from ref. [1]. $\beta = 0.25$ is our estimate transmission rate in Hong Kong. $l = 0$ means perfect isolation while $l = 1$ means no isolation.	26
2.2	The median and the interquartile range (IQR) of the distribution of the basic reproductive number (\mathcal{R}_0) of SARS for Toronto, Hong Kong and Singapore obtained from our uncertainty analysis.	29
2.3	Partial rank correlation coefficients (PRCCs) between each of the input parameters and \mathcal{R}_0 from Monte Carlo sampling of size 10^4 for different distributions of the isolation effectiveness (l) as described in the text.	29
2.4	Sensitivity Indices for Toronto with $l = 0.1$	36
2.5	Sensitivity Indices for Hong Kong with $l = .43$	36
3.1	Parameter definitions and baseline estimates (time is given in days) obtained from the best fit of the model equations (4.3) to the epidemic-curve data of the Congo 1995 and Uganda 2000 outbreaks (Figure 3.5). The parameters were optimized by a computer program (Berkeley Madonna, Berkeley, CA) using a <i>least squares</i> fitting technique and appropriate initial conditions for the parameters ($0 < \beta < 1$, $0 < q < 100$, $1 < 1/k < 21$ [2], $3.5 < 1/\gamma < 10.7$ [3]). The optimization process was repeated 10 times (each time the program is fed with two different initial conditions for each parameter) before the “best fit” was chosen.	47
3.2	Population parameters and estimated R_0 for the Congo 1995 and the Uganda 2000 Ebola outbreaks. Notice that even though our expression for R_0 is independent of N , our model is not independent of N and hence the corresponding population sizes for Congo and Uganda are used in the least-squares estimation of the parameters.	49
4.1	Distribution of the number of counties per state and the average number of farms per county (N_j).	64
4.2	Distribution of the total number of infected farms among the different Uruguayan states within each defined contiguous region.	65

4.3	Parameter definitions and estimates obtained from least-squares fitting of the non-spatial epidemic model (4.2) to the cumulative number of infected farms over time (days) in Region I (Figure 4.4). All the parameters have units 1/ days.	73
4.4	Parameter definitions and estimates obtained from least-squares fitting of the spatial epidemic model (4.4) to the cumulative number of infected farms over time (days) in Region I (Figure 4.5). All the parameters have units 1/ days except for q whose units are 1/Km. * Small values of q lead to widespread influence, whereas large q supports local spread. Great mobility and frequent interactions among farms would lead to small values of q	75
5.1	Sample section of a TRANSIMS activity file. In this example, person 115 arrives for a social recreational activity at location 33005 at 19.25 o'clock and departs at 21.00 o'clock.	87
5.2	Statistical properties of the Portland's location-based network. S is the size of the largest component of the cumulative network during the whole day.	90
5.3	Size of the largest component just before and after 6 a.m., the time at which a sharp transition occurs. At midnight, all but 14 locations belong to the largest component (Table 2).	95

LIST OF FIGURES

- | | | |
|-----|---|----|
| 1.1 | A schematic representation of the flow of individuals between the different classes. The model considers two distinct susceptible classes: S_1 , the most susceptible, and S_2 . $\beta \frac{I+qE+lJ}{N}$ is the transmission rate to S_1 from E , I and J . p is a measure of reduced susceptibility to SARS in class S_2 . E is the class composed of asymptomatic, possibly infectious individuals. The class I denotes infected, symptomatic, infectious, and undiagnosed individuals. I -individuals move into the diagnosed class J at the rate α . Individuals recover from class I at the rate γ_1 and γ_2 from the J class. The rate δ is SARS' disease-induced mortality. The classes R and D are included to keep track of the cumulative number of diagnosed, recovered and dead individuals, respectively. The quantity C is for comparison with epidemiological statistics; it tracks the total number of diagnosed individuals. | 8 |
| 1.2 | The cumulative number of SARS cases from March 31 to April 14 (lin-log scale) for the World (top data), Hong Kong(second row), Ontario, Canada (fourth row), all of Canada (third row) and Singapore (bottom row). The data were obtained from WHO [4] except for the Canadian data which are from the Canadian Ministry of Health [5]. The Ontario data includes suspected and probable cases since March 31. This inclusion explains the jump in the data for Ontario on March 31st. The rates of growth of the SARS outbreak (computed using data from March 31 to April 14) are: 0.041 (world), 0.050 (Hong Kong), 0.037 (Singapore), 0.054 (Canada) and 0.054 (Ontario). | 10 |

1.3	The circles are the cumulative number of suspected or probable SARS cases in Ontario beginning on day 61 (March 31st, the day of the jump) and the number of probable cases up until day 60. The lines are the cumulative number of “diagnosed” cases C from the SEIJR model. The fit to the data is given by a change in the values of α and l on March 26th. Prior to March 26th, $\alpha = 1/6$, $l = 0.76$. Because the model is poorly constrained prior to day 61, the real purpose of this part of the model is to generate sufficiently large classes of E and I relative to J on March 26th to give the fast increase in C from day 61 to day 67. After March 26th, three scenarios are shown. The fit to the data is given by $\alpha = 1/3$, $l = 0.05$ (rapid diagnosis and effective isolation of diagnosed cases, dashed line). The second curve is given by $\alpha = 1/6$, $l = 0.05$ (slow diagnosis and effective isolation, dotted line) and the third curve by $\alpha = 1/3$, $l = 0.3$ (rapid diagnosis with improved but imperfect isolation, dash-dot line). An index case is assumed on February 1 st . The transmission rate β is computed using the estimated rate of growth ($r = 0.0543$) for the Ontario data as described in the text.	14
1.4	Cumulative number of SARS cases in Hong Kong and Singapore as a function of time (SEIJR model) with $l = 0.38$ (Hong Kong) and $l = 0.40$ (Singapore). Singapore has $\beta = 0.68$, all other parameters are from Table 1. The data are fitted starting March 31 (see Figure 1.2) because of the jump in reporting on March 30th.	15
2.1	Histograms of the 6 distributed parameters appearing in eqn. 1 with sample size 10^4 . The transmission rate was assumed exponentially distributed with mean 0.25, our estimate transmission rate in Hong Kong. Here l is assumed to have a Beta distribution ($l \sim \mathcal{B}(1, 2)$). Alternative distributions for l were also used as described in the text. All other distributions were taken from ref. [1].	25
2.2	Empirical (dots) and stretched exponential estimated probability density function $Prob(\mathcal{R}_0) = ae^{-(\mathcal{R}_0/b)^c}$ (solid line) [6] of \mathcal{R}_0 for the cases of Toronto ($a = 0.186$, $b = 0.803$, $c = 0.957$, after control measures had taken place), Hong Kong ($a = 0.281$, $b = 1.312$, $c = 0.858$) and Singapore($a = 0.213$, $b = 1.466$, $c = 0.883$) obtained from our uncertainty analysis. The distribution for the case of perfect isolation ($l = 0$, $a = 0.369$, $b = 0.473$, $c = 0.756$) is shown as a reference.	27
2.3	(β, l) parameter space when $\mathcal{R}_0 < 1$ obtained from the uncertainty analysis (black dots). The deterministic (β, l) level curve when $\mathcal{R}_0 = 1$ is shown in yellow. All other parameters in eqn. 1 were fixed to their baseline values (Table 3.1). $l = 0$ denotes perfect isolation while $l = 1$ denotes no isolation.	28

2.4	Boxplot of the sensitivity of \mathcal{R}_0 estimates to varying values of l , isolation effectiveness. l ($0 \leq l \leq 1$) was divided in 20 equally spaced intervals going from perfect isolation ($l = 0$, level 1) to no isolation ($l = 1$, level 21). The boxplot shows the median and the interquartile range of \mathcal{R}_0 obtained from Monte Carlo sampling of size 10^5	30
2.5	Level curve of (l, α) where $l(\alpha + 2\gamma_1 + 2\delta) = \delta + \gamma_2$	37
3.1	A schematic representation of the flow of individuals between epidemiological classes. $\beta \frac{I}{N}$ is the transmission rate to susceptibles S from I ; E is the class of infected (not yet infectious) individuals; k is the rate at which E -individuals move to the symptomatic and infectious class I ; Infectious individuals (I) either die or recover at rate γ . C is not an epidemiological state but keeps track of the cumulative number of cases after the time of onset of symptoms.	41
3.2	On the left, we have the <i>daily</i> number of cases by date of symptom onset during the Ebola outbreak in Congo 1995 (Mar 6-Jul 12). On the right, we have the <i>weekly</i> number of cases by date of symptom onset during the Ebola outbreak in Uganda 2000 (Aug 20-Jan 07). Data has been taken from refs. [7, 8].	45
3.3	95% confidence intervals for t_h ($t_h = \frac{\log(2)}{q}$), the time to achieve a transmission rate of $\frac{\beta_0 + \beta_1}{2}$, obtained from the likelihood ratio as described in the text.	48
3.4	(Top) cumulative number of cases (log-lin scale) during the exponential growth phase of the Congo 1995 epidemic as identified by the date of start of interventions (09 May 1995 [7]). The model-free initial growth rate of the number of cases for Congo 1995 is 0.07 (linear regression); (bottom) estimated distribution of R_0 from our uncertainty analysis (see text). R_0 lies in the interquartile range (IQR) (1.66 – 2.28) with a median of 1.89. Notice that 100% of the weight lies above $R_0 = 1$	51
3.5	(Top) Comparison of the cumulative number of Ebola cases during the Congo 1995 and Uganda 2000 Ebola outbreaks, as a function of the time of onset of symptoms. Black circles are data. The solid line is the average of 250 Monte Carlo replicates and the error bars represent the standard error around the mean from the simulation replicates using our parameter estimates (Table 3.1). For the case of Congo 1995, simulations were begun on 13 Mar 1995. A reduction in the transmission rate β due to the implementation of interventions occurs on 09 May 1995 (day 56) [7]. For the case of Uganda 2000, simulations start on 27 August 2000 and interventions take place on 22 October 2000 (day 56) [8]; (bottom) comparison of the residuals (difference between the data and the model best fit) scaled by the standard deviation for the cases of Congo and Uganda.	53

3.6	The final epidemic size distributions for the cases of Congo 1995 and Uganda 2000 obtained from 250 Monte Carlo replicas. Crosses (X) represent the final epidemic size from data.	54
3.7	Sensitivity of the final epidemic size to the time of start of interventions. Here negative numbers represent number of days before the actual reported intervention date (Table 3.2) and positive numbers represent a delay after the actual reported intervention date ($\tau = 0$). All other parameters have been fixed to their baseline values (Table 3.2). The final epidemic size grows exponentially as expected with the time of interventions with a rate of 0.06 for the case of Congo and 0.05 for the case of Uganda.	55
4.1	a) Daily and b) cumulative number of reported infected farms during the 2001 Foot and Mouth Disease in Uruguay. The epidemic reached its maximum of 66 cases on day 33 (25 May 2001). 1763 cases had been reported by day 79 (10 July 2001). Data has been taken from refs. [9, 10, 11]. The periodic dips in the data are due to low reporting rates on the weekends.	60
4.2	a) The initial intrinsic growth rate r in Region I, II and III are 0.65, 0.35, and 0.19 respectively ; b) Region I, II and III comprise 3, 7 and 8 Uruguayan states respectively (see Table 4.2). We estimate the intrinsic growth rate in region III using the cumulative number of cases from 02 May to 07 May 2001 due to underreporting of number of cases before 02 May 2001. The intrinsic growth rate after 07 May 2001 is approximately the same in the three regions once movement restrictions and some depletion in the number of susceptible farms had taken place. Mass vaccination started on 05 May 2001.	63
4.3	a) Map of Uruguay with state (color) and county divisions; b) distribution of inter-county (euclidean) distances which were obtained using a geographic information system (GIS). The centroide of each county is used to compute euclidean distances.	68
4.4	a) The daily and b) cumulative number of reported infected farms in Region I (Figure 4.2) where the outbreak started (23 April 2001) and focused (57% of cases). Movement restrictions were implemented on 27 April 2001 and mass vaccination started on 05 May 2001. Circles are the data and the solid line is the best-fit solution of the deterministic model equations of the nonspatial model (4.2) to the data via least squares fitting (parameter estimates are given in Table 4.3).	72

4.5	a) The daily and b) cumulative number of reported infected farms in Region I (Figure 4.2) where the outbreak started (23 April 2001) and focused (57% of cases). Movement restrictions were implemented on 27 April 2001 and mass vaccination started on 05 May 2001. Circles are the data and the solid line is the best-fit solution of the deterministic model equations of the spatial model (4.4) to the data via least squares fitting (parameter estimates are given in Table 4.4).	74
4.6	a) The daily and b) cumulative number of reported infected farms in Region I (Figure 4.2) where the outbreak started (23 April 2001) and focused (57% of cases). Movement restrictions were implemented on 27 April 2001 and mass vaccination started on 05 May 2001. Circles are the data and the solid line is the best-fit solution of the deterministic model equations (4.4) to the data via least squares fitting (parameter estimates are given in Table 4.4). Three scenarios are shown: (dash-dot) no mass vaccination implemented after movement restrictions (total of 5252 cases); (dot-dot) mass vaccination with a 5-day delay (1551 cases) and (dash-dash) 5 days before the actual date at which mass vaccination started (604 cases).	76
4.7	Sensitivity of the final epidemic size (Region I) to the time of start of the mass vaccination program. Negative numbers represent number of days before the actual reported start of the mass vaccination programme (05 May 2001) while positive numbers represent a delay (days).	77
5.1	Structure of the location-based network of the city of Portland. The nodes represent locations connected via directed edges based on the traffic or movement of individuals (activities) between the locations. The weights (w_{ij}) of the edges represent the daily traffic from location i to location j	88
5.2	The number of people active in (a) work activities, (b) school activities, (d) social activities, and (d) home activities as a function of time (hours) during a ‘typical’ day in Portland, Oregon.	89
5.3	Log-log plots of the clustering coefficient as a function of the out-degree for subnetworks constructed from work activities, school activities, social activities, and all the activities. The dotted line has slope -1 . Notice the scaling k^{-1} for the school and social/recreational activities. However, for the subnetwork constructed from work activities, the clustering coefficient is almost independent of the out-degree k	92
5.4	The size of the largest component (cluster) over time. A sharp transition is observed at about 6 a.m when people move from home to work or school.	93

5.5	(a) The number of components $X(t)$ between 4 a.m. and 8 a.m. (b) Probability distribution $P(m)$ of the normalized component sizes at two different times of the day. The component sizes (m) have been normalized by S , the size of the largest component of the cumulative network during the whole day (Table 1).	94
5.6	Distribution of the out-degrees of the location-based network of the city of Portland. There are approximately the same number of nodes (locations) with out-degree $k = 1, 2, \dots, 10$. For $k > 10$ the number of nodes with a given out-degree decays as a power law $P(k) \propto k^{-\gamma}$ with (a) $\gamma \approx 2.7$ for the morning (6 a.m.-12 p.m.), $\gamma \approx 2.43$ for the workday (6 a.m.-6 p.m.) and (b) $\gamma \approx 2.4$ for the full day.	96
5.7	The out-traffic distribution of the location-based network of the city of Portland follows a power law ($P(k) \propto k^{-\gamma}$) with (a) $\gamma \approx 3.56$ (morning), $\gamma \approx 3.74$ (afternoon), and (b) $\gamma \approx 3.76$ (full day). Hence a few connections have high traffic but most connections have low traffic.	97
5.8	Distribution of the total out-traffic for the location-based network of the city of Portland. There are approximately the same number of locations (nodes) with small total out-traffic. The number of locations where more than 30 people (approximately) leave each day decays as a power law with $\gamma \approx 2.74$	98
5.9	Correlation between the out-degree and the total out-traffic. The correlation coefficient is $\rho = 0.94$ on a log-log scale. Most (95%) of the locations have fewer than 100 people leaving during the day.	99
5.10	(a) Joint distribution $F(k, v)$ plot (b) \log_e density of $F(k, v)$ plot between the out-degree k and the total out-traffic v in the location-based network of the city of Portland.	100

Chapter 1

SARS Outbreaks in Ontario, Hong Kong and Singapore: The Role of Diagnosis and Isolation as a Control Mechanism *

Severe acute respiratory syndrome (SARS) is a new respiratory disease which was first identified in China's southern province of Guangdong. SARS is not merely a local endemic disease: it poses a serious risk to the medical community, is a threat to international travelers, is having a substantial negative economic impact in parts of East Asia and is spreading world-wide. The serious danger SARS poses to the medical community is illustrated by the numerous cases of transmission to health-care workers. Startlingly, the man who awakened the world to the dangers of SARS, Dr. Carlo Urbani, succumbed to the disease. Cases of transmission between aircraft passengers are suspected, and relatively short visits to epidemic regions have resulted in infection. The most striking feature of SARS, however, has proven to be its ability to rapidly spread on a global scale. One man with SARS made 7 flights: from Hong Kong to München to Barcelona to Frankfurt to London, back to München and Frankfurt before finally returning to Hong Kong [12]. Another individual, a 26-year-old airport worker, appears to have transmitted the disease to 112 people [13]. Clearly, there is an unfortunate interaction between the incubation period of the virus, the widely distributed severity and infectiousness of SARS in different people and the speed and volume of passenger air travel.

*G. Chowell , P. W. Fenimore, M. A. Castillo-Garsow and C. Castillo-Chavez. SARS Outbreaks in Ontario, Hong Kong and Singapore: the role of diagnosis and isolation as a control mechanism. *J. Theor. Biol.* 24, 1-8 (2003).

The adverse economic impact in parts of East Asia far exceeds the disruption of previous outbreaks of avian influenza, earning comparison with the 1998 financial market crisis in that part of the world [14, 15, 16]. Although the causative agent of SARS has been determined [17, 18], a detailed understanding of the causative virus' pathogenticity and routes of transmission and the dynamics of the epidemic is still at a very early stage. It is uncertain how the virus is transmitted: by droplet or airborne transmission or person-to-person contact. The recent development of laboratory tests promises to improve the epidemiological situation somewhat [19].

SARS is a public health crisis on a scale rarely seen. The obvious question in such a crisis is, "can SARS be contained?" In this study, we report transmission parameters and epidemic dynamics from a model based on classes of people who are susceptible, exposed, infectious, diagnosed, and recovered ("SEIJR") that includes the effect of patient isolation. Our model is consistent with the possibility of containment in Toronto, Ontario.

1.1 SARS epidemiology and related issues

SARS was first identified in November 2002 in the Guongdong Province of China [20]. By February 26, 2003 officials in Hong Kong reported their first cases of SARS and no later than March 14th of this year the virus reached Canada [21]. As of April 17th, Canada is the only location outside of Asia which has seen deaths as a result of SARS (13 so far) [22]. U.S. health officials are currently investigating 199 cases in 34 states (Apri 17, 2003) [23].

An individual exposed to SARS may become infectious after an incubation period of 2 – 7 days (or longer) [24] with 3 – 5 days being most common [25]. Most infected individuals either recover, typically after 7 to 10 days, or suffer 4%

mortality or higher [26, 27, 28]. SARS appears to be most serious in people over age 40, especially those who have other medical problems such as heart or liver disease. Its symptoms are similar to pneumonia or other respiratory ailments and include a high fever ($\geq 38^{\circ}\text{C}$), shortness of breath, dry cough, headache, stiff or achy muscles, fatigue and diarrhea [29]. These symptoms, however, are not uniform. In the US, for example, the disease seems to be a milder one than in Asia [30]. The result has been that SARS was, and for the moment remains, a diagnosis of exclusion.

Presently, there is no treatment for SARS [31] and diagnostic tests are just becoming available [19]. The mortality rate is reported to be 4% or higher worldwide[27, 28]. Experts estimate that between 80 and 90 percent of people with SARS recover without medical intervention, while the condition of the remaining victims requires medical care [29]. As of April 17, 2003, the World Health Organization (WHO) reported 3,389 cases (a mixture of probable or suspected cases) in 26 countries. 165 victims are reported to have died [23].

Although researchers in the Erasmus Medical Center in Rotterdam recently demonstrated that a coronavirus (some of which produce common colds) is the causative agent of SARS, the mode of transmission still remains unknown [23]. The current hypothesis is that SARS is transmitted mainly by close person-to-person contact which may explain the relatively slow transmission scale. However, it could also be transmitted through contaminated objects, air or by other unknown ways [32]. It is also a mystery how the disease originated, whether in birds, pigs or other animals, nor is it known if the origin is rural or urban [33].

In this article, a simple model for SARS outbreaks is formulated (see [34]). The model is used in conjunction with *global and local* SARS data to estimate the initial

growth rate of the SARS epidemic. These rates are used to estimate SARS' *basic reproductive number*, R_0 , the classical epidemiological measure associated with the reproductive power of a disease. R_0 estimates the *average* number of secondary cases of infection generated by a *typical* infectious individual in a population of susceptibles [35] and hence, it is used to estimate the initial growth of a SARS outbreak. We estimate (using data from Ontario, Hong Kong and Singapore) that R_0 is about 1.2. This value is not too different from past estimates of R_0 for influenza (see [36]) despite the fact that *superspreaders* of SARS have been identified. In fact, the parameter values resulting on this R_0 , on our population-scaled model, can lead to extremely high levels of infection). We show, via simple extrapolation, that the estimated rate of growth is consistent with the reported date for the first cases of SARS in Hong Kong, however the first cases in Toronto may be several weeks earlier than the February 23 date of the first case reported by the Canadian Health Ministries [5]. Our best "rough" estimate for Toronto is that the first case occurred sometime around January 29th, and not later than February 28th. The data for Hong Kong are fitted by fixing the parameters k , δ and γ_1 based on estimates of the observed rates for the corresponding processes. The growth rate β is estimated from observed "model-free" exponential growth in Singapore and Hong Kong. The *average* diagnostic rate α and the measure of heterogeneity between the two susceptible classes p and the effectiveness of patient isolation measures (related to l) are then varied to fit the initial data for Hong Kong and Singapore. To model the data in Toronto, we must postulate that the parameters describing the rate of diagnosis (α) and isolation (l) in the Canadian outbreak changed radically on March 27. Two hospitals in Toronto were closed about that time: Scarborough Grace Hospital on March 25th and York Central

Hospital on March 28th [37]. The remainder of this article is organized as follows: Section 4 introduces the basic model and gives an approximate formula for R_0 in the special case where class E only makes a minor contribution to basic reproductive rate; Section 5 describes the results of simulations and connections to data; and, Section 6 collects our final thoughts.

1.2 SARS’ Transmission Model

U.S. data is limited and sparsely distributed [38, 39] while the quality of China’s data is hard to evaluate [40]. On the other hand, there appears to be enough data for Toronto [5], Singapore and Hong Kong [4] to make limited preliminary predictions using a model that includes the effects of *suspected* mechanisms for the spread of SARS. Limited data and inconclusive epidemiological information place severe restrictions on efforts to model the global spread of the SARS etiological agent.

Thus, we model *single* outbreaks, ignoring demographic processes other than the impact of SARS on survival. The model is applied to data from Toronto, Hong Kong and Singapore. Because the outbreak dynamics in Singapore and Hong Kong are different from those in Toronto, some of the results may only be indicative of what is happening in those regions of the world (in particular our parameters α and l may change). The situation must be re-evaluated frequently as SARS continues its travels around the world.

Here we describe a model that incorporates, in a *rather crude* way, some of the important characteristics suggested in the literature (unequal susceptibility, symptomatic and asymptomatic individuals, mode of transmission, superspreaders, etc.) [32, 41, 42, 38]. The goal is to use the results for single outbreaks as

a first step in our efforts to gauge the *global* impact of SARS. Hence, we focus on three “closed” populations (Southern Ontario (Toronto), Singapore and Hong Kong) and postulate differences in the degree of susceptibility to SARS [13, 29]. These differences may be due to variations in contact rates, age-dependent susceptibility or “unknown” genetic factors. This last assumption is handled (in a rather crude and arbitrary way) via the introduction of two distinct susceptible classes: S_1 , the most susceptible, and S_2 , less so. Initially, $S_1 = \rho N$ and $S_2 = (1 - \rho)N$ where ρ is the proportion of the population size N that is initially at higher risk of SARS infection. The parameter p is a measure of reduced susceptibility to SARS in class S_2 [29, 13]. E (“exposed”) denotes the class composed of asymptomatic, possibly infectious (at least some of the time) individuals. Typically, it takes some time before asymptomatic infected individuals become infectious. The possibility of limited transmission from class E is included, in a rather crude way, via the parameter q (see Table 1). The class I denotes infected, symptomatic, infectious, and undiagnosed individuals. I -individuals move into the diagnosed class J at the rate α . Individuals recover at the rates γ_1 (I class) and γ_2 (J class). The rate δ denotes SARS’ disease-induced mortality. The classes R is included to keep track of the cumulative number of diagnosed and recovered, respectively. Furthermore, it is assumed that diagnosed individuals are handled with *care*. Hence, they might not be (*effectively*) as infectious as those who have not been diagnosed (if l is small). The parameter l takes into account their reduced impact on the transmission process (small l represents effective measures taken to isolate diagnosed cases and *visa versa*). Table 1 includes parameters’ definitions and the initial values used. Our SARS epidemiological model is given by the following nonlinear system of differential equations:

$$\begin{aligned}
\dot{S}_1 &= -\beta S_1 \frac{(I+qE+lJ)}{N}, \\
\dot{S}_2 &= -\beta p S_2 \frac{(I+qE+lJ)}{N}, \\
\dot{E} &= \beta(S_1 + pS_2) \frac{(I+qE+lJ)}{N} - kE, \\
\dot{I} &= kE - (\alpha + \gamma_1 + \delta)I, \\
\dot{J} &= \alpha I - (\gamma_2 + \delta)J, \\
\dot{R} &= \gamma_1 I + \gamma_2 J,
\end{aligned} \tag{1.1}$$

which is referred to as “SEIJR,” after the variables used to name the classes (Figure 5.3).

The values of p and q are not known and are fixed arbitrarily while l and α are varied and optimized to fit the existing data (least-squares criterion) for Hong Kong, Singapore and Toronto. We did not explore the sensitivity of the model to variations in p and q because they are not known and cannot be controlled. All other parameters were roughly estimated from data [5, 4] and current literature [32, 24, 25, 26]. In particular, the transmission rate β is calculated from the dominant root of the third order equation obtained from the linearization around the disease-free equilibrium [35]. The parameters l and α were allowed to vary when fitting the data for each location (Singapore, Hong Kong and Toronto). Some restrictions apply, for example, the value of $\alpha > \gamma_1$. We also require that $1/\gamma_2 = 1/\gamma_1 - 1/\alpha$, a statement that members of the diagnosed class J recover at the same rate as members of the undiagnosed class I . $1/\gamma_1$ has been reported to be between 7 and 10 days [27, 26].

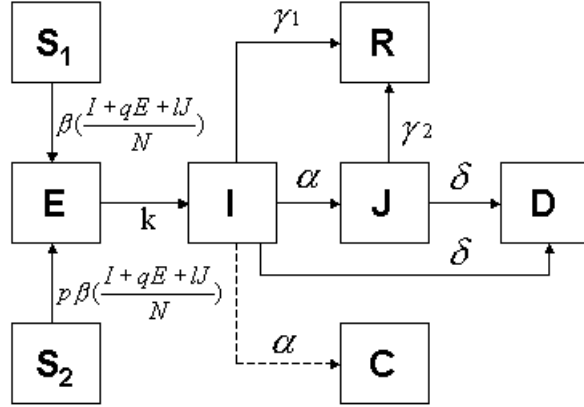


Figure 1.1: A schematic representation of the flow of individuals between the different classes. The model considers two distinct susceptible classes: S_1 , the most susceptible, and S_2 . $\beta \frac{I + qE + lJ}{N}$ is the transmission rate to S_1 from E , I and J . p is a measure of reduced susceptibility to SARS in class S_2 . E is the class composed of asymptomatic, possibly infectious individuals. The class I denotes infected, symptomatic, infectious, and undiagnosed individuals. I -individuals move into the diagnosed class J at the rate α . Individuals recover from class I at the rate γ_1 and γ_2 from the J class. The rate δ is SARS' disease-induced mortality. The classes R and D are included to keep track of the cumulative number of diagnosed, recovered and dead individuals, respectively. The quantity C is for comparison with epidemiological statistics; it tracks the total number of diagnosed individuals.

Table 1.1: Parameter definitions and values that fit the cumulative number of cases in class J (“diagnosed”) for Hong Kong. These parameters are used to compute the basic reproductive number R_0 .

Parameter	Definition	Value
β	Transmission rate per day	0.75
q	Relative measure of infectiousness for class E	0.1
l	Relative measure of reduced risk for class J	0.38
p	Relative measure of reduced risk for class S_2	0.1
$1/k$	Mean incubation period (days)	3
$1/\alpha$	Mean time before diagnosis (days)	3
$1/\gamma_1$	Mean time before recovery (days)	8
$1/\gamma_2$	Mean time before recovery for class J (days)	5
δ	SARS-induced mortality per day	0.006
ρ	Proportion of the population at higher risk	0.4

From the second generator approach [35], we obtain the following expression for the basic reproductive number:

$$\mathcal{R}_0 = \{\beta [\rho + p(1 - \rho)]\} \left\{ \frac{q}{k} + \frac{1}{\alpha + \gamma_1 + \delta} + \frac{\alpha l}{(\alpha + \gamma_1 + \delta)(\gamma_2 + \delta)} \right\} \quad (1.2)$$

which can be easily given an epidemiological interpretation (see Appendix). The use of parameters estimated from Hong Kong (Table 5.1) gives a values of $R_0 = 1.2$ (Hong Kong) and $R_0 = 1.2$ (Toronto, assuming exponential growth) and $R_0 = 1.1$ (Singapore).

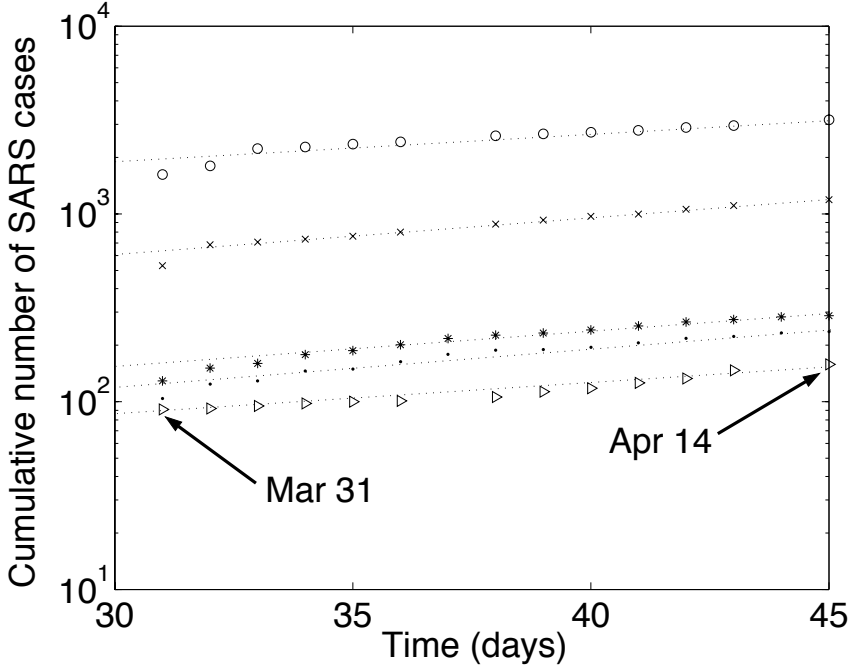


Figure 1.2: The cumulative number of SARS cases from March 31 to April 14 (lin-log scale) for the World (top data), Hong Kong(second row), Ontario, Canada (fourth row), all of Canada (third row) and Singapore (bottom row). The data were obtained from WHO [4] except for the Canadian data which are from the Canadian Ministry of Health [5]. The Ontario data includes suspected and probable cases since March 31. This inclusion explains the jump in the data for Ontario on March 31st. The rates of growth of the SARS outbreak (computed using data from March 31 to April 14) are: 0.041 (world), 0.050 (Hong Kong), 0.037 (Singapore), 0.054 (Canada) and 0.054 (Ontario).

1.3 Simulation Results

Initial rates of growth for SARS outbreaks in different parts of the world (see Figure 1.2) are computed using the data provided by WHO [4] and the Canadian Ministry of Health [5]. These rates are computed exclusively from the number of cases reported between March 31 and April 14. The values obtained are 0.0405 (world data), 0.0496 (Hong Kong), 0.054 (Canada), 0.054 (Toronto) and 0.037 (Singapore).

Table 1.2: Estimated starting times of the SARS outbreak

Country	Estim. start of the outbreak
Canada	February 1st
Hong Kong	November 20th
Singapore	December 6th
World data	November 5th

For our numerical simulations, we start with an infectious individual (not yet diagnosed, $I(0) = 1$) and *crude* estimates for the start of SARS outbreaks (t_0) are obtained from the formula $t_0 = t - (\frac{1}{r} \log(x(t)))$, which assumes initial exponential growth (r , the estimated “model-free” rate of growth from the time series $x(t)$ of the cumulative number of SARS cases). Results for Toronto, Hong Kong, Singapore and aggregated world data are shown in Table 5.2. The estimated “world” start of the outbreak is November 5, a date consistent with the fact that the first SARS case was detected in Guangdong, China in November [20]. These dates are used as the starting time of the respective outbreaks.

For the case of the Province of Ontario, Canada the total population N is approximately 12 million. We assume that the population at *major* risk of SARS infection lives in Ontario’s southern part (particularly Toronto), and is approximately 40% of the total population ($\rho = 0.4$ in our model). It is worth pointing out that this value of ρ is not critical (that is, the most sensitive) in the model. The “model-free” approximately exponential growth rates for the various regions of the world are roughly similar *except for Canada* from March 31st (day 61) to April 6th (beginning the day of the jump in the number of reported Canadian cases), the number of diagnosed cases grew $\sim \exp(0.081t)$, where t is measured in days. This

rate is substantially higher than elsewhere in the world. In the subsequent week (beginning April 7th, day 68) the number of probable or suspected Canadian cases rapidly rolls over to a smaller growth rate not too far from the rest of the world (Figure 5.4). We conclude, based on the coincidence of the Canadian hospital closures, the jump in the reported number of Canadian SARS cases on March 31st and the rapid rise in recognized cases in the following week, that Canadian doctors were rapidly diagnosing pre-existing cases of SARS (in either class E or I on March 26th). If we make the assumption that the fundamental disease spreading parameters other than α and l are roughly constant throughout the world prior to March 26th, we can reach two important conclusions. Beginning on March 26th, in Toronto:

- α changed from a number $1/\alpha \approx 1/\gamma_1 - 2 \approx 6$ days to $1/\alpha_1 \leq 3$ days, and
- l changed from an uncertain and relatively large value $l > 1/2$ to $l \leq 0.1$.

If we assume that the fundamental growth rate β is essentially constant from one region of the world to another, it is difficult for our model to produce growth rates r well above the world average, except as a transient response to differences in diagnostic rate α (due to delays in response or change in policy). Similarly, the SEIJR model requires fairly small values of l to achieve a rapid roll-over in the growth rate of recognized cases. The parametric details of how a “second” initial condition for Toronto on March 26th is generated do not affect the qualitative aspect of this argument: the Canadian data prior to March 31st (the day of the large jump) are probably not as meaningful as data after that date, and hence only bound the model from below prior to March 26th. The essential aspect of this before-and-after hospital closure argument is that there were substantially

Table 1.3: Long-time model results for Ontario, Canada, assuming various changes in behavior on March 26th, 2003.

l	α	Infected with SARS	Diagnosed with SARS
0.05	1/3	0.0077%	0.0055%
0.30	1/3	18%	13%
0.05	1/6	21%	13%

more undiagnosed people in classes E and I than in class J on March 26th. This is a reasonable assumption given that the number of cases reported by Canadian officials more than double from March 30th to March 31st. The introduction of behavioral changes starting on March 26 ($t = 57$ days), alters the fate of the disease in a dramatic fashion (see Table 5.3).

Fitting the model to the Hong Kong and Singapore data is carried out in a similar fashion with $\rho = 0.4$, (Hong Kong has about 7.5 million inhabitants, Singapore 4.6 million). The estimated transmission rate from Hong Kong data is $\beta \approx 0.75$ and for Singapore $\beta \approx 0.68$. Both Hong Kong and Singapore's data are fit with the value $q = 0.1$. Hong Kong and Singapore's measure of contact between diagnosed SARS cases and susceptibles are $l = 0.38$ and 0.40 , respectively (see Figure 4). Even though there is some heterogeneity in the parameters for Hong Kong and Singapore, they provide an important calibration of our model. Their values for l and α are roughly consistent with each other, indicating that the difference with Toronto is significant within our model, and pointing to the joint importance of rapid diagnosis $\alpha \approx 1$ and good isolation of diagnosed patients $l \approx 0$ in controlling an outbreak. While there is some indication in the data from Hong Kong of a possible slowing of the outbreak, we did not attempt to analyze the slowing or assess its significance.

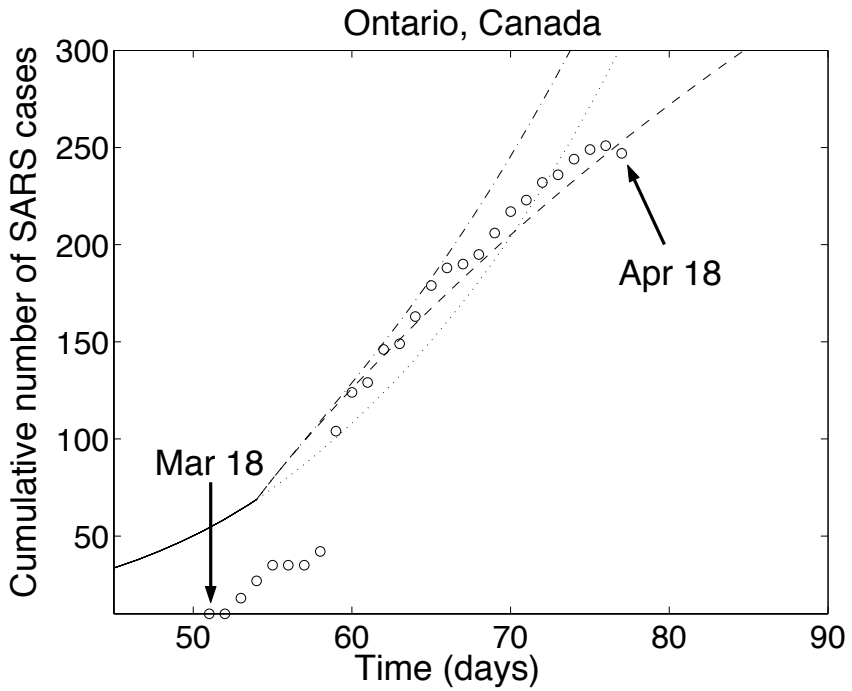


Figure 1.3: The circles are the cumulative number of suspected or probable SARS cases in Ontario beginning on day 61 (March 31st, the day of the jump) and the number of probable cases up until day 60. The lines are the cumulative number of “diagnosed” cases C from the SEIJR model. The fit to the data is given by a change in the values of α and l on March 26th. Prior to March 26th, $\alpha = 1/6$, $l = 0.76$. Because the model is poorly constrained prior to day 61, the real purpose of this part of the model is to generate sufficiently large classes of E and I relative to J on March 26th to give the fast increase in C from day 61 to day 67. After March 26th, three scenarios are shown. The fit to the data is given by $\alpha = 1/3$, $l = 0.05$ (rapid diagnosis and effective isolation of diagnosed cases, dashed line). The second curve is given by $\alpha = 1/6$, $l = 0.05$ (slow diagnosis and effective isolation, dotted line) and the third curve by $\alpha = 1/3$, $l = 0.3$ (rapid diagnosis with improved but imperfect isolation, dash-dot line). An index case is assumed on February 1st. The transmission rate β is computed using the estimated rate of growth ($r = 0.0543$) for the Ontario data as described in the text.

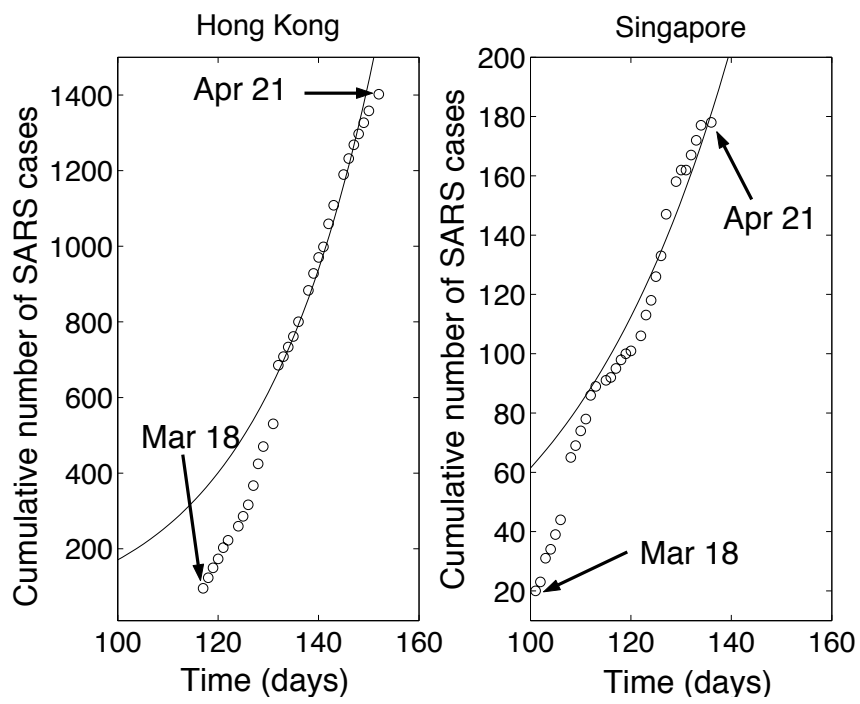


Figure 1.4: Cumulative number of SARS cases in Hong Kong and Singapore as a function of time (SEIJR model) with $l = 0.38$ (Hong Kong) and $l = 0.40$ (Singapore). Singapore has $\beta = 0.68$, all other parameter are from Table 1. The data are fitted starting March 31 (see Figure 1.2) because of the jump in reporting on March 30th.

1.4 Conclusions

A simple model that can capture the effect of average infectiousness in a heterogeneous population and the effect of isolating diagnosed patients has been introduced to explore the role of patient isolation and diagnostic rate in controlling a SARS outbreak. By examining two cases with relatively clean exponential growth curves for the number of recognized cases, we are able to calibrate a SEIJR model with parameters $\alpha = 1/3$ (SARS' diagnostic rate) and $l \approx 0.4$ (isolation effectiveness). We then use our SEIJR model to examine the non-exponential dynamics of the Toronto outbreak. Two features of the Toronto data, the steep increase in the number of recognized cases after March 31st and rapid slowing in the growth of new recognized cases, robustly constrained the SEIJR model by requiring that $l \approx 0.05$ and $\alpha > 1/3 \text{ days}^{-1}$.

The model is also used to look at the impact of drastic control measures (isolation). The fitting of data shows that the initial rates of SARS' growth are quite similar in most regions leading to estimates of R_0 between 1.1 and 1.2 despite the recent identification of *superspreaders*. Model simulations are fitted to SARS reported data for the province of Ontario, Hong Kong and Singapore. Good fits are obtained for reasonable values of α , the rate of identification of SARS infections; “reasonable” values of the control parameters l (a measure of isolation); possible values of p , a *crude* measure of reduced susceptibility (due to genetic factors, age or reduced contact rates); q a *crude* measure of the relative degree of infectiousness of asymptomatic individuals; possible values of ρ a measure of initial levels of population heterogeneity; and, reasonable values of N the *effective* population size. It is worth noticing that for values of N larger than 100,000 the predictions (proportion of cases at the end of the outbreak, etc.) are *roughly* the same. The

introduction of behavioral changes that follow the identification of the first case (reduce values of l at the time of the identification and moving aggressively to identify cases of SARS by increasing $1/\alpha$) result in a dramatic reduction in the total number of cases and on mortality in Toronto. Given the fact that SARS appears to kill between three and seven percent of infected (diagnosed) cases ([28]), it seems quite appropriate to isolate diagnosed people. Although we do not examine the effect of quarantine by varying q , it seems intuitive that quarantining those who came into close contact with positively diagnosed individuals will reduce the total number of cases.

Model results and simple estimates suggest that *local* outbreaks may follow similar patterns. Furthermore, the use of relative extreme isolation measures in conjunction with rapid diagnosis has strong impact on the local dynamics (Toronto's situation). However, if SARS has shown us anything it is that “undetected” and “unchecked” local disease dynamics can rapidly become a global issue.

The research on this article used the latest data available (April 18 for Canada and April 21 for Hong Kong and Singapore). Recent disclosures [43] reaffirm the importance of carrying out the analysis excluding data from China. We have redone the analysis including the data collected up to April 25 and, our conclusions, remain the same. Current data seem to support higher values for SARS induced mortality rates [28]. However, our model is *most sensitive* to the parameters l (effectiveness of isolation) and (α) diagnostic rate. It is not as sensitive to changes in δ . In fact, the consideration of a 7% mortality ($\delta \approx 0.01$) rather than 4% reduces the number of cases by about 12%. In Toronto, we have estimated 612 diagnosed cases with ($l = 0.05$ and $\alpha = 1/3$ after March 26th). Perfect isolation after March 26th, ($l = 0.00$) reduces this number to 396 diagnosed cases. The assumption of

homogenous mixing implies that our model is likely to overestimate the size of the outbreak. Hence, the situation in Toronto seems to support the view that this *outbreak* is being contained. Obviously, the case of the crude model (by design) cannot handle high levels of variability (an stochastic model would be desirable). This possibility is tested (as it is often done in deterministic models) by looking at the sensitivity of the model to parameters (α and l being the most critical). Such sensitivity analyses can also help “estimate” the variability in R_0 .

1.5 Appendix

Following the second generator approach [35], we obtain the next generation matrix FV^{-1} where

$$J = \begin{pmatrix} \beta q(\rho + p(1 - \rho)) & \beta(\rho + p(1 - \rho)) & \beta l(\rho + p(1 - \rho)) \\ 0 & 0 & 0 \\ 0 & 0 & 0 \end{pmatrix}$$

and

$$J = \begin{pmatrix} k & 0 & 0 \\ -k & \alpha + \gamma_1 + \delta & 0 \\ 0 & -\alpha & \gamma_2 + \delta \end{pmatrix}$$

F represents the paths to infection (derivatives of the infection terms) and V represents the remaining dynamics (derivatives of all other terms). The three columns and rows correspond to the compartments E , I and J .

The basic reproductive number is the dominant eigenvalue of FV^{-1}

$$\mathcal{R}_0 = \{\beta [\rho + p(1 - \rho)]\} \left\{ \frac{q}{k} + \frac{1}{\alpha + \gamma_1 + \delta} + \frac{\alpha l}{(\alpha + \gamma_1 + \delta)(\gamma_2 + \delta)} \right\} \quad (1.3)$$

β is the common scale for the rate of infection. ρ is the fraction of compartment S_1 susceptibles in the population and $(1 - \rho)$ is the fraction of compartment S_2 susceptibles. The infection rates for the latter are attenuated by p . Infectives stay

in compartment E for $\frac{1}{k}$ days on average, where their infection rate is $q\beta$, they then all progress to compartment I for $\frac{1}{\alpha+\gamma_1+\delta}$ days (on average) where their infection rate is β . A fraction $\frac{\alpha}{\alpha+\gamma_1+\delta}$ infectives progress from compartment I to J where their infection rate is $l\beta$. Infectives spend, on average, $\frac{1}{\gamma_2+\delta}$ days in compartment J .

Chapter 2

Implications of an Uncertainty and Sensitivity Analysis for SARS' Basic Reproductive Number for General Public Health Measures *

2.1 Introduction

Severe Acute Respiratory Syndrome (SARS), a viral respiratory disease, has been reported in 32 countries (July 11, 2003). SARS is believed to have originated in Guangdong Province, China during November 2002 [44]. Researchers at the Erasmus Medical Center in Rotterdam identified a corona virus as the agent responsible for the infection of 8437 individuals worldwide (813 deaths, July 11, 2003) [4]. According to recent epidemiological data from Hong Kong [1], an individual exposed to SARS enters an incubation period with a mean length of 6.4 days. Symptomatic individuals in that study were diagnosed (hospitalized) at a mean rate $1/4.85 \text{ days}^{-1}$. Those who recovered were discharged a mean of 23.5 days after diagnosis, while the mean period to death was 35.9 days after diagnosis. Because no specific treatment for SARS exists, control of the epidemic has relied on rapid diagnosis and isolation of patients [44], an approach that is reported to be effective [45]. However, the majority of the early SARS cases in Toronto occurred

*G. Chowell , C. Castillo-Chavez, P.W. Fenimore, C. Kribs-Zaleta, L. Arriola, J.M. Hyman. Implications of an Uncertainty and Sensitivity analysis for SARS's Basic Reproductive Number for General Public Health Measures, Emerging Infectious Diseases 10 (7) (2004).

in hospitals, with the movement of SARS patients between hospitals contributing significantly to its initial spread [46]. In Taiwan 94% percent of SARS cases occurred due to transmission in hospital wards [47] (similar effects occurred in Hong Kong and Singapore [48]). Although the SARS epidemic was eventually controlled, the measures used to achieve that control varied greatly in scope from one place to another. Control of an outbreak relies partly on identifying what disease parameters are likely to lead to a significant reduction in \mathcal{R}_0 . Here we calculate the dependence of \mathcal{R}_0 on model parameters.

2.2 Methods

The basic reproductive number \mathcal{R}_0 is the average number of secondary cases generated by a primary case during its infectious period. If $\mathcal{R}_0 < 1$ the disease can not be sustained. On the other hand, if $\mathcal{R}_0 > 1$ an epidemic outbreak typically occurs. Two models of the SARS epidemic that incorporate the effects of quarantine and early detection of new cases that report a basic reproductive number between 2 and 4 but assume perfect isolation were recently introduced [49, 50]. A slightly different model (Chowell et al. [51]) was used to quantify the role that fast diagnosis and efficient isolation of patients played in Toronto's outbreak [51]. The estimates of \mathcal{R}_0 from this general model were significantly lower than those found in other work. This model predicted control in Toronto and showed that lack of immediate action would have been catastrophic [52]. Differences in the susceptibility of the population [1] are incorporated in the model by dividing the population into classes S_1 (high risk) and S_2 (low risk). The low risk class (S_2) has a reduced susceptibility to SARS, measured by the parameter p . While $p = 0$ would denote that S_2 has no susceptibility to SARS, $p = 1$ would indicate that both susceptible

classes are equally susceptible to SARS. Initially, $S_1 = \rho N$ and $S_2 = (1 - \rho)N$ where N is the total population size and ρ is the initial fraction of individuals in the most susceptible class S_1 . Susceptibles exposed to SARS (assumed to be asymptomatic) enter the exposed class with a rate proportional to β and remain there for a mean incubation period of $1/k$. The possibility of reduced transmission from the exposed class is included through the parameter q ($0 < q < 1$), a relative measure of infectiousness. Once symptomatic, exposed individuals progress to the infectious class (not yet diagnosed) where they may recover at the rate γ_1 , die at rate δ , or enter the diagnosed class at the rate α . Isolation mechanisms may be put in place in the diagnosed class to reduce their impact on the transmission process. The relative infectiousness after isolation is measured by the parameter l ($0 < l < 1$) so that $l = 0$ denotes perfect isolation while $l = 1$ denotes ineffective isolation.

The basic reproductive number derived from our model [51] is given by the formula:

$$\mathcal{R}_0 = \{\beta [\rho + p(1 - \rho)]\} \left\{ \frac{q}{k} + \frac{1}{\alpha + \gamma_1 + \delta} + \frac{\alpha l}{(\alpha + \gamma_1 + \delta)(\gamma_2 + \delta)} \right\}. \quad (2.1)$$

This equation includes 10 parameters of which two, the diagnostic rate (α) and the isolation effectiveness (l) are amenable to modification by medical intervention. Definitions for the remaining parameters are in Table 3.1. We use a Monte Carlo procedure (simple random sampling) to quantify the uncertainty of the basic reproductive number \mathcal{R}_0 and the sensitivity of \mathcal{R}_0 to model parameters when these parameters are distributed. Similar methodology has been used before [53, 54, 55]. The probability distributions for k , γ_2 , δ , α (Figure 2.1) are taken from [1]. Because it is still not known whether asymptomatic individuals (exposed class) can transmit the disease, we have fixed $q = 0.1$ (the relative infectiousness of exposed and asymptomatic individuals) as in ref. [51]. The observed heterogeneity in trans-

mission rates during the SARS epidemic is modelled here by assuming that β is distributed exponentially with mean $0.25 \text{ person}^{-1}\text{day}^{-1}$ (our estimate of the transmission rate in Hong Kong). We revise earlier estimates for ρ and p [51] (both have an impact on \mathcal{R}_0) using data from the age distribution of residents and the age-specific incidence of SARS in Hong Kong as reported in [1]. The revised estimates are $\rho = 0.77$ (the initial proportion of the population at higher risk) and $p = 1/3$ (the measure of reduced susceptibility in S_2). The lower risk subpopulation lies in the age range (0 – 19). It constitutes approximately 23% of Hong Kong's population [1]. The fact that most of the SARS cases used in the epidemiological studies of Toronto [46] were generated in hospitals limits the use of general demographic data from Toronto in the estimation of ρ and p . Hence, we use the parameters estimated from the situation in Hong Kong. In addition, we have generated new estimates for the transmission rate β ($\beta = 0.25$ for Hong Kong) and the isolation effectiveness (l) in Hong Kong ($l = 0.43$), Singapore ($l = 0.49$) and Toronto ($l = 0.1$, after control measures were put in place) by least squares fitting of our model [51] to epidemic curve data [4, 5] using the revised values of $p = 1/3$ and $\rho = 0.77$.

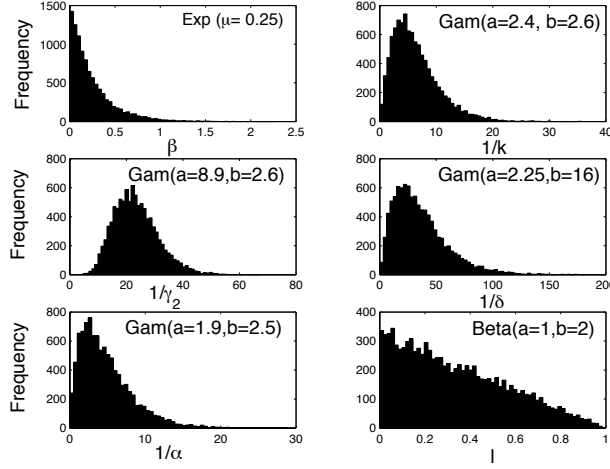


Figure 2.1: Histograms of the 6 distributed parameters appearing in eqn. 1 with sample size 10^4 . The transmission rate was assumed exponentially distributed with mean 0.25, our estimate transmission rate in Hong Kong. Here l is assumed to have a Beta distribution ($l \sim \mathcal{B}(1, 2)$). Alternative distributions for l were also used as described in the text. All other distributions were taken from ref. [1].

2.3 Results

2.3.1 Uncertainty analysis

Monte Carlo simulations with 10^5 samples from the distributions of various epidemic parameters (Figure 2.1) and fixed values of $l = 0.1$ and $\alpha = 1/3$ day $^{-1}$ for Toronto (i.e. after the implementation of control measures on March 26th) give a median and interquartile range for the distribution of the basic reproductive number $\mathcal{R}_0 = 0.58$ (0.24, 1.18) (Table 2.2). The same Monte Carlo procedure but with lower rate of diagnosis $\alpha = 1/4.85$ day $^{-1}$ and the levels of patient isolation in Hong Kong ($l = 0.43$) and Singapore ($l = 0.49$) gives $\mathcal{R}_0 = 1.10$ (0.44 – 2.29) and 1.17 (0.47 – 2.47) respectively (see Figure 2.2). These values for \mathcal{R}_0 are in agreement with the *empirical* \mathcal{R}_0 observed from the data of the first week of the SARS outbreak in Singapore [49]. Perfect isolation gives $\mathcal{R}_0 = 0.49$ (0.19 – 1.08).

Table 2.1: Parameters definitions and baseline values for our model. Baseline values for k , γ_2 , α , ρ , p and δ have been taken from ref. [1]. $\beta = 0.25$ is our estimate transmission rate in Hong Kong. $l = 0$ means perfect isolation while $l = 1$ means no isolation.

Parameter	Definition	Baseline value
p	Reduction in risk of infection for class S_2	0.33
ρ	Initial proportion of the population at higher risk	0.77
β	Transmission rate per day	0.25
$1/k$	Mean incubation period (days)	6.37
$1/\gamma_1$	Mean period before recovery (days)	28.35
$1/\gamma_2$	Mean period before recovery for class J (days)	23.5
$1/\alpha$	Mean period before diagnosis (days)	4.85
δ	SARS' induced mortality rate per day	0.0279
q	Relative measure of infectiousness for class E	0.1
l	Relative measure of reduced risk for class J	[0, 1]

Especially noteworthy is that even in cases when eventual control of an outbreak is achieved (Toronto and a hypothetical case of perfect isolation), 25% of the weight of the distribution of \mathcal{R}_0 lies at $\mathcal{R}_0 > 1$. Furthermore, the median and interquartile range of R_0 are larger when $p = 1$, as it has been assumed ([49]). In Figure 2.3 we show the (β, l) parameter space when $R_0 < 1$ obtained from our uncertainty analysis [55].

2.3.2 Sensitivity analysis

We rank model parameters according to the size of their effect on \mathcal{R}_0 . Partial rank correlation coefficients (PRCCs) [53, 54, 56] were computed between each of the parameters (with the exception of p , q , and ρ which where held fixed) and \mathcal{R}_0 as

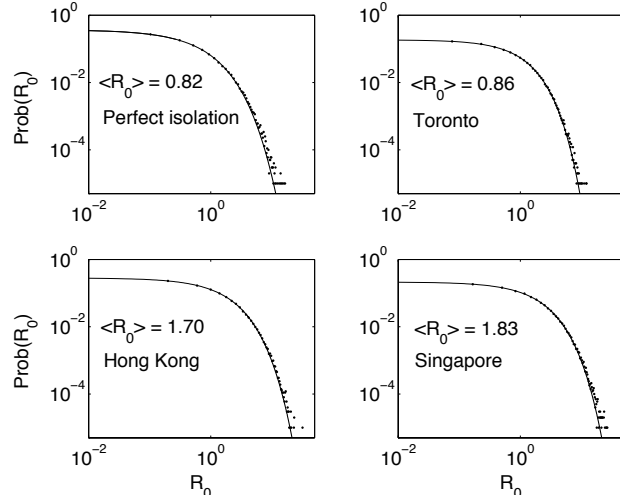


Figure 2.2: Empirical (dots) and stretched exponential estimated probability density function $Prob(\mathcal{R}_0) = ae^{-(\mathcal{R}_0/b)^c}$ (solid line) [6] of \mathcal{R}_0 for the cases of Toronto ($a = 0.186$, $b = 0.803$, $c = 0.957$, after control measures had taken place), Hong Kong ($a = 0.281$, $b = 1.312$, $c = 0.858$) and Singapore($a = 0.213$, $b = 1.466$, $c = 0.883$) obtained from our uncertainty analysis. The distribution for the case of perfect isolation ($l = 0$, $a = 0.369$, $b = 0.473$, $c = 0.756$) is shown as a reference.

samples were drawn from the distributions, thus quantifying the strength of the parameter's linear association with \mathcal{R}_0 . The larger the partial rank correlation coefficient, the larger the influence of the input parameter on the magnitude of \mathcal{R}_0 . Because the distribution of the parameter l (isolation effectiveness) is not known, we studied the sensitivity of \mathcal{R}_0 to various distributions of l . The systematic decline in \mathcal{R}_0 with increasing l in the range $[0, 1]$ is illustrated in Figure 2.4. Distributions of l used for the Monte Carlo calculation of the partial rank correlation coefficients are: (a) $l \sim \mathcal{B}(a = 2, b = 2)$ where \mathcal{B} is used to denote a beta distribution. Here, the likelihood of l is bell-shaped with mean 0.5 and variance 0.05; (b) $l \sim \mathcal{B}(a = 1, b = 2)$, the likelihood of l decreases linearly in the $[0,1]$ interval; and (c) $l \sim \mathcal{B}(a = 2, b = 1)$, the likelihood of l increases linearly in the $[0,1]$ interval.

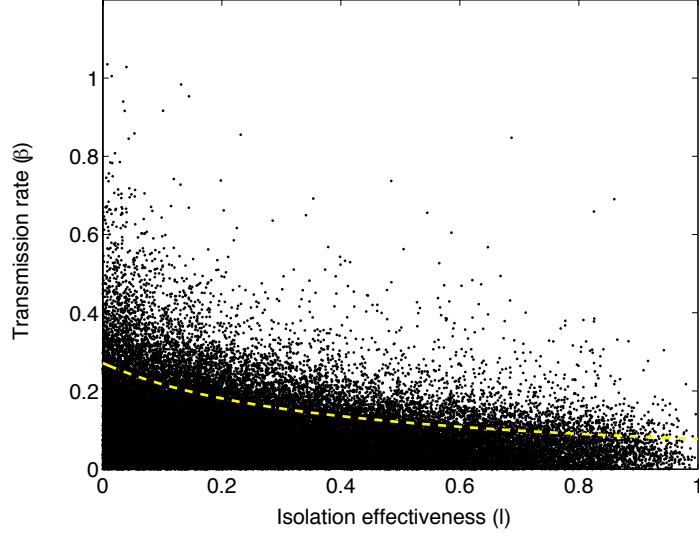


Figure 2.3: (β, l) parameter space when $\mathcal{R}_0 < 1$ obtained from the uncertainty analysis (black dots). The deterministic (β, l) level curve when $\mathcal{R}_0 = 1$ is shown in yellow. All other parameters in eqn. 1 were fixed to their baseline values (Table 3.1). $l = 0$ denotes perfect isolation while $l = 1$ denotes no isolation.

The transmission rate β and isolation effectiveness (l) are the most influential parameters in determining \mathcal{R}_0 . Table 2.3 shows the partial rank correlation coefficients for three possible distributions of l . The transmission rate is ranked first independent of the distribution of l . Isolation effectiveness is ranked second when l comes from distributions (a) and (b) and ranked third when it comes from distribution (c). Our sensitivity analysis is corroborated by computing local derivatives on \mathcal{R}_0 (see appendix). Achieving control ($\mathcal{R}_0 < 1$) can require changing parameters other than those with the highest partial rank correlation coefficient. For example ref. [51] showed that control of the outbreak in Toronto relied on both a reduction in l and $1/\alpha$, even though α is ranked fairly low by the partial rank correlation coefficient.

Table 2.2: The median and the interquartile range (IQR) of the distribution of the basic reproductive number (\mathcal{R}_0) of SARS for Toronto, Hong Kong and Singapore obtained from our uncertainty analysis.

Country	\mathcal{R}_0 mean	\mathcal{R}_0 median	\mathcal{R}_0 IQR
Toronto, Canada ($l = 0.10$)	0.86	0.58	(0.24-1.18)
Hong Kong ($l = 0.43$)	1.70	1.10	(0.44-2.29)
Singapore ($l = 0.49$)	1.83	1.17	(0.47-2.47)

Table 2.3: Partial rank correlation coefficients (PRCCs) between each of the input parameters and \mathcal{R}_0 from Monte Carlo sampling of size 10^4 for different distributions of the isolation effectiveness (l) as described in the text.

Probability distrib.	Parameters sorted by decreasing PRCC
Beta($a = 2, b = 2$)	β (0.92), l (0.57), δ (0.53), γ_2 (0.35), α (0.32), k (0.13)
Beta($a = 1, b = 2$)	β (0.90), l (0.60), δ (0.44), α (0.39), γ_2 (0.26), k (0.12)
Beta($a = 2, b = 1$)	β (0.92), δ (0.60), l (0.51), γ_2 (0.40), α (0.22), k (0.11)

2.4 Conclusion

We have estimated the basic reproductive number (\mathcal{R}_0) for the cases of Toronto, Hong Kong and Singapore (Table 2.2) via an uncertainty analysis carried on Equation 2.2. Input parameters to \mathcal{R}_0 have been taken or derived from [1, 51] (Figure 2.1). A stretched exponential distribution fits well the resulting distributions of \mathcal{R}_0 for the different locations (Figure 2.2). Even though the median of \mathcal{R}_0 is less than one under the assumption of perfect patient isolation ($l = 0$), we find that 25% of our \mathcal{R}_0 distribution lies at $\mathcal{R}_0 > 1$, even when control is achieved.

Our expression for R_0 incorporates the effects of diagnosis-isolation strategies. Moreover, our approach includes differential susceptibility (p) and/or effective population size (ρ). Most models take $p = 1$ even though data from Hong Kong shows

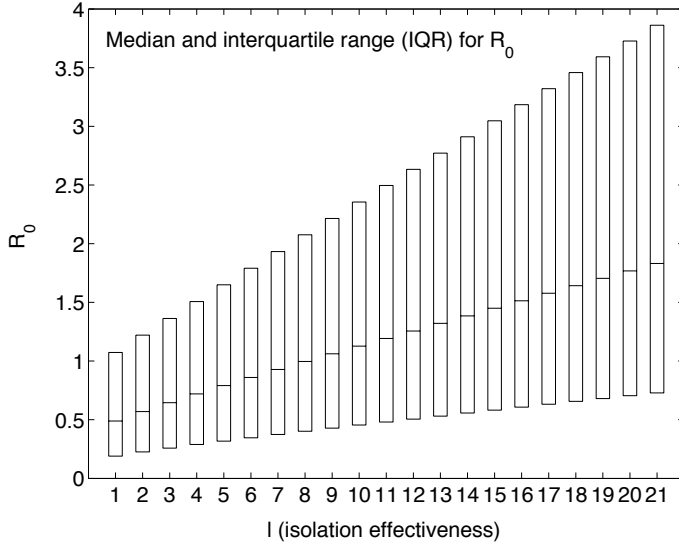


Figure 2.4: Boxplot of the sensitivity of \mathcal{R}_0 estimates to varying values of l , isolation effectiveness. l ($0 \leq l \leq 1$) was divided in 20 equally spaced intervals going from perfect isolation ($l = 0$, level 1) to no isolation ($l = 1$, level 21). The boxplot shows the median and the interquartile range of \mathcal{R}_0 obtained from Monte Carlo sampling of size 10^5 .

that a low risk subpopulation lies in the age range (0 – 19), approximately 23% of Hong Kong’s population [1]. The assumption $p = 1$ thus overestimates R_0 .

Our sensitivity analysis shows that the transmission rate (β) and the isolation effectiveness in hospitals (l) have the largest effect on \mathcal{R}_0 . The absence of clear policies that would modify β directly means that a significant effort must be (and has been) made, by the medical community, to modify alternative parameters, such as the diagnostic rate. Hence, the strong sensitivity of \mathcal{R}_0 to the transmission rate β indicates that efforts in finding intervention strategies that manage to lower the contact rate of individuals promise an effective means for lowering R_0 . Such strategies include, but are not limited to, the use of face masks (the probability of transmission per contact is reduced), hand washing, and avoiding large crowd gatherings (large public events).

Associated with the role of screening, diagnosis, and the effective isolation of patients is the issue of cost. The value of stringent quarantine measures and the likelihood of compliance combined with the economic impact of lost wages (thousands were quarantined in Taiwan, Hong Kong and Singapore [57]); the costs associated with screening at airports and hospitals; the cost associated with the closure of hospitals; and, the costs associated with the isolation of SARS cases and exposed individuals cannot be ignored or minimized (see appendix for a brief discussion).

2.5 Appendix

Our Monte Carlo sampling of the parameter space provides *globally* averaged measure of the sensitivity of \mathcal{R}_0 to model parameters. Another approach consists in computing sensitivity indices of the model parameters through local derivatives [58]. This approach only provides a *local* measure as the sensitivity indices can change when the parameter values change. Here we use local sensitivity analysis to corroborate our *global* sensitivity analysis and discuss how this approach can be applied in the analysis of resource allocation.

Let λ represent any of the ten nonnegative parameters $\beta, \rho, p, q, k, \gamma_1, \gamma_2, \delta, \alpha$ and l that define the basic reproductive number of our model [51]

$$\mathcal{R}_0 = \{\beta[\rho + p(1 - \rho)]\} \left\{ \frac{q}{k} + \frac{1}{\alpha + \gamma_1 + \delta} + \frac{\alpha l}{(\alpha + \gamma_1 + \delta)(\gamma_2 + \delta)} \right\}. \quad (2.2)$$

If a “small” perturbation $\delta\lambda$ is made to the parameter λ , a corresponding change will occur in \mathcal{R}_0 as $\delta\mathcal{R}_0$, where

$$\begin{aligned} \delta\mathcal{R}_0 &= \mathcal{R}_0(\lambda + \delta\lambda) - \mathcal{R}_0(\lambda) \\ &\approx \delta\lambda \frac{\partial\mathcal{R}_0}{\partial\lambda}. \end{aligned}$$

The normalized sensitivity index Ψ_λ is the ratio of the corresponding normalized changes and is defined as

$$\Psi_\lambda := \frac{\delta\mathcal{R}_0}{\mathcal{R}_0} \Big/ \frac{\delta\lambda}{\lambda} = \frac{\lambda}{\mathcal{R}_0} \frac{\partial\mathcal{R}_0}{\partial\lambda}. \quad (2.3)$$

An approximation of the perturbed value of \mathcal{R}_0 , in terms of the sensitivity index is

$$\mathcal{R}_0(\lambda + \delta\lambda) \approx \left(1 + \frac{\delta\lambda}{\lambda} \Psi_\lambda\right) \mathcal{R}_0(\lambda),$$

where the ten normalized sensitivity indices are

$$\begin{aligned}
\Psi_\beta &= 1 \\
\Psi_\rho &= \frac{\rho(1-p)}{\eta} \\
\Psi_p &= \frac{p(1-\rho)}{\eta} \\
\Psi_q &= \frac{q\beta\eta}{k\mathcal{R}_0} = -\Psi_k \\
\Psi_\alpha &= -\frac{\alpha\beta\eta}{\mathcal{R}_0(\alpha+\gamma_1+\delta)} \left(\frac{\mathcal{R}_0}{\beta\eta} - \frac{q}{k} - \frac{l}{\delta+\gamma_2} \right) \\
\Psi_{\gamma_1} &= -\frac{\gamma_1\beta\eta}{\mathcal{R}_0(\alpha+\gamma_1+\delta)} \left(\frac{\mathcal{R}_0}{\beta\eta} - \frac{q}{k} \right) \\
\Psi_{\gamma_2} &= -\frac{\alpha\beta\eta}{\mathcal{R}_0(\alpha+\gamma_1+\delta)} \frac{l\gamma_2}{(\delta+\gamma_2)^2} \\
\Psi_\delta &= -\frac{\delta\beta\eta}{\mathcal{R}_0(\alpha+\gamma_1+\delta)} \left(\frac{\mathcal{R}_0}{\beta\eta} - \frac{q}{k} + \frac{\alpha l}{(\delta+\gamma_2)^2} \right) \\
\Psi_l &= \frac{\beta\eta}{\mathcal{R}_0(\alpha+\gamma_1+\delta)} \frac{\alpha l}{(\delta+\gamma_2)},
\end{aligned}$$

with $\eta := p(1-\rho) + \rho$ and $\gamma_2 := \alpha\gamma_1/(\alpha - \gamma_1)$. For the values of the parameters used in this model, the sensitivity indices Ψ_β , Ψ_ρ , Ψ_p , Ψ_q and Ψ_l are positive, $\Psi_k = -\Psi_q$ and the remaining indices are negative. Furthermore, since all of the indices (except Ψ_β) are functions of the parameters, the sensitivity indices will change as the parameter values change.

For our specific case where $\beta = .25$, $q = .1$, $p = 1/3$, $k = .15707$, $\alpha = .2061$, $\gamma_1 = .035285$, $\gamma_2 = .0426$, $\delta = .0279$ and $\rho = .77$, and Toronto ($l = .1$) or Hong Kong ($l = .43$) the normalized sensitivity indices are computed. The sensitivity indices and the associated % changes needed to affect a 1% decrease in \mathcal{R}_0 are given in Tables 2.5 and 2.5. Since the effective rate of patient isolation and the average rate of diagnosis provide feasible intervention strategies, we examine how changes to the parameters l and α affect the basic reproductive number (\mathcal{R}_0).

Let us first consider the outbreak in Hong Kong. The value $\alpha = .2061$ means that the mean time to diagnose an infected individual is approximately 4.85 days. The sensitivity index $\Psi_\alpha = -.1933$ means that a 5.2% increase in α , which in turn requires a decrease of 5.7 hours of mean time to diagnosis, would result in a decrease of approximately 1% in \mathcal{R}_0 . Similarly, the sensitivity index $\Psi_l = .5183$ suggests that a 1.9% decrease in the value of l , that is, when l goes from 0.43 to 0.42 (isolation effectiveness*) results in a 1% decrease in \mathcal{R}_0 . In other words, a 5.2% increase in α or a 1.9% decrease in l result in approximately a 1% decrease in \mathcal{R}_0 . For the particular values of the parameters chosen for Hong Kong, the most effective way to reduce \mathcal{R}_0 is to decrease the transmission rate β and the parameter l (improve the effective isolation rate). In the case of Toronto, $\Psi_\alpha = -.4758$ which means that a 2.1% increase in α , results in a 1% decrease in \mathcal{R}_0 . Whereas $\Psi_l = .2001$ means that a 5% decrease in l results in a 1% decrease in \mathcal{R}_0 .

As can be seen from these two examples, the importance or ranking of the sensitivity indices can change as the values of the parameters change. Specifically, the sensitivity indices Ψ_l and Ψ_α satisfy the relationship

$$\|\Psi_l\| < \|\Psi_\alpha\| \iff l < \frac{\delta + \gamma_2}{\alpha + 2\gamma_1 + 2\delta}. \quad (2.4)$$

For the particular values of the parameters given above, Figure (2.5) shows the level curve for the pair (l, α) , where $l(\alpha + 2\gamma_1 + 2\delta) = \delta + \gamma_2$. The particular parameter values are either for Toronto $(l, \alpha) = (.1, .2064)$ or for Hong Kong $(l, \alpha) = (.43, .2064)$. Choosing the parameter values (l, α) below the level curve means that $\|\Psi_l\| < \|\Psi_\alpha\|$ and the converse is true if (l, α) is chosen above the curve. Along the level curve, the magnitude of the sensitivities are equal. Notice

*Recall that $l = 0$ corresponds to complete isolation, whereas $l = 1$ means no effective isolation occurs. Hence, a decrease in l means an increase in the effective isolation of the infected individuals.

that the level curve divides the parameter space into two regions, each of area A_{below} and A_{above} , respectively. Since $A_{\text{above}} \gg A_{\text{below}}$, Ψ_l will be the dominant sensitivity index for randomly chosen (l, α) .

The implementation of an efficient intervention policy must consider the fact that there are limited resources. If one assumes, for example, that the strategies of isolation and diagnosis have associated 1% incremental costs in implementation of δC_I and δC_D , respectively, then a mixed strategy could be formulated that maximizes the effectiveness of a combined intervention. Specifically, if x denotes the magnitude of % decrease in l and y denotes the magnitude of % increase in α and, it is assumed that there is a maximum amount of total additional resources available (δC_T), then the total additional cost of a new mixed isolation and diagnosis intervention policy must satisfy the inequality $\delta C_I x + \delta C_D y \leq \delta C_T$. Since the objective is to maximize the decrease in the reproductive number \mathcal{R}_0 , this means we want to maximize the objective function $P := \|\Psi_l\|x + \|\Psi_\alpha\|y$ under appropriate constraints. In a more general setting, additional nonlinear constraints could be involved, in which case one would need to solve a nonlinear optimization problem. The situation where the cost of diagnosis of infected individuals may be much greater than the cost of isolation or viceversa is certainly of interest.

Table 2.4: Sensitivity Indices for Toronto with $l = 0.1$

Positive Sensitivity Indices		Negative Sensitivity Indices	
$\Psi_\beta = 1$	-1%	$\Psi_\alpha = -.4758$	2.10%
$\Psi_\rho = .6063$	-1.65%	$\Psi_\delta = -.1707$	5.86%
$\Psi_l = .2001$	-4.99%	$\Psi_{\gamma_2} = -.1208$	8.28%
$\Psi_q = .1172$	-8.53%	$\Psi_k = -.1172$	8.53%
$\Psi_p = .0906$	-11.04%	$\Psi_{\gamma_1} = -.1156$	8.65%

Table 2.5: Sensitivity Indices for Hong Kong with $l = .43$

Positive Sensitivity Indices		Negative Sensitivity Indices	
$\Psi_\beta = 1$	-1%	$\Psi_{\gamma_2} = -.3129$	3.19%
$\Psi_\rho = .6063$	-1.65%	$\Psi_\delta = -.3016$	3.32%
$\Psi_l = .5183$	-1.93%	$\Psi_\alpha = -.1933$	5.17%
$\Psi_p = .0906$	-11.04%	$\Psi_{\gamma_1} = -.1216$	8.22%
$\Psi_q = .0706$	-14.16%	$\Psi_k = -.0706$	14.16%

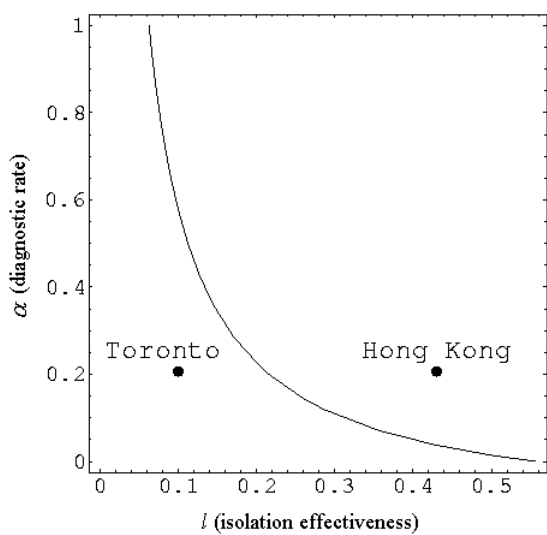


Figure 2.5: Level curve of (l, α) where $l(\alpha + 2\gamma_1 + 2\delta) = \delta + \gamma_2$.

Chapter 3

The Basic Reproductive Number of Ebola and the Effects of Public Health Measures: The Cases of Congo and Uganda *

3.1 Introduction

Ebola hemorrhagic fever is a highly infectious and lethal disease named after a river in the Democratic Republic of the Congo (formerly Zaire) where it was first identified in 1976 [59]. Twelve outbreaks of Ebola have been reported in Congo, Sudan, Gabon, and Uganda as of September 14, 2003 [60, 61]. Two different strains of the Ebola virus (Ebola-Zaire and the Ebola-Sudan) have been reported in those regions. Despite extensive search, the reservoir of the Ebola virus has not yet been identified [62, 63]. Ebola is transmitted by physical contact with body fluids, secretions, tissues or semen from infected persons [59, 64]. Nosocomial transmission has been typical as patients are often treated by unprepared hospital personnel (barrier nursing techniques need to be observed). Individuals exposed to the virus who become infectious do so after a mean incubation period of 6.3 days (1 – 21 days) [2]. Ebola is characterized by initial flu-like symptoms which rapidly progress to vomiting, diarrhea, rash, and internal and external bleeding.

*G. Chowell , N. W. Hengartner, C. Castillo-Chavez, P. W. Fenimore, and J. M. Hyman. The Reproductive Number of Ebola and the Effects of Public Health Measures: The cases of Congo and Uganda, forthcoming in Journal of Theoretical Biology.

Infected individuals receive limited care as no specific treatment or vaccine exists. Most infected persons die within 10 days of their initial infection [65] (50% – 90% mortality [64]).

Using a simple SEIR (susceptible-exposed-infectious-removed) epidemic model (Figure 5.3) and data from two well-documented Ebola outbreaks (Congo 1995 and Uganda 2000), we estimate the number of secondary cases generated by an index case in the absence of control interventions (R_0). Our estimates of R_0 are 1.83 (SD 0.06) for Congo (1995) and 1.34 (SD 0.03) for Uganda (2000). We model the course of the outbreaks via an SEIR epidemic model that includes a smooth transition in the transmission rate after control interventions are put in place. We also perform an uncertainty analysis on the basic reproductive number R_0 to account for its sensitivity to disease-related parameters and analyze the model sensitivity of the final epidemic size to the time at which interventions begin. We provide a distribution for the final epidemic size. A two-week delay in implementing public health measures results in an approximated doubling of the final epidemic size.

3.2 Methods

We fit data from Ebola hemorrhagic fever outbreaks in Congo (1995) and Uganda (2000) to a simple deterministic (continuous time) SEIR epidemic model (Figure 5.3). The least-squares fit of the model provides estimates for the epidemic parameters. The fitted model can then be used to estimate the basic reproductive number R_0 and quantify the impact of intervention measures on the transmission rate of the disease. Interpreting the fitted model as an expected value of a Markov process, we use multiple stochastic realizations of the epidemic to estimate

a distribution for the final epidemic size. We also study the sensitivity of the final epidemic size to the timing of interventions and perform an uncertainty analysis on R_0 to account for the high variability in disease-related parameters in our model.

3.2.1 Epidemic Models

Individuals are assumed to be in one of the following epidemiological states (Figure 5.3): susceptibles (at risk of contracting the disease), exposed (infected but not yet infectious), infectives (capable of transmitting the disease), and removed (those who recover or die from the disease).

Differential Equation Model

Susceptible individuals in class S in contact with the virus enter the exposed class E at the per-capita rate $\beta I/N$, where β is transmission rate per person per day, N is the total effective population size, and I/N is the probability that a contact is made with a infectious individual (i.e. uniform mixing is assumed). Exposed individuals undergo an average incubation period (assumed asymptomatic and uninfected) of $1/k$ days before progressing to the infectious class I . Infectious individuals move to the R -class (death or recovered) at the per-capita rate γ (see Figure 5.3). The above transmission process is modeled by the following system of nonlinear ordinary differential equations [66, 34]:

$$\begin{aligned}
\dot{S}(t) &= -\beta S(t)I(t)/N \\
\dot{E}(t) &= \beta S(t)I(t)/N - kE(t) \\
\dot{I}(t) &= kE(t) - \gamma I(t) \\
\dot{R}(t) &= \gamma I(t) \\
\dot{C}(t) &= kE(t),
\end{aligned} \tag{3.1}$$

where $S(t)$, $E(t)$, $I(t)$, and $R(t)$ denote the number of susceptible, exposed, infectious, and removed individuals at time t (the dot denotes time derivatives). $C(t)$ is not an epidemiological state but serves to keep track of the cumulative number of Ebola cases from the time of onset of symptoms.

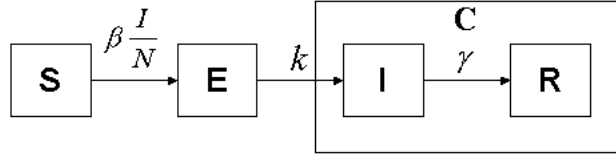


Figure 3.1: A schematic representation of the flow of individuals between epidemiological classes. $\beta \frac{I}{N}$ is the transmission rate to susceptibles S from I ; E is the class of infected (not yet infectious) individuals; k is the rate at which E -individuals move to the symptomatic and infectious class I ; Infectious individuals (I) either die or recover at rate γ . C is not an epidemiological state but keeps track of the cumulative number of cases after the time of onset of symptoms.

Markov Chain Model

The analogous stochastic model (continuous time Markov chain) is constructed by considering three events: *exposure*, *infection* and *removal*. The transition rates are defined as:

Event	Effect	Transition rate
Exposure	$(S, E, I, R) \rightarrow (S-1, E+1, I, R)$	$\beta(t)SI/N$
Infection	$(S, E, I, R) \rightarrow (S, E-1, I+1, R)$	kE
Removal	$(S, E, I, R) \rightarrow (S, E, I-1, R+1)$	γI

The event times $0 < T_1 < T_2 < \dots$ at which an individual moves from one state to another are modeled as a renewal process with increments distributed exponentially,

$$P(T_k - T_{k-1} > t | T_j, j \leq k-1) = e^{-t\mu(T_{k-1})}$$

where $\mu(T_{k-1}) = (\beta(T_{k-1})S(T_{k-1})I(T_{k-1})/N + kE(T_{k-1}) + \gamma I(T_{k-1}))^{-1}$.

The final epidemic size is $Z = C(T)$ where $T = \min\{t > 0, E(t) + I(t) = 0\}$, and its empirical distribution can be computed via Monte Carlo simulations [67].

3.2.2 The Transmission Rate and the Impact of Interventions

The intervention strategies to control the spread of Ebola include surveillance, placement of suspected cases in quarantine for three weeks (the maximum estimated length of the incubation period), education of hospital personnel and community members on the use of strict barrier nursing techniques (i.e protective clothing and equipment, patient management), and the rapid burial or cremation of patients who die from the disease [64]. Their net effect, in our model, is to

reduce the transmission rate β from β_0 to $\beta_1 < \beta_0$. In practice, the impact of the intervention is not instantaneous. Between the time of the onset of the intervention to the time of full compliance, the transmission rate is assumed to decrease gradually from β_0 to β_1 according to

$$\beta(t) = \begin{cases} \beta_0 & t < \tau \\ \beta_1 + (\beta_0 - \beta_1)e^{-q(t-\tau)} & t \geq \tau \end{cases}$$

where τ is the time at which interventions start and q controls the rate of the transition from β_0 to β_1 . One key question is whether the speed at which control measures are implemented might benefit from improvement. As we will see, this seems unlikely. Another interpretation of the parameter q can be given in terms of $t_h = \frac{\ln(2)}{q}$, the time to achieve $\beta(t) = \frac{\beta_0 + \beta_1}{2}$.

3.2.3 Epidemiological data

The data for the Congo (1995) and Uganda (2000) Ebola hemorrhagic fever outbreaks include the identification dates of the causative agent and data sources. The reported data are (t_i, y_i) , $i = 1, \dots, n$ where t_i denotes the i^{th} reporting time and y_i the cumulative number of infectious cases from the beginning of the outbreak to time t_i .

Congo 1995. This outbreak began in the Bandundu region, primarily in Kikwit, located on the banks of the Kwilu River. The first case (January 6) involved a 42-year old male charcoal worker and farmer who died on January 13. The Ebola virus was not identified as the causative agent until May 9. At that time, an international team implemented a control plan that involved active surveillance (identification

of cases) and education programs for infected people and their family members. Family members were visited for up to three weeks (maximum incubation period) after their last identified contact with a probable case. Nosocomial transmission (transmission from patients within hospital settings) occurred in Kikwit General Hospital. Transmission was halted through the institution of strict barrier nursing techniques that included the use of protective equipment and special isolation wards. A total of 315 cases of Ebola were identified (81% case fatality). Daily Ebola cases by date of symptom onset from March 1 through July 12 are available (Figure 4.1) [7].

Uganda 2000. A total of 425 cases (53% case fatality) of Ebola were identified in three districts of Uganda: Gulu, Masindi and Mbarara. The onset of symptoms for the first reported case was on August 30, but the cause was not identified as Ebola until October 15 by the National Institute of Virology in Johannesburg (South Africa). Active surveillance started during the third week of October. A plan that included the voluntary hospitalization of probable cases was then put in place. Suspected cases were closely followed for up to three weeks. Other control measures included community education (avoiding crowd gatherings during burials) and the systematic implementation of protective measures by health care personnel and the use of special isolation wards in hospitals. Weekly Ebola cases by date of symptom onset are available from the WHO (World Health Organization) [8] (from August 20, 2000 through January 7, 2001) (Figure 4.1).

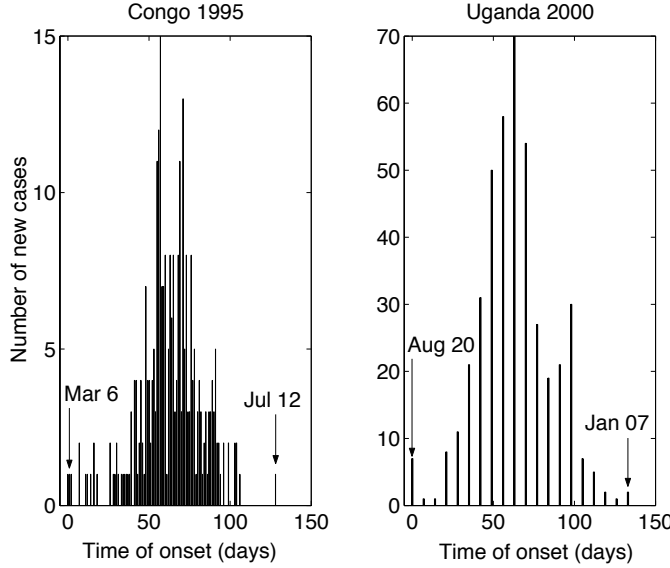


Figure 3.2: On the left, we have the *daily* number of cases by date of symptom onset during the Ebola outbreak in Congo 1995 (Mar 6-Jul 12). On the right, we have the *weekly* number of cases by date of symptom onset during the Ebola outbreak in Uganda 2000 (Aug 20-Jan 07). Data has been taken from refs. [7, 8].

3.2.4 Parameter Estimation

Empirical studies in Congo suggest that the incubation period is less than 21 days with a mean of 6.3 days [2] and the infectious period is between 3.5 and 10.7 days. The model parameters $\Theta = (\beta_0, \beta_1, k, q, \gamma)$ are fitted to the Congo (1995) and Uganda (2000) Ebola outbreak data by *least squares* fit to the cumulative number of cases $C(t, \Theta)$ in eqn. (4.3). We used a computer program (Berkeley Madonna, Berkeley, CA) and appropriate initial conditions for the parameters ($0 < \beta < 1$, $0 < q < 100$, $1 < 1/k < 21$ [2], $3.5 < 1/\gamma < 10.7$ [3]). The optimization process was repeated 10 times (each time the program is fed with two different initial conditions for each parameter) before the “best fit” was chosen. The asymptotic variance-covariance $AV(\hat{\theta})$ of the least-squares estimate is

$$AV(\hat{\theta}) = \sigma^2 \left(\sum_{i=1}^n \nabla C(t_i, \Theta_0) \nabla C(t_i, \Theta_0)^T \right)^{-1}$$

which we estimate by

$$\hat{\sigma}^2 \left(\sum_{i=1}^n \hat{\nabla} C(t_i, \hat{\Theta}) \hat{\nabla} C(t_i, \hat{\Theta})^T \right)^{-1}$$

where n is the total number of observations, $\hat{\sigma}^2 = \frac{1}{n-5} \sum (y_i - C(t_i, \hat{\Theta}))^2$ and $\hat{\nabla} C$ are numerical derivatives of C .

For small samples, the confidence intervals based on these variance estimates may not have the nominal coverage probability. For example, for the case of Zaire 1995, the 95% confidence interval for q based on asymptotic normality is $(-0.26, 2.22)$. It should be obvious that this interval is not “sharp” as it covers negative values whereas we know $q \geq 0$. The likelihood ratio provides an attractive alternative to build confidence sets (Figure 3.3). Formally, these sets are of the form

$$\left\{ \Theta : \frac{\sum (y_i - C(t_i, \Theta))^2}{\sum (y_i - C(t_i, \hat{\Theta}))^2} \leq A_\alpha \right\}$$

where A_α is the $1 - \alpha$ quantile of an F distribution with appropriate degrees of freedom. Parameter estimates are given in Table 3.1.

3.2.5 The Reproductive Number

The basic reproductive number R_0 measures the average number of secondary cases generated by a primary case in a pool of mostly susceptible individuals [66, 34] and

Table 3.1: Parameter definitions and baseline estimates (time is given in days) obtained from the best fit of the model equations (4.3) to the epidemic-curve data of the Congo 1995 and Uganda 2000 outbreaks (Figure 3.5). The parameters were optimized by a computer program (Berkeley Madonna, Berkeley, CA) using a *least squares* fitting technique and appropriate initial conditions for the parameters ($0 < \beta < 1$, $0 < q < 100$, $1 < 1/k < 21$ [2], $3.5 < 1/\gamma < 10.7$ [3]). The optimization process was repeated 10 times (each time the program is fed with two different initial conditions for each parameter) before the “best fit” was chosen.

Param.	Definition	Congo 1995		Uganda 2000	
		Estim.	S. D.	Estim.	S. D.
β_0	Pre-interven. transm. rate	0.33	0.06	0.38	0.24
β_1	Post-interven. transm. rate	0.09	0.01	0.19	0.13
t_h	Time to achieve $\frac{\beta_0+\beta_1}{2}$	0.71	(0.02, 1.39) [†]	0.11	(0, 0.87) [†]
$1/k$	Mean incubation period	5.30	0.23	3.35	0.49
$1/\gamma$	Mean infectious period	5.61	0.19	3.50	0.67

is an estimate of the epidemic growth at the start of an outbreak if everyone is susceptible. That is, a primary case generates $R_0 = \frac{\beta_0}{\gamma}$ new cases on the average where β_0 is the pre-interventions transmission rate and $1/\gamma$ is the mean infectious period.

The effective reproductive number at time t , $R_{eff}(t) = \frac{\beta(t)}{\gamma}x(t)$, measures the average number of secondary cases per infectious case t time units after the introduction of the initial infections and $x(t) = \frac{S(t)}{N} \approx 1$ as the population size is much larger than the resulting size of the outbreak (Table 3.2). Hence, $R_{eff}(0) = R_0$. In a closed population, the effective reproductive number $R_{eff}(t)$ is non-increasing as the size of the susceptible population decreases. The case $R_{eff}(t) \leq 1$ is of special interest as it highlights the crossing of the threshold to eventual control of the outbreak. An intervention is judged successful if it reduces the effective reproductive number to a value less than one. In our model, the post-intervention

reproductive number $R_p = \frac{\beta_1}{\gamma}$ where β_1 denotes the post-intervention transmission rate. In general, the smaller β_1 , the faster an outbreak is extinguished. By the delta method [68], the variance of the estimated basic reproductive number \hat{R}_0 is approximately

$$V(\hat{R}_0) \approx \hat{R}_0^{-2} \left\{ \frac{V(\hat{\beta}_0)}{\hat{\beta}_0^2} + \frac{V(\hat{\gamma})}{\hat{\gamma}^2} - \frac{2Cov(\hat{\beta}_0, \hat{\gamma})}{\hat{\beta}_0 \hat{\gamma}} \right\}.$$

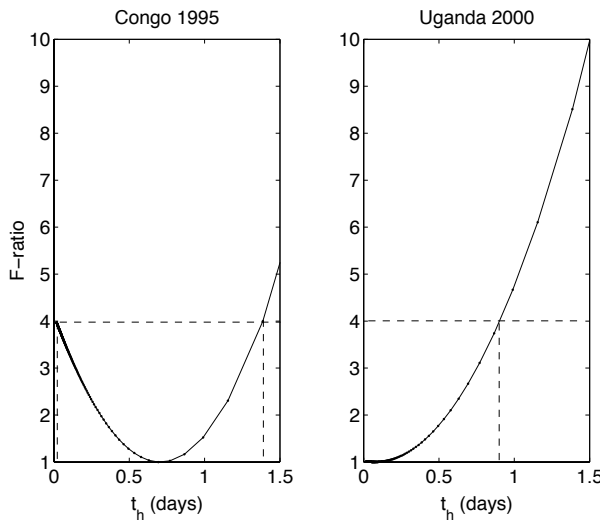


Figure 3.3: 95% confidence intervals for t_h ($t_h = \frac{\log(2)}{q}$), the time to achieve a transmission rate of $\frac{\beta_0 + \beta_1}{2}$, obtained from the likelihood ratio as described in the text.

3.2.6 The Effective Population Size

A rough estimate of the population size in the Bandundu region of Congo (where the epidemic developed) in 1995 is computed from the population size of the Bandundu region in 1984 [69] and annual population growth rates [70] (Table 3.2). For the case of Uganda (2000), we adjusted the population sizes of the districts of Gulu,

Masindi and Mbara in 1991 and annual population growth rates [71] (Table 3.2). These estimates are an upper bound of the effective population size (those at risk of becoming infected) for each region. Estimates of the effective population size are essential when the incidence is modeled with the pseudo mass-action assumption ($\beta(t)SI$) which implies that transmission grows linearly with the population size and hence the basic reproductive number $R_0(N) = \beta_0 N / \gamma$. In our model, we use the true mass-action assumption ($\beta(t)SI/N$) which makes the model parameters (homogeneous system of order 1) independent of N and hence the basic reproductive number can be estimated by $R_0 = \beta_0 / \gamma$ [72]. In fact, comparisons between the pseudo mass-action and the true mass-action assumptions with experimental data have concluded in favor of the later [73]. The model assumption that N is constant is not critical as the outbreaks resulted in a small number of cases compared to the size of the population.

Table 3.2: Population parameters and estimated R_0 for the Congo 1995 and the Uganda 2000 Ebola outbreaks. Notice that even though our expression for R_0 is independent of N , our model is not independent of N and hence the corresponding population sizes for Congo and Uganda are used in the least-squares estimation of the parameters.

Outbreak	Eff. Pop. (N)	Start of interv.	Fatal. rate (%)	R_0	S.D. R_0
Congo 1995	5,364,500*	May 9, 1995 [7]	81% [7]	1.83	0.06
Uganda 2000	1,867,200 †	Oct 22, 2000 [8]	53% [8]	1.34	0.03

†95 % CI (Figure 3.3).

*Adjusted from population size of the Bandundu region in 1984 [69] using the annual population growth rates [70].

¶Adjusted from the population sizes of the districts of Gulu, Masindi and Mbara (where the outbreak developed) in 1991 using the annual population growth rates [71].

3.2.7 Uncertainty Analysis on R_0

Log-normal distributions seem to model well the incubation period distributions for a large number of diseases [74]. Here, a log-normal distribution is assumed for the incubation period of Ebola in our uncertainty analysis. Log-normal distribution parameters are set from empirical observations (mean incubation period is 6.3 and the 95% quantile is 21 days [2]). The infectious period is assumed to be uniformly distributed in the range (3.5 – 10.7) days [3].

A formula for the basic reproductive number R_0 that depends on the initial per-capita rate of growth r in the number of cases (Figure 3.4), the incubation period ($1/k$) and the infectious period ($1/\gamma$) can be obtained by linearizing equations \dot{E} and \dot{I} of system (4.3) around the disease-free equilibrium with $S = N$. The corresponding Jacobian matrix is given by:

$$J = \begin{pmatrix} -k & \beta \\ k & -\gamma \end{pmatrix},$$

and the characteristic equation is given by:

$$r^2 + (k + \gamma)r + (\gamma - \beta)k = 0$$

where the early-time and per-capita free growth r is essentially the dominant eigenvalue. By solving for β in terms of r , k and γ , one can obtain the following expression for R_0 using the fact that $R_0 = \beta/\gamma$:

$$R_0 = 1 + \frac{r^2 + (k + \gamma)r}{k\gamma}.$$

Our estimate of the initial rate of growth r for the Congo 1995 epidemic is $r = 0.07$

day^{-1} , obtained from the time series $y(t)$, $t < \tau$ of the cumulative number of cases and assuming exponential growth ($y(t) \propto e^{rt}$). The distribution of R_0 (Figure 3.4) lies in the interquartile range (IQR) (1.66 – 2.28) with a median of 1.89, generated from Monte Carlo sampling of size 10^5 from the distributed epidemic parameters ($1/k$ and $1/\gamma$) for fixed r [54]. We give the median of R_0 (not the mean) as the resulting distribution of R_0 from our uncertainty analysis is skewed to the right.

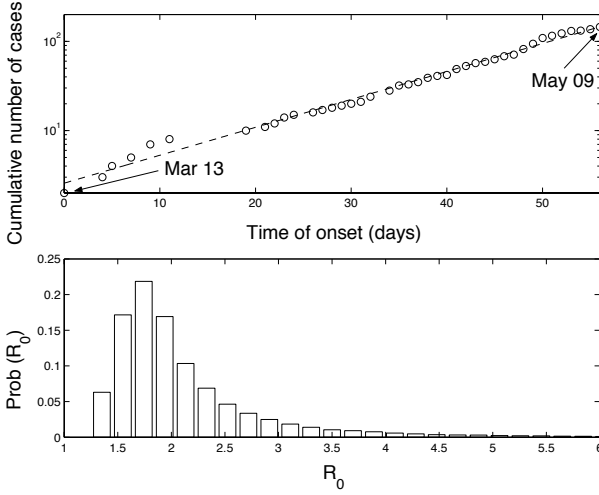


Figure 3.4: (Top) cumulative number of cases (log-lin scale) during the exponential growth phase of the Congo 1995 epidemic as identified by the date of start of interventions (09 May 1995 [7]). The model-free initial growth rate of the number of cases for Congo 1995 is 0.07 (linear regression); (bottom) estimated distribution of R_0 from our uncertainty analysis (see text). R_0 lies in the interquartile range (IQR) (1.66 – 2.28) with a median of 1.89. Notice that 100% of the weight lies above $R_0 = 1$.

3.3 Results

Using our parameter estimates (Table 3.1), we estimate an R_0 of 1.83 (SD 0.06) for Congo (1995) and 1.34 (SD 0.03) for Uganda (2000). The effectiveness of interventions is often quantified in terms of the reproductive number R_p after interventions are put in place. For the case of Congo $R_p = 0.51$ (SD 0.04) and $R_p = 0.66$ (SD

0.02) for Uganda allowing us to conclude that in both cases, the intervention was successful in controlling the epidemic. Furthermore, the time to achieve a transmission rate of $\frac{\beta_0 + \beta_1}{2}$ (t_h) is 0.71 (95% CI (0.02, 1.39)) days and 0.11 (95% CI (0, 0.87)) days for the cases of Congo and Uganda respectively after the time at which interventions begin.

We use the estimated parameters to simulate the Ebola outbreaks in Congo (1995) and Uganda (2000) via Monte Carlo simulations of the stochastic model of Section 2.1 [67]. There is very good agreement between the mean of the stochastic simulations and the reported cases despite the “wiggle” captured in the residuals around the time τ of the start of interventions (Figure 3.5). The empirical distribution of the final epidemic sizes for the cases of Congo 1995 and Uganda 2000 are given in Figure 3.6.

The final epidemic size is sensitive to the start time of interventions τ . Numerical solutions (deterministic model) show that the final epidemic size grows exponentially fast with the initial time of interventions (not surprising as the intial epidemic growth is driven by exponential dynamics). For instance, for the case of Congo, our model predicts that there would have been 20 more cases if interventions had started one day later (Figure 4.7).

3.4 Discussion

Using epidemic-curve data from two major Ebola hemorrhagic fever outbreaks [7, 8], we have estimated the basic reproductive number (R_0) (Table 3.2). Our estimate of R_0 (median is 1.89) obtained from an uncertainty analysis [54] by simple random sampling (Figure 3.4) of the parameters k and γ distributed according to empirical data from the Zaire (now the Democratic Republic of Congo) 1976 Ebola

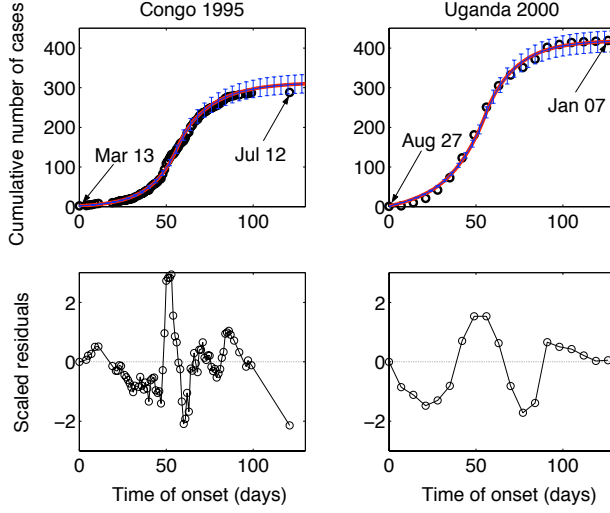


Figure 3.5: (Top) Comparison of the cumulative number of Ebola cases during the Congo 1995 and Uganda 2000 Ebola outbreaks, as a function of the time of onset of symptoms. Black circles are data. The solid line is the average of 250 Monte Carlo replicates and the error bars represent the standard error around the mean from the simulation replicates using our parameter estimates (Table 3.1). For the case of Congo 1995, simulations were begun on 13 Mar 1995. A reduction in the transmission rate β due to the implementation of interventions occurs on 09 May 1995 (day 56) [7]. For the case of Uganda 2000, simulations start on 27 August 2000 and interventions take place on 22 October 2000 (day 56) [8]; (bottom) comparison of the residuals (difference between the data and the model best fit) scaled by the standard deviation for the cases of Congo and Uganda.

outbreak [2, 3] is in agreement with our estimate of $R_0 = 1.83$ from the outbreak in Congo 1995 (obtained from least squares fitting of our model (4.3) to epidemic curve data).

The difference in the basic reproductive numbers R_0 between Congo and Uganda is due to our different estimates for the infectious period ($1/\gamma$) observed in these two places. Their transmission rates β_0 are quite similar (Table 3.1). Our estimate for the infectious period for the case of Congo (5.61 days) is slightly larger than that of Uganda (3.50 days). Clearly, a larger infectious period increases the likelihood of infecting a susceptible individual and hence increases the basic reproductive num-

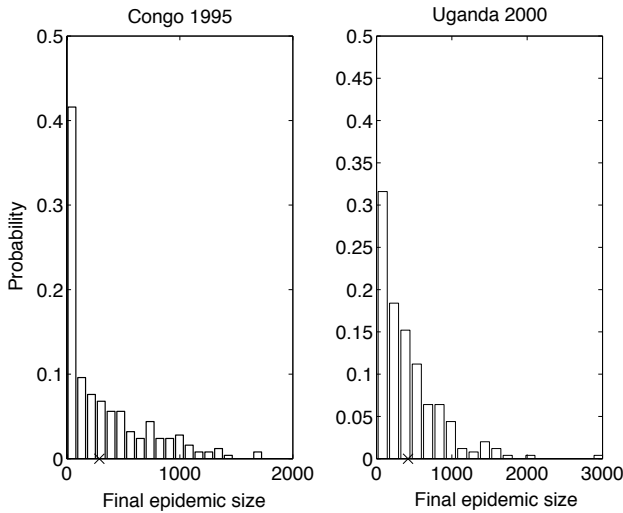


Figure 3.6: The final epidemic size distributions for the cases of Congo 1995 and Uganda 2000 obtained from 250 Monte Carlo replicas. Crosses (X) represent the final epidemic size from data.

ber. The difference in the infectious periods might be due to differences in virus subtypes [75]. The Congo outbreak was caused by the Ebola-Zaire virus subtype [7] while the Uganda outbreak was caused by the Ebola-Sudan virus subtype [8]. The significant reduction from the basic reproductive number (R_0) to the post-intervention reproductive number (R_p) in our estimates for Congo and Uganda shows that the implementation of control measures such as education, contact tracing and quarantine will have a significant effect on lowering the effective reproductive rate of Ebola. Furthermore, estimates for the time to achieve $\frac{\beta_0+\beta_1}{2}$ have been provided (Table 3.1).

We have explored the sensitivity of the final epidemic size to the starting time of interventions. The exponential increase of the final epidemic size with the time of start of interventions (Figure 4.7) supports the idea that the rapid implementation of control measures should be considered as a critical component in any contingency plan against disease outbreaks specially for those like Ebola and SARS for

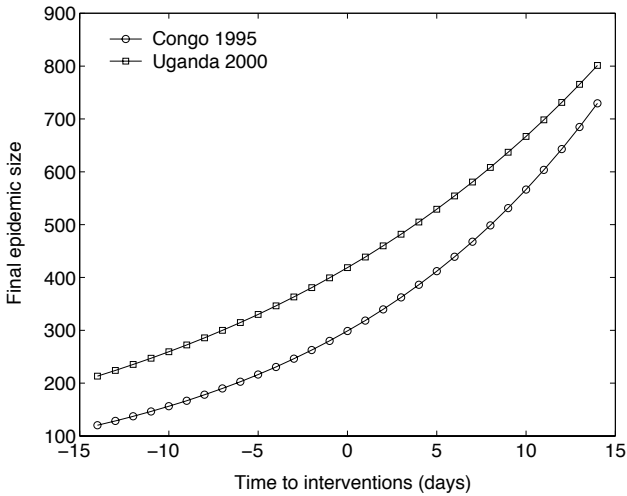


Figure 3.7: Sensitivity of the final epidemic size to the time of start of interventions. Here negative numbers represent number of days before the actual reported intervention date (Table 3.2) and positive numbers represent a delay after the actual reported intervention date ($\tau = 0$). All other parameters have been fixed to their baseline values (Table 3.2). The final epidemic size grows exponentially as expected with the time of interventions with a rate of 0.06 for the case of Congo and 0.05 for the case of Uganda.

which no specific treatment or vaccine exists. A two-week delay in implementing public health measures results in an approximated doubling of the final outbreak size. Moreover, because the existing control measures cut the transmission rate to less than half, we should seek and support further improvement in the effectiveness of interventions for Ebola. A mathematical model that considers basic public health interventions for SARS control in Toronto supports this conclusion [51, 76]. Simulation results show that small perturbations on the rate q at which interventions are put fully in place do not have a significant effect on the final epidemic size. The rapid identification of an outbreak, of course, remains the strongest determinant of the final outbreak size.

Field studies of Ebola virus are difficult to conduct due to the high risk imposed on the scientific and medical personnel [77]. Recently, a new vaccine that makes

use of an *adenovirus technology* has been shown to give cynomolgus macaques protection within 4 weeks of a single jab [78, 79]. If the vaccine turns out to be effective in humans, then its value should be tested. A key question would be “What are the conditions for a successful target vaccination campaign during an Ebola outbreak?” To address questions of this type elaborate models need to be developed.

Chapter 4

Modeling the 2001 Foot-and-Mouth Epidemic in Uruguay using Geo-referenced Data

4.1 Introduction

Foot and mouth disease (FMD) is a highly infectious illness caused by an aphthovirus that affects cloven-hoofed animals such as pigs, cattle, and sheep. Infected animals shed large amounts of the virus through the mouth and nose. Viral particles can survive in objects such as shoes, clothes, or vehicle tires. The wind can carry the virus long distances [80]. Typically one outbreak will not reoccur in one region for a long time. For instance, Japan had been FMD free for 92 years until an outbreak was confirmed in 2000 [81] and Great Britain was FMD free for 33 years before the recent epidemic in 2001 [82].

The power of an infectious disease to cause an epidemic depends on several factors including the epidemiology of the disease in question, the susceptibility of the landscape where the infectious agent is introduced and the timely response and effectiveness of interventions. The basic reproductive number, R_0 , is the number of secondary cases generated by a primary case when this is introduced in a population of fully susceptible individuals [66, 34]. That is, R_0 measures the power of a disease to spread under a scenario that facilitates maximal growth (beginning of epidemic). Once an epidemic starts, the number of livestock decreases and

control measures are implemented causing the reproductive number $R(t)$ (where $R(0) = R_0$) to decay. The objective of any contingency plan is to make $R(t) < 1$ as soon as possible.

Transmission of FMD can be localized (between adjacent farms [83, 84, 85]). Long distance transmission through daily milk collection, meat transportation, animal movement, etc. are also possible. Hence, invalid predictions about the epidemic could result from ignoring an appropriate spatial component [86, 87]. A movie of the FMD epidemic in Uruguay in 2001 [88] shows the spatial spread of FMD. The movie illustrates the importance of including a topology of transmission when modeling FMD epidemics. Such topology of transmission may include the distance among farms and the road network.

At least 4 million animals were destroyed during the 2001 FMD epidemic in Great Britain. The catastrophic economic consequences linked to FMD epidemics make FMD of great concern to governments. Once an epidemic is put under control, the exportation of animal goods is not permitted for a period of 6-12 months post outbreak [80]. Hence, governments frequently revise FMD control policy. The value of selected FMD control policies depends strongly on available data and the “tools” (models) used to test the policies. For example, during the 2001 FMD epidemic in Great Britain, two teams of researchers developed highly refined models to aid in the decision-making process [83, 84]. Both teams concluded that a culling policy was the best strategy to control the ongoing FMD epidemic. Their conclusions relied on data that included the location of farms, farm animal density and animal heterogeneity within farms. Longitudinal data on the number of farms infected and the culling process was available [80].

4.1.1 The 2001 Foot-and-Mouth Epidemic in Uruguay

The first case of the 2001 Foot-and-Mouth Disease (FMD) epidemic in Uruguay was reported in the state of Soriano close to the border with Argentina on April 23rd [89, 90]. In just a few days, the epidemic had disseminated over the whole country. The epidemic reached its peak incidence of 66 new cases on May 25th and 1763 cases were reported by July 10th, 2001 (Figure 4.1). From April 25 to April 29 slaughter was implemented (total: 5,295 cattle; 1,481 sheep; 332 pigs) and animal movement restrictions enforced by the police and the army were implemented on April 27. However, people movement was never banned (farm personnel continued to come in and out during the roadblock period). Other control measures included an awareness campaign to farmers via press release and personal visits by veterinarians to farms. Controls were implemented in borders, airports and harbours [90]. Mass vaccination (60 – 70% expected efficacy) started on May 5 with May 28 as the expected completion date (peak protective levels of the serum antibodies may take up to 14-28 days depending on the vaccine composition). No high potency vaccines (where the protective immunity is reached within 3-4 days [91]) were used. The vaccination program did not include calves younger than 3 months, pigs or goats. Vaccines were delivered to county/district veterinarians. Farmers picked them up and administered them to their own herds. The second round of mass vaccination (booster vaccination with expected 100% efficacy) started on June 15 and was completed on July 22. The fact that this was an infection introduced into a region where previously it was known to be absent (exotic disease) and the fact that geo-referenced data exist about its epidemic, the 2001

FMD epidemic in Uruguay provides an excellent test bed for the evaluation of a geo-deterministic model.

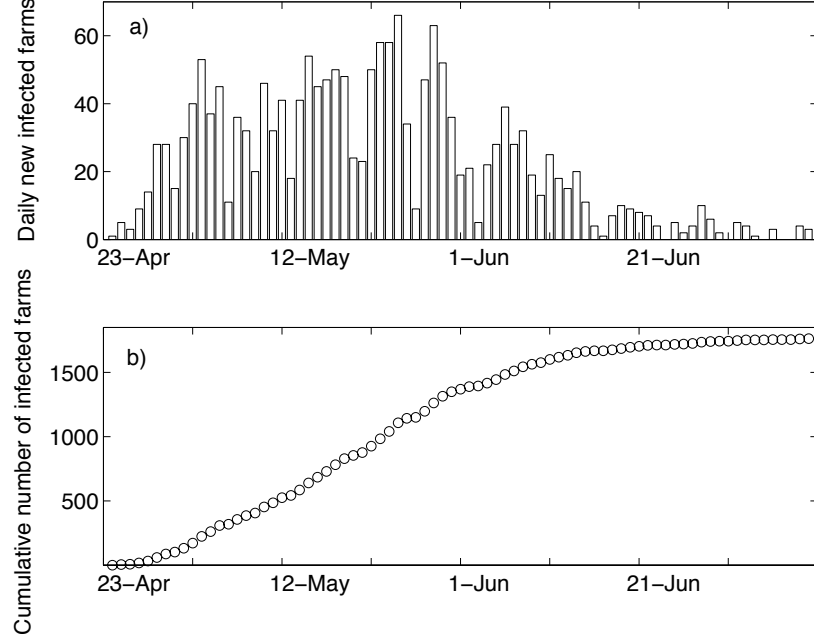


Figure 4.1: a) Daily and b) cumulative number of reported infected farms during the 2001 Foot and Mouth Disease in Uruguay. The epidemic reached its maximum of 66 cases on day 33 (25 May 2001). 1763 cases had been reported by day 79 (10 July 2001). Data has been taken from refs. [9, 10, 11]. The periodic dips in the data are due to low reporting rates on the weekends.

It has been recently shown experimentally in pigs and cattle that the rate of spread, the incubation period, and the severity of disease depend on the dose received, the route of introduction, the animal species and husbandry conditions [92]. These factors are not independent. For example, the dose received is correlated to the length of the incubation period. The FMD virus is excreted up to 11 days once symptoms appear [93]. The incubation period for FMD has been reported to be between 3 – 6 days with a maximum of 14 days [94, 95, 96]. A recent experimental study in cattle reports the presence of viral RNA (mouth and nasal swabs) in all

infected cattle within 24 h post infection and peak levels were reached 1 – 2.5 days post infection. In some animals viral RNA was not detected until 7 – 18 days post infection [97]. Latent animals progress to an infectious state that lasts for about 8 days. Animals are asymptomatic during the first 5 days of the infectious period [83]. The remaining 3 – 5 days (symptomatic and infectious) [97] is the time that it takes on average to detect and remove/isolate the infected animals from the rest. Most animals recover with reduced weight gain or milk yield [84] .

In this article, we model the 2001 FMD epidemic in Uruguay using a spatial deterministic epidemic model that includes geo-referenced data (i.e. euclidean distances between farms, as estimated in relation to distances between county centroides). Our spatial model is validated by means of a non-spatial model. We estimate epidemiological and control parameters via least-squares fitting. We then compute the internal (within counties) and external (across counties) reproductive numbers before and after interventions were implemented. We also explore the expected impact of a mass vaccination policy depending on when (how early/late) it is implemented after an epidemic starts.

4.2 Materials and Methods

The data used in this study includes the inter-county distances (i.e. euclidean distances between farms, as estimated in relation to distances between county centroides) as a measure of the connectivity between counties, the times at which different control strategies were implemented, and epidemic-curve data on the number of cases reported over time identified by counties obtained from geo-referenced

case reports.

We first introduce a non-spatial deterministic model with and without interventions. We use this model to validate our deterministic model under spatial considerations before and after interventions. We classify the number of secondary cases generated by a primary case during its entire period of infectiousness as *internal* and *external*. Internal secondary cases are generated within counties and external secondary cases are generated across counties. Since interventions are not expected to be implemented from the beginning of the epidemic, control model parameters are time dependent which we estimate by least-squares fitting techniques. Standard deviations for each of the estimated parameters are also provided which can be used to construct confidence intervals.

4.2.1 Data

We grouped the 19 Uruguayan states into three contiguous regions (Region I, II and III) in the map of Uruguay (Figure 4.2 b). Table 4.1 shows the distribution of the number of counties per state and the mean density of farms per county in each Uruguayan state. Figure 4.3 shows the distribution of all the inter-county distances. Using geo-referenced case reports obtained from public records of the Uruguayan Ministry of Livestock, Agriculture, and Fisheries (MGAP), the Pan-american Health Organization, and the World Organization for Animal Health (OIE) [9, 10, 11], we generate a table of the number of daily new reported infected farms during the first 79 days of the epidemic. That is, a table of the form (t_i, x_i) , $i = 1, \dots, 1763$ where t_i denotes the time and x_i the location of the i^{th} reporting infected farm. Each infected farm can be associated geographically to a region,

state, and county. Table 4.2 shows that the focus of the epidemic was in region I where the epidemic started (57% of total infected farms) which includes states of Soriano (26%), Colonia (21%) and Rio Negro (10%).

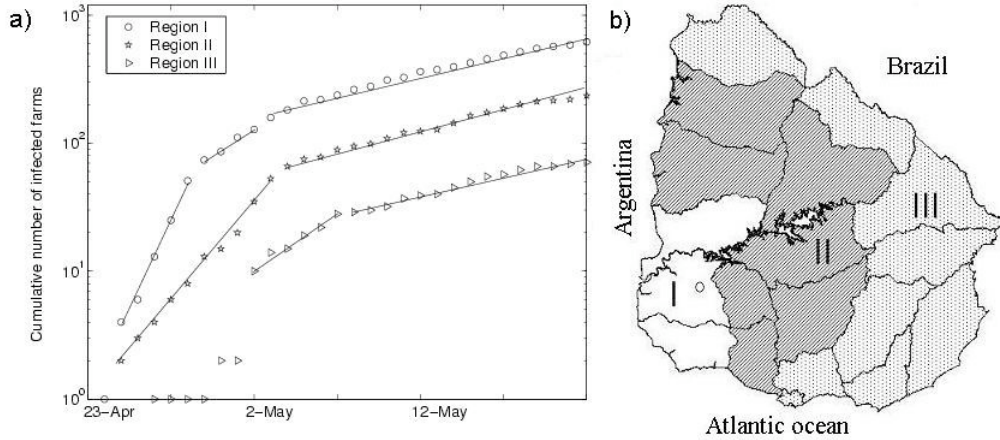


Figure 4.2: a) The initial intrinsic growth rate r in Region I, II and III are 0.65, 0.35, and 0.19 respectively ; b) Region I, II and III comprise 3, 7 and 8 Uruguayan states respectively (see Table 4.2). We estimate the intrinsic growth rate in region III using the cumulative number of cases from 02 May to 07 May 2001 due to underreporting of number of cases before 02 May 2001. The intrinsic growth rate after 07 May 2001 is approximately the same in the three regions once movement restrictions and some depletion in the number of susceptible farms had taken place. Mass vaccination started on 05 May 2001.

4.2.2 Non-spatial Epidemic Model

Susceptible farms (class S) in contact with the virus enter the latent class L at the rate $\hat{\beta}I/N$, where $\hat{\beta}_0$ is transmission rate per day, N is the total number of farms, and I/N is the probability that a contact is made with a infectious farm (i.e. uniform mixing). Latent farms progress to the infectious state after a mean time of $1/\hat{k}$ days and stay there for a mean time of $1/\hat{\alpha}_0$ days until these are properly “removed/isolated” from the rest (class J). The above transmission process is modeled by the following system of nonlinear ordinary differential equations [66, 34, 98]:

Table 4.1: Distribution of the number of counties per state and the average number of farms per county (N_j).

Region I			Region II			Region III		
State	Count.	N_j	State	Count.	N_j	State	Count.	N_j
Soriano	12	140	Paysan.	13	121	Artigas	12	118
Colonia	18	151	Salto	16	111	Rivera	10	206
Rio Negro	13	71	S. Jose	10	243	C. Largo	14	196
			Flores	9	91	Lavalleja	14	235
			Florida	16	152	Rocha	12	190
			Tacuar.	16	7	T. y Tres	11	163
			Durazno	15	136	Maldon.	13	136
						Canelones	27	141

$$\begin{aligned}
 \dot{S}(t) &= -\hat{\beta}_0 S(t)I(t)/N \\
 \dot{L}(t) &= \hat{\beta}_0 S(t)I(t)/N - \hat{k}L(t) \\
 \dot{I}(t) &= \hat{k}L(t) - \hat{\alpha}_0 I(t) \\
 \dot{J}(t) &= \hat{\alpha}_0 I(t)
 \end{aligned} \tag{4.1}$$

where $S(t)$, $L(t)$, $I(t)$, and $J(t)$ denote the number of susceptible, exposed, infectious, and removed/isolated farms at time t (the dot denotes rate of change with respect to time). The basic reproductive number \hat{R}_0 for this model is the product of the transmission rate and the period of infectiousness:

$$\hat{R}_0 = \hat{\beta}_0/\hat{\alpha}_0.$$

Table 4.2: Distribution of the total number of infected farms among the different Uruguayan states within each defined contiguous region.

Region I			Region II			Region III		
State	Inf.	Tot.	State	Inf.	Tot.	State	Inf.	Tot.
Soriano	463	1682	Paysan.	64	1567	Artigas	34	1421
	362	2724	Salto	56	1783	Rivera	14	2064
	Rio Negro	925	S. Jose	68	2430	C. Largo	26	2744
			Flores	62	816	Lavalleja	15	3296
			Florida	109	2436	Rocha	12	2284
			Tacuar.	111	2427	T. y Tres	59	1797
			Durazno	92	2043	Maldon.	12	1773
						Canelones	25	3800
Overall Tot.	1003	5331		562	13502		198	19179

4.2.3 Non-spatial Epidemic Model with Interventions

Our non-spatial model with interventions is given by the system of nonlinear ordinary differential equations:

$$\begin{aligned}
 \dot{S}(t) &= -\hat{\beta}(t)S(t)I(t)/N - \hat{\nu}S \\
 \dot{V}(t) &= \hat{\nu}S - \hat{\beta}(t)V(t)I(t)/N - \hat{\mu}V \\
 \dot{L}(t) &= \hat{\beta}(t)(S(t) + V(t))I(t)/N - \hat{k}L(t) \\
 \dot{I}(t) &= \hat{k}L(t) - \hat{\alpha}I(t) \\
 \dot{J}(t) &= \hat{\alpha}I(t) \\
 \dot{P}(t) &= \hat{\mu}V(t)
 \end{aligned} \tag{4.2}$$

Here V is the class of vaccinated but not yet protected farms. The farms in

V are not fully protected since it takes a few days before vaccinated farms reach protective levels. As the farms in V become fully protected, they enter the protected class P . Susceptible farms are vaccinated at rate $\hat{\nu}$ and vaccinated farms in class P reach protective levels at rate $\hat{\mu}$. The parameters $\beta(t)$, $\alpha(t)$, $\nu(t)$, and $\mu(t)$ depend on time since control measures cannot be implemented simultaneously but rather at different times during the epidemic.

$$\beta(t) = \begin{cases} \hat{\beta}_0 & t < \tau_m \\ \hat{\beta} & t \geq \tau_m \end{cases}$$

$$\alpha(t) = \begin{cases} \hat{\alpha}_0 & t < \tau_v \\ \hat{\alpha} & t \geq \tau_v \end{cases}$$

$$\nu(t) = \begin{cases} 0 & t < \tau_v \\ \hat{\nu} & t \geq \tau_v \end{cases}$$

$$\mu(t) = \begin{cases} 0 & t < \tau_v \\ \hat{\mu} & t \geq \tau_v \end{cases}$$

Here τ_m (27 April 2001) is the time at which movement restrictions were put in place and τ_v (05 May 2001) is the time at which mass vaccination started.

4.2.4 Spatial Epidemic Model

We model the FMD epidemic at the level of farms or premises aggregated at the level of counties (Table 4.1). We classify farms as susceptible (S), latent (L), infectious and undetected (I), and detected and removed (J). A susceptible farm

in county i in contact with the virus enters the latent (uninfectious and asymptomatic) class (L) at rate $\sum_{j=1}^n \beta_{ij} I_j$ that includes the influence from all the infected farms in all counties j where the transmission rate β_{ij} between farms in counties i and j decays exponentially fast with the euclidean distance of their respective county centroids. Hence, the transmission rate β_{ij} between farms in counties i and j (mixing matrix [99]) can be expressed as:

$$\beta_{ij} = \beta_0 e^{-qd_{i,j}}$$

where β_0 is the average transmission rate of infectious farms within each county, d_{ij} is the distance between counties i and j (i.e. euclidean distances between farms, as estimated in relation to distances between county centroids, Figure 4.3), and q quantifies the extent of local spread (or $1/q$ can be interpreted as the FMD mean transmission range). Latent farms progress to the infectious state after a mean time of $1/k$ days and the infectious farms are detected and isolated from the rest at rate α . The spatial transmission dynamics of Foot-and-Mouth Disease can be modeled by the system of nonlinear ordinary differential equations:

$$\begin{aligned}\dot{S}_i &= -S_i \sum_{j=1}^n \beta_{ij} I_j \\ \dot{L}_i &= S_i \sum_{j=1}^n \beta_{ij} I_j - k L_i \\ \dot{I}_i &= k L_i - \alpha I_i \\ \dot{J}_i &= \alpha I_i\end{aligned}\tag{4.3}$$

The dot denotes time derivatives where S_i , L_i , I_i , and J_i denote the number of susceptible, latent, infectious, and removed/isolated farms in each county i ($i = 1, 2, \dots, n$). The distribution of the number of farms in the different counties is

given in Table 4.1. Our spatially dependent transmission rate β_{ij} is analogous to the patch connectivity index in the context of metapopulation dynamics [100, 101] where d_{ij} could be some measure of the influence of the landscape on migration [102]. d_{ij} could be used as an “index” that could incorporate wind direction and animal heterogeneity within farms (dairy, beef, etc.). Here, we assume that the county connectivity d_{ij} is well approximated by the distance between counties.

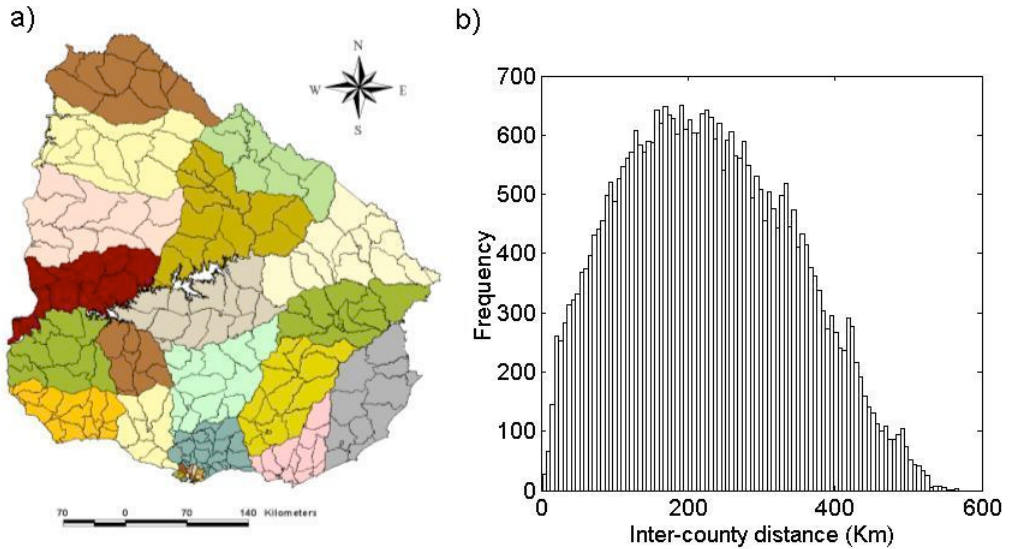


Figure 4.3: a) Map of Uruguay with state (color) and county divisions; b) distribution of inter-county (euclidean) distances which were obtained using a geographic information system (GIS). The centroide of each county is used to compute euclidean distances.

The Basic Reproductive Number R_0

Unfortunately, we do not know an analytical expression for R_0 for our multi-county model (4.3). However, we can estimate the basic reproductive number using model parameter estimates [103].

We define the *internal* (within counties) basic reproductive number of county i , R_{0i}^{in} , as the number of secondary cases generated by a primary case in county

i within the same county and is given by $R_{0i}^{in} = \beta_0 N_i / \alpha$. Similarly, we define the *external* (across counties) basic reproductive number of county i , R_{0i}^{out} , as the number of secondary cases generated by a primary case in county i in any other county j where $j \neq i$ and is given by $R_{0i}^{out} = \sum_{j \neq i}^n \beta_0 N_j e^{-qd_{ij}} / \alpha$.

4.2.5 Spatial Epidemic Model with Interventions

Our model with interventions is given by the system of nonlinear ordinary differential equations:

$$\begin{aligned}\dot{S}_i &= -S_i(t) \sum_{j=1}^n \beta_{ij}(t) I_j(t) - \nu(t) S_i(t) \\ \dot{V}_i &= \nu(t) S_i(t) - V_i(t) \sum_{j=1}^n \beta_{ij}(t) I_j(t) - \mu(t) V_i(t) \\ \dot{L}_i &= (S_i(t) + V_i(t)) \sum_{j=1}^n \beta_{ij}(t) I_j(t) - k(t) L_i(t) \\ \dot{I}_i &= k(t) L_i(t) - \alpha(t) I_i(t) \\ \dot{J}_i &= \alpha(t) I_i(t) \\ \dot{P}_i &= \mu(t) V_i(t)\end{aligned}\tag{4.4}$$

where susceptible farms in county i (S_i) are vaccinated at rate ν (V_i). Vaccinated farms in V_i enter the protected class P_i at rate μ . The total cumulative number of reported infected farms as a function of time is given by $C(t) = \sum_{i=1}^n J_i(t)$ and the daily number of new reported infected farms is given by $\dot{C}(t)$. The parameters $\beta(t)$, $\alpha(t)$, $\nu(t)$, and $\mu(t)$ depend on time in the same manner as in the non-spatial model.

The Reproductive Number

Once movement restrictions (the first intervention implemented) were implemented five days after the first reported infected farm, the *internal* and *external* reproductive numbers of county i are given by $R_{m_i}^{in} = \beta N_i / \alpha$ and $R_{m_i}^{out} = \sum_{j \neq i}^n \beta N_j e^{-qd_{ij}} / \alpha$. The second type of interventions consisted of a mass vaccination program that started nine days after movement restrictions were implemented. The reproductive number that considers the effects of the mass vaccination program after movement restrictions can be defined as a function of the effective time T elapsed from the beginning of mass vaccination at time t_v to time t . That is, $T = t - t_v - 1/\mu$ where $1/\mu$ is the mean time it takes vaccinated farms to reach protective antibody levels. The *internal* and *external* reproductive numbers can be estimated using $R(T)_i^{in} = (\beta N_i / \alpha) s_i^*$ and $R(T)_i^{out} = (\sum_{j \neq i}^n \beta N_j e^{-qd_{ij}} s_j^* / \alpha)$ where $i = 1, 2, \dots, n$ counties and $s_i^* = \begin{cases} 0 & 1 \leq T\nu \\ 1 - T\nu & T\nu < 1 \end{cases}$.

4.2.6 Parameter Estimation

The model parameters $\Theta = (\beta(t), k(t), \alpha(t), q(t), \nu(t), \mu(t))$ are fitted to the cumulative number of reported farms (t_i, y_i) where t_i denotes the i^{th} reporting time (79 reporting days) and y_i is the cumulative number of reported farms by least-squares fit to $C(t, \Theta)$ in Region I (where the outbreak started and the majority of cases occurred). This gives a system of 5 (equations per county) * 42 (counties in region I) = 210 differential equations. Farm density of each county is given in Table 4.1. We wrote a MATLAB program to carry out the least squares fitting procedure with appropriate initial conditions ($0 < \beta < 100$, $1/5 < k < 1/3$, $1/12 < \alpha < 1/4$, $0 < q < 10$, $0 < \nu < 10$, $0 < \mu < 10$).

The asymptotic variance-covariance $AV(\hat{\theta})$ of the least-squares estimate using a Brownian bridge in the error structure is

$$AV(\hat{\theta}) = \sigma^2 \mathbf{B}(\Theta_0) \nabla C(\Theta_0)^T \mathbf{G} \nabla C(\Theta_0) \mathbf{B}(\Theta_0)$$

where $\mathbf{B}(\Theta_0) = [\nabla C(\Theta_0)^T \nabla C(\Theta_0)]^{-1}$. $AV(\hat{\theta})$ is estimated by

$$\sigma^2 \hat{\mathbf{B}}(\hat{\Theta}) \nabla \hat{C}(\hat{\Theta})^T \mathbf{G} \nabla \hat{C}(\hat{\Theta}) \hat{\mathbf{B}}(\hat{\Theta})$$

where $\hat{\mathbf{B}}(\hat{\Theta}) = [\nabla \hat{C}(\hat{\Theta})^T \nabla \hat{C}(\hat{\Theta})]^{-1}$, n is the total number of observations, \mathbf{G} is an $n \times n$ matrix such that $G_{i,j} = (1/n) \min(i, j) - (ij)/n^2$, $\hat{\sigma}^2 = 1/(I_{1xn} \mathbf{G} I_{nx1}) \sum(y_i - C(t_i, \hat{\Theta}))^2$ and $\nabla \hat{C}$ are numerical derivatives of $C(\hat{\Theta})$.

4.3 Results

The initial intrinsic growth rate r (assuming initial exponential growth rate $y \propto e^{rt}$) is 0.65, 0.35, and 0.19 for Regions I, II, and III respectively (Figure 4.2 b). These growth rates decayed as awareness of the epidemic increased and enforced movement restrictions (epidemic started to spread from Region I onwards) became more established. After 07 May 2001 the rate of growth was about the same in the three regions (see Figure 4.2 a). Therefore to reduce the complexity, we analyze the case incidence data of Region I, where the epidemic focused (57% of total cases).

The non-spatial epidemic model (4.2) fit to the cumulative number of infected

farms shows a systematic deviation from the epidemic data during the first 20 days of the epidemic (Figure 4.4). The model parameter estimates are given in Table 4.3. We then fit the cumulative number of reported farms in Region I using our spatial model with interventions (4.4). Our model agrees well with the data (Figure 4.5) and the parameter estimates are in agreement with FMD epidemiology (see Table 4.4). Furthermore, our model predicts a two-hump epidemic with the second hump being of higher amplitude. Such dynamics can be explained by sparks of infection reaching pockets of susceptible farms [83].

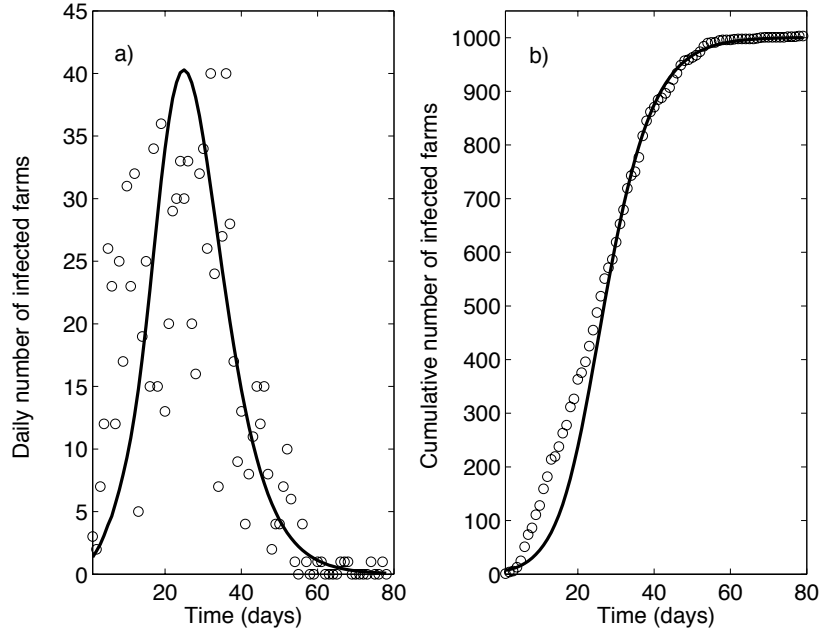


Figure 4.4: a) The daily and b) cumulative number of reported infected farms in Region I (Figure 4.2) where the outbreak started (23 April 2001) and focused (57% of cases). Movement restrictions were implemented on 27 April 2001 and mass vaccination started on 05 May 2001. Circles are the data and the solid line is the best-fit solution of the deterministic model equations of the nonspatial model (4.2) to the data via least squares fitting (parameter estimates are given in Table 4.3).

The “free course” of the epidemic only includes approximately 5 days of data

Table 4.3: Parameter definitions and estimates obtained from least-squares fitting of the non-spatial epidemic model (4.2) to the cumulative number of infected farms over time (days) in Region I (Figure 4.4). All the parameters have units 1/ days.

Params.	Definition	Estim.	SD
$\hat{\beta}_0$	Transm. rate between farms <i>before</i> mov. restrict.	0.77	0.04
$\hat{\beta}$	Transm. rate between farms <i>after</i> mov. restrict.	0.49	0.08
$\hat{\alpha}_0$	Rate of removal from inf. state <i>before</i> mov. restrict.	0.16	0.07
$\hat{\alpha}$	Rate of removal from inf. state <i>after</i> mov. restrict.	0.14	0.02
\hat{k}	Rate of progression from latent to infectious state	0.26	0.07
$\hat{\nu}$	Vaccination rate of susceptible farms	0.16	0.04
$\hat{\mu}$	Rate at which vaccinated farms become protected	0.31	0.05

(movement restrictions were rapidly enforced by the police and the army) and hence parameter estimates of the transmission rate and the infectious period during the initial “free” growth of the epidemic could be somewhat uncertain. Our estimate of the transmission rate (β_0) before movement restrictions is 0.33 (SD 0.13) $\text{farm}^{-1} \text{ day}^{-1}$ compared to our estimate $\beta = 0.10$ (SD 0.03) $\text{farm}^{-1} \text{ days}^{-1}$ after movement restrictions were put in place. The difference between the rates of identification isolation of infected farms before and after movement restrictions were put in place ($\alpha_0 = 0.14$ (SD 0.02), $\alpha = 0.14$ (SD 0.02)) is not statistically significant.

Our estimate of the basic reproductive number ($R_0 \approx 355$) from model (4.3) was computed following van den Driessche & Watmough [103] approach based on the difference of the rate of inflow of new infections in compartment j (f_j) and the inflow and outflow rates of individuals in compartment j by all other epidemiological processes (v_j). This large estimate of R_0 reflects the explosive rate at which

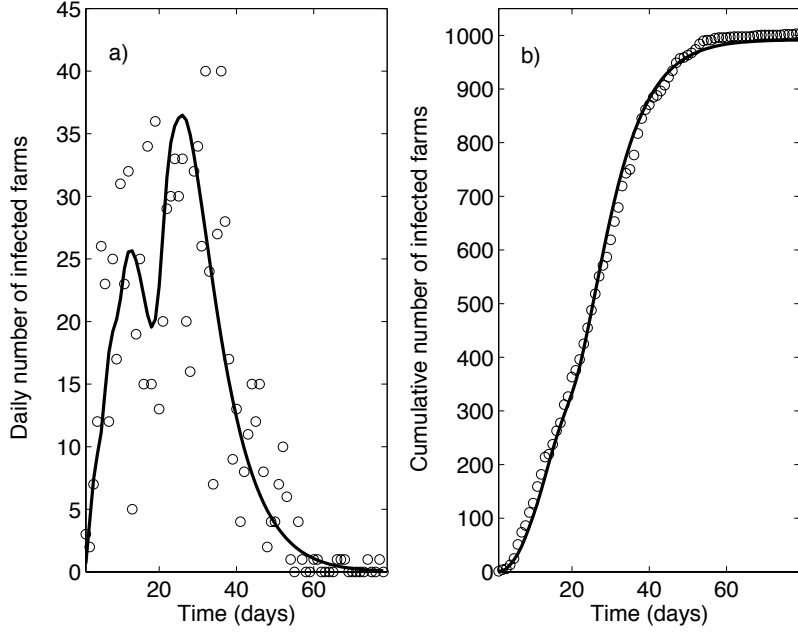


Figure 4.5: a) The daily and b) cumulative number of reported infected farms in Region I (Figure 4.2) where the outbreak started (23 April 2001) and focused (57% of cases). Movement restrictions were implemented on 27 April 2001 and mass vaccination started on 05 May 2001. Circles are the data and the solid line is the best-fit solution of the deterministic model equations of the spatial model (4.4) to the data via least squares fitting (parameter estimates are given in Table 4.4).

FMD can spread.

The average *internal* and *external* basic reproductive numbers $\bar{R}_0^{in} \approx 280.47$ and $\bar{R}_0^{out} \approx 2.64$ respectively before movement restriction were enforced. After movement restrictions were implemented, $\bar{R}_m^{in} \approx 87.20$ and $\bar{R}_m^{out} \approx 0.82$. After mass vaccination started, our model predicts that the *internal* basic reproductive number rapidly decreased to a number less than one on day 25 (16 May 2001) of the epidemic.

Our estimate of the vaccination rate of susceptible farms (ν) is 0.25 (SD 0.09). That is, we estimate a mean time of approximately 4 days before a susceptible farm was successfully vaccinated. Since it takes a few days before vaccinated animals reach

Table 4.4: Parameter definitions and estimates obtained from least-squares fitting of the spatial epidemic model (4.4) to the cumulative number of infected farms over time (days) in Region I (Figure 4.5). All the parameters have units 1/ days except for q whose units are 1/Km. * Small values of q lead to widespread influence, whereas large q supports local spread. Great mobility and frequent interactions among farms would lead to small values of q .

Params.	Definition	Estim.	SD
β_0	Transm. rate within counties <i>before</i> mov. restrict.	0.33	0.13
β	Transm. rate within counties <i>after</i> mov. restrict.	0.10	0.03
α_0	Rate of removal from inf. state <i>before</i> mov. restrict.	0.14	0.02
α	Rate of removal from inf. state <i>after</i> mov. restrict.	0.14	0.02
k	Rate of progression from latent to infectious state	0.28	0.05
q^*	Positive constant quantifying extent of local spread	1.03	0.10
ν	Vaccination rate of susceptible farms	0.25	0.09
μ	Rate at which vaccinated farms become protected	0.14	0.03

protective levels, we estimate the rate at which vaccinated farms reach protective antibody levels (μ). Our estimate is 0.14 (SD 0.03) days⁻¹. That is, we estimate 7.14 days before successfully vaccinated farms became protected. The mass vaccination program implemented during the 2001 FMD epidemic in Uruguay reduced the final epidemic size to 1003 (18.8%) infected farms in Region I compared to 5251 (98.5%) if no mass vaccination had been implemented after movement restrictions (multiple outbreaks are observed, Figure 4.6). A 5-day delay in its implementation with respect to the actual implementation date yields 1501 (28.2%) infected farms. Moreover, if the vaccination program had been implemented 5 days prior to the actual date, our model predicts only 629 (11.8%) infected farms (Figure 4.6). The sensitivity of the final epidemic size to the time of starts of the mass vaccination program is shown in Figure 4.7.

We quantify the extent of local spread through the parameter q . Small values of q lead to widespread influence, whereas large q supports local spread. Our estimate for q is 1.03 1/Km (SD 0.10). That is, our estimate of the mean transmission range ($1/q$) is approximately 0.97 Km.

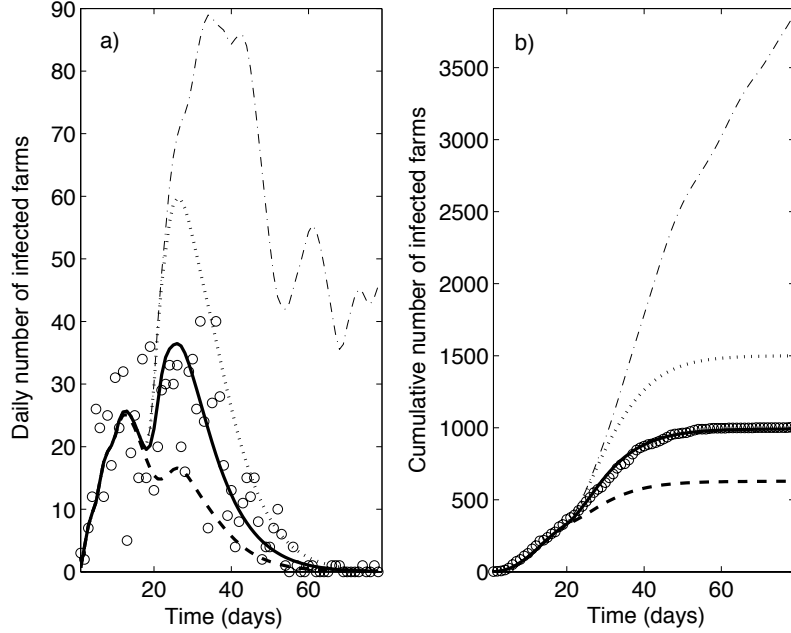


Figure 4.6: a) The daily and b) cumulative number of reported infected farms in Region I (Figure 4.2) where the outbreak started (23 April 2001) and focused (57% of cases). Movement restrictions were implemented on 27 April 2001 and mass vaccination started on 05 May 2001. Circles are the data and the solid line is the best-fit solution of the deterministic model equations (4.4) to the data via least squares fitting (parameter estimates are given in Table 4.4). Three scenarios are shown: (dash-dot) no mass vaccination implemented after movement restrictions (total of 5252 cases); (dot-dot) mass vaccination with a 5-day delay (1551 cases) and (dash-dash) 5 days before the actual date at which mass vaccination started (604 cases).

4.4 Discussion

Mathematical models have played an important role in the decision-making process in the control of FMD epidemics and its economic consequences [82, 84, 83,

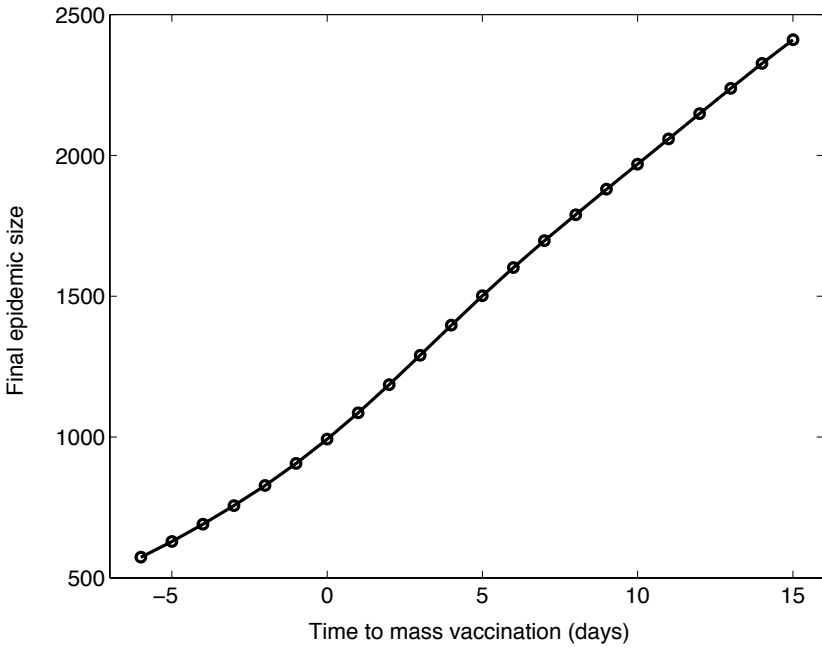


Figure 4.7: Sensitivity of the final epidemic size (Region I) to the time of start of the mass vaccination program. Negative numbers represent number of days before the actual reported start of the mass vaccination programme (05 May 2001) while positive numbers represent a delay (days).

104, 105, 106, 107, ?, 108]. During the 2001 FMD epidemic in Great Britain different approaches were used and included “moment closure” technique [84] and stochastic models [83, 104]. Here, we model the 2001 FMD epidemic in Uruguay using a deterministic model that takes into account the distance among counties in the transmission process (Figure 4.3), farm density within counties (Table 4.1) and information on the intervention strategies that were put in place during the outbreak.

Our spatial deterministic model is validated by means of a non-spatial model (4.2) that assumes uniform risk of infection among farms. Our spatial model differed with its non-spatial counterpart in: a) non-spatial model fit to the data shows a systematic deviation from epidemic data during the initial epidemic take-off and

b) the spatial model displays a double hump in the time series of the daily number of infected farms, pattern not observed under the non-spatial model. We assume that the spatial location of farms play an important role in the transmission dynamics of FMD as a first order approximation. As most models for FMD, our model do not include *road density* considerations. Nevertheless, given data become available, the road density factor could play a significant role in capturing higher resolution epidemic patterns within states or counties as this measure can be highly heterogeneous. We did not incorporate farm heterogeneity (i.e dairy, beef, etc) in the transmission process [109] and may be considered if appropriate data become available. Notwithstanding the relatively basic aspects of FMD transmission considered here, our model is able to capture regional patterns of the 2001 Uruguay FMD epidemic.

By fitting our model to epidemic-curve data on the cumulative number of reported farms, we are able to estimate relevant epidemiological parameters including the average transmission rate within counties (before and after movement restrictions were put in place) (β_0, β), the incubation period ($1/k$), the infectiousness period (before and after movement restrictions were put in place) ($1/\alpha_0, 1/\alpha$), and control parameters: mean time before susceptible farms are vaccinated ($1/\nu$) and the mean time it takes for vaccinated farms to achieve protective antibody levels ($1/\mu$). Epidemiological and control parameter estimates are given in Table 4.4. We observe a reduction by a factor of 3 in the transmission rate before and after movement restrictions were enforced (Table 4.4). However, we find no difference between the infectious period before and after movement restrictions were implemented.

Our spatial epidemic model captures a two-hump outbreak in the transmission dynamics of the 2001 FMD epidemic in Uruguay (Figure 4.5). Such dynamics can-

not be reproduced using fully mixed systems. In our spatial model, such dynamics arise from long distance sparks of infection which can trigger secondary outbreaks. Moreover, secondary “humps” of infection can be of higher intensity as the 2001 FMD epidemic in Uruguay showed (Figure 4.5).

Our estimate of the basic reproductive number ($R_0 \approx 355$) is large and this can be explained by the spatial transmission parameter that dominate the course of FMD epidemics. The basic reproductive number for spatial models must be much higher for epidemics to occur [110] because of the more localized transmission dynamics. Woolhouse et al. (1996) [111] report a basic reproductive number for an FMD-infected animal to be between 2 and 73. Our R_0 estimates are given in terms the number of secondary infected farms generated by a primary infectious farm during its infectious period in a fully susceptible landscape.

More useful information can be obtained by looking at the number of secondary cases generated within counties and between counties. Before movement restrictions were implemented, the average number of secondary cases generated externally to counties (*external* basic reproductive number) was $\bar{R}_0^{out} \approx 2.64$. However, once movement restriction had been enforced on 27 April 2001, the average number of external secondary cases declined to a number less than one ($\bar{R}_m^{out} \approx 0.82$) which indicates that once movement restrictions had been put in place, the transmission process was mostly confined to within counties with rarely long distance (at the level of counties) transmission events. This drop in the reproductive number is in agreement with the reduction of the intrinsic growth rate r observed in the data (Figure 4.2 a). This is also supported by our parameter estimate $1/q = 0.97$ (Km) characterizing the extent of local spread or the average transmission range of the disease under the assumption of uniform mixing of farms within counties.

We estimate that the reproductive number within counties decayed to a number less than one approximately 12 days after the mass vaccination program started. Our model predicts a reduction in the final epidemic size of 374 infected farms in Region I (see Figure 4.6 b) if mass vaccination had started 5 days prior to the actual date. Moreover, our model predicts no secondary “humps” of infection of higher intensity under this scenario (Figure 4.5) which can be explained by the higher number of vaccinated farms achieved by starting mass vaccination earlier. A 5-day delay in its implementation had generated 498 more cases (Figure 4.6). This highlights the effects of delays in the implementation of control measures which are tightly linked to the economic impact of the epidemic. Figure 4.7 shows the sensitivity of the final epidemic size in Region I to the time of start of mass vaccination.

There is only few data on the different aspects of the vaccine and the vaccination program including the vaccination coverage (since not all the susceptible animals are vaccinated for several reasons) and the vaccine efficacy which can be very different from the one observed in the field. During the epidemic, neither young calves were vaccinated (< 3 month-olds). Pigs and sheep were not vaccinated either [90]. The vaccine utilized for the mass vaccination program was specific. That is, the vaccine targetted to the virus observed during the FMD epidemic (virus type *A₂₄* [90]). The age, health, and stress of the livestock influences the animal’s response and the effectiveness of the vaccine (the “responders” index). Furthermore, some animals do not reach protective antibody levels from those who generate immune response. For the 2001 FMD epidemic in Uruguay, we estimate 7.14 days for successfully vaccinated farms to reach antibody protective levels.

4.5 Conclusions

- FMD epidemic models incorporating spatial structures can capture regional patterns of spread
- Long distance sparks of infection reaching areas of susceptible farms can generate multiple peaks in the global infection rates. In contrast to spatially structured models, spatially homogeneous models are unable to reproduce such patterns of infection
- Our model predicts the basic reproductive number will rapidly decrease after movement restrictions are imposed. This observation agrees with the rapid decrease in the intrinsic growth rate observed in the incidence data (Figure 4.2 a)
- There was a rapid drop in the external reproductive number to less than one after movement restrictions were enforced. Following these restrictions, transmissions were localized and there was a very low probability for long-range transmission events. Hence, ensuring that movement restrictions are strictly enforced is crucial in any contingency plan against FMD
- Mass vaccination implemented along with a policy of movement restrictions is an effective means of control and significantly reduces the final epidemic size.
- The 2001 FMD Uruguayan epidemic data and analysis can be used for comparison when assessing other control measures such as culling policies and higher potency vaccines implemented alone or in combination with other interventions.

Chapter 5

Scaling laws for the movement of people between locations in a large city *

5.1 Introduction

Similar scaling laws and patterns have been detected in a great number of systems found in nature, society, and technology. Networks of scientific collaboration [112][113][114], movie actors [115], cellular networks [116][117], food webs [118], the Internet [119], the *World Wide Web* [120, 121], friendship networks [122] and networks of sexual relationships [123] among others have been analyzed up to some extent. Several common properties have been identified in such systems. One such property is the short average distance between nodes, that is, a small number of edges need to be traversed in order to reach a node from any other node. Another common property is high levels of clustering [115, 124], a characteristic absent in random networks [125]. Clustering measures the probability that the neighbors of a node are also neighbors of each other. Networks with short average distance between nodes and high levels of clustering have been dubbed “small worlds” [115, 124]. Power-law behavior in the degree distribution is another common property in many real world networks [126]. That is, the probability that a randomly chosen node has degree k decays as $P(k) \sim k^{-\gamma}$ with γ typically between 2 and 3. Barabási and Albert (BA) introduced an algorithm capable of generating networks with a power-law connectivity distribution ($\gamma = 3$). The BA algorithm generates

*G. Chowell , J. M. Hyman, S. Eubank, C. Castillo-Chavez. Scaling Laws for the Movement of People between Locations in a Large City. Physical Review E 68 (2003).

networks where nodes connect, with higher probability, to nodes that have accumulated higher number of connections and stochastically generates networks with a power-law connectivity distributions in the appropriate scale.

Social networks are often difficult to characterize because of the different perceptions of what a link constitutes in the social context and the lack of data for large social networks of more than a few thousand individuals. Even though detailed data on the daily movement of people in a large city does not exist, these systems have been statistically sampled and the data used to build detailed simulations for the full population. The insights gained by studying the simulated movement of people in a virtual city can help guide research in identifying what scaling laws or underlying structures may exist and should be looked for in a real city. In this article we analyze a social mobility network that can be defined accurately by the simulated movement of people between locations in a large city. We analyze the cumulative directed graph generated from the simulated movement of 1.6 million individuals *in* or *out* of 181,206 locations during a typical day in Portland, OR. The 181,206 nodes represent locations in the city and the edges connections between nodes. The edges are weighted by daily traffic (movement of individuals) *in* or *out* of these locations. The statistical analysis of the cumulative network reveals that it is a small world with power-law decay in the out-degree distribution of locations (nodes). The resulting graph as well as subgraphs based on different activity types exhibit scaling laws consistent with an underlying hierarchical structure [127, 128]. The out-traffic (weight of the full network) and the total out-traffic (total weight of the out edges per node) distributions are also fitted to power laws. We show that the joint distribution of the out-degree and total out-traffic distributions decays linearly in an appropriate scale. We also explore the time evolution

of the largest component and the distribution of the component sizes.

5.1.1 Transportation Analysis Simulation System (TRANSIMS)

TRANSIMS [129] is an agent-based simulation model of the daily movement of individuals in virtual region or city with a complete representation of the population at the level of households and individual travelers, daily activities of the individuals, and the transportation infrastructure. The individuals are endowed with demographic characteristics taken from census data and the households are geographically distributed according to the population distribution. The transportation network is a precise representation of the city's transportation infrastructure. Individuals move across the transportation network using multiple modes including car, transit, truck, bike, walk, on a second-by-second basis. DMV records are used to assign vehicles to the households so that the resulting distribution of vehicle types matches the actual distribution. Individual travelers are assigned a list of activities for the day (including home, work, school, social/recreational, and shop activities) obtained from the household travel activities survey for the metropolitan area [130] (Figure 5.2 shows the frequency of four activity types in a typical day). Data on activities also include origins, destinations, routes, timing, and forms of transportation used. Activities for itinerant travelers such as bus drivers are generated from real origin/destination tables.

TRANSIMS consists of six major integrated modules: Population synthesizer, Activity Generator, Router, Microsimulation and Emissions Estimator. Detailed information on each of the modules is available [129]. TRANSIMS has been designed to give transportation planners accurate, complete information on traffic

impacts, congestion, and pollution.

For the case of the city of Portland, OR, TRANSIMS calculates the simulated movements of 1.6 million individuals in a typical day. The simulated Portland data set includes the time at which each individual leaves a location and the time of arrival to its next destination (node). These data are used to calculate the average number of people at each location and the traffic between any two locations on a typical day. (Table 1 shows a sample of a Portland activity file generated by TRANSIMS). Locations where activities are carried out are estimated from observed land use patterns, travel times and costs of transportation alternatives. These locations are fed into a routing algorithm that finds the minimum cost paths that are consistent with individual choices [131, 132, 133]. The simulation land resolution is of 7.5 meters. The simulator provides an updated estimate of time-dependent travel times for each edge in the network, including the effects of congestion, to the *Router and location estimation algorithms* [129], which generate traveling plans. Since the entire process estimates the demand on a transportation network from census data, land use data, and activity surveys, these estimates can thus be applied to assess the effects of hypothetical changes such as building new infrastructures or changing downtown parking prices. Methods based on observed demand cannot handle such situations, since they have no information on what generates the demand. Simulated traffic patterns compare well to observed traffic and, consequently, TRANSIMS provides a useful planning tool.

Until recently, it has been difficult to obtain useful estimates on the structure of social networks. Certain classes of random graphs (scale-free networks [126], small-world networks [122, 124], or Erdos-Renyi random graphs [125, 134]), have been postulated as good representatives. In addition, data based models while

useful are limited since they have naturally focused on small scales [135]. While most studies on the analysis of real networks are based on a single snapshot of the system, TRANSIMS provides powerful time dependent data of the evolution of a location-based network.

5.2 Portland’s location-based network

A “typical” realization by the Transportation Analysis Simulation System (TRANSIMS) simulates the dynamics of 1.6 million individuals in the city of Portland as a directed network, where the nodes represent locations (i.e. buildings, households, schools, etc.) and the directed edges (between the nodes) represent the movement (traffic due to activities) of individuals between locations (nodes). We have analyzed the cumulative network of the whole day as well as cumulative networks that comprise different time intervals of the day. Here we use the term “activity” to denote the movement of an individual to the location where the activity will be carried out. Traffic intensity is modeled by the nonsymmetric mobility matrix $W = (w_{ij})$ of traffic weights assigned to all directed edges in the network ($w_{ij} = 0$ means that there is no directed edge connecting node i to node j).

5.3 Power law distributions

We calculate the statistical properties of a typical day in the location-based network of this virtual city from the cumulative mobility data generated by TRANSIMS (see Table 2).

The *average out-degree* is $\langle k \rangle = \sum_{i=1}^n k_i/n$ where k_i is the degree for node i and n is the total number of nodes in the network. For the portland network

Table 5.1: Sample section of a TRANSIMS activity file. In this example, person 115 arrives for a social recreational activity at location 33005 at 19.25 o'clock and departs at 21.00 o'clock.

Person ID	Location ID	Arriv. time(hrs)	Depart. time(hrs)	Activity type
115	4225	0.0000	7.00	home
115	49296	8.00	11.00	work
115	21677	11.2	13.00	work
115	49296	13.2	17.00	work
115	4225	18.00	19.00	home
115	33005	19.25	21.00	social/rec
115	4225	21.3	7.00	home
220	8200	0.0000	8.50	home
220	10917	9.00	14.00	school
220	8200	14.5	18.00	home
220	3480	18.2	20.00	social/rec
220	8200	20.3	8.6	home

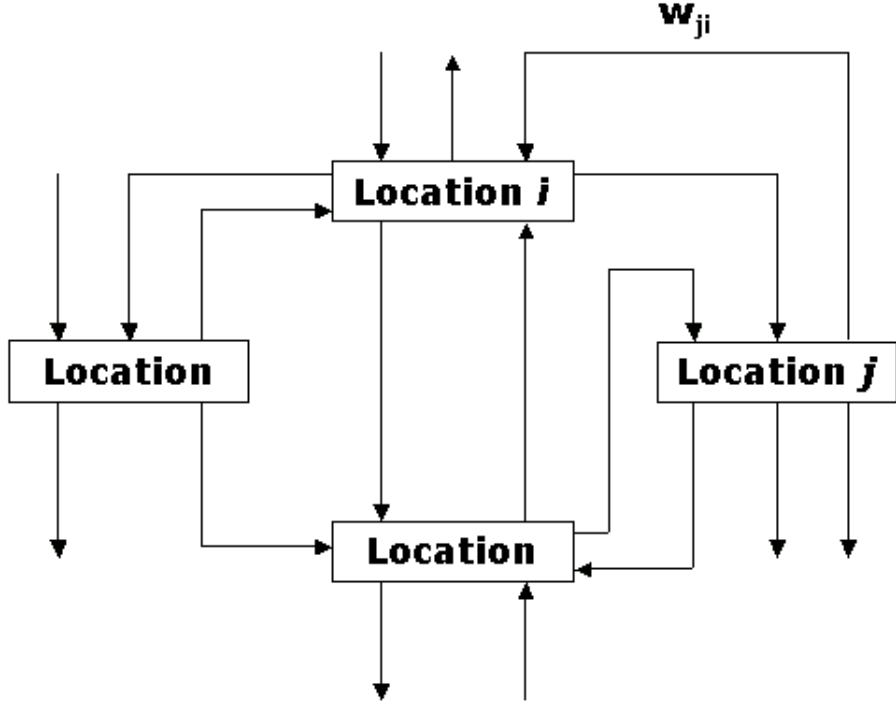


Figure 5.1: Structure of the location-based network of the city of Portland. The nodes represent locations connected via directed edges based on the traffic or movement of individuals (activities) between the locations. The weights (w_{ij}) of the edges represent the daily traffic from location i to location j .

$\langle k \rangle = 29.88$ and the *out-degree distribution* exhibits power law decay with scaling exponent ($\gamma \approx 2.7$). The *out-traffic* (edge weights) and the *total out-traffic* (edge-weights per node) distributions are also fitted well by power laws.

The *average distance* between nodes L is defined as the median of the means L_i of the shortest path lengths connecting a vertex $i \in V(G)$ to all other vertices [136]. For our network, $L = 3.1$, which is small when compared to the size of the network. In fact, the *diameter* (D) of the graph (the largest of all possible shortest paths between all the locations) is only 8. L and D are measured using a breadth first search (BFS) algorithm [137] ignoring the edge directions.

The *clustering coefficient*, C , quantifies the extent to which neighbors of a node

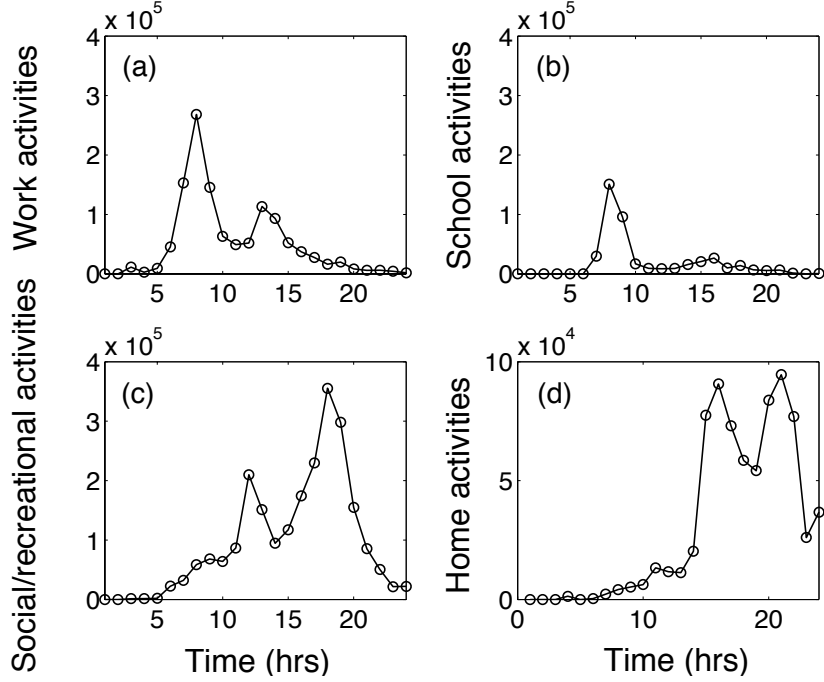


Figure 5.2: The number of people active in (a) work activities, (b) school activities, (d) social activities, and (d) home activities as a function of time (hours) during a ‘typical’ day in Portland, Oregon.

are also neighbors of each other [136]. The clustering coefficient of node i , C_i , is given by

$$C_i = |E(\Gamma_i)| / \binom{k_i}{2}$$

where $|E(\Gamma_i)|$ is the number of edges in the neighborhood of i (edges connecting the neighbors of i not including i itself) and $\binom{k_i}{2}$ is the maximal number of edges that could be drawn among the k_i neighbors of node i . The clustering coefficient C of the whole network is $C = \sum_{i=1}^n C_i/n$. For a *scale-free* random graph (BA model) [126] with 181,206 nodes and $m = 16$ [138], the clustering coefficient $C_{rand} \approx \frac{(m-1)}{8} \frac{(\ln N)^2}{N} \approx 0.0015$ [139, 140]. The clustering coefficient for our location-

Table 5.2: Statistical properties of the Portland’s location-based network. S is the size of the largest component of the cumulative network during the whole day.

Statistical properties	Value
Total nodes (N)	181,206
Size of the cumulative largest component (S)	181,192
Total directed edges (E)	5,416,005
Average out-degree ($< k >$)	29.88
Clustering coefficient (C)	0.0584
Average distance between nodes (L)	3.1
Diameter (D)	8.0

based network, ignoring edge directions, is $C = 0.0584$, which is roughly 39 times larger than C_{rand} .

Highly clustered networks have been observed in other systems [115] including the electric power grid of western US. This grid has a clustering coefficient $C = 0.08$, about 160 times larger than the expected value for an equivalent random graph [136]. The few degrees of separation between the locations of the (highly clustered) network of the city of Portland “make” it a small world [124, 122, 136].

Many real-world networks exhibit properties that are consistent with underlying hierarchical organizations. These networks have groups of nodes that are highly interconnected with few or no edges connected to nodes outside their group. Hierarchical structures of this type have been characterized by the clustering coefficient function $C(k)$, where k is the node degree. A network of movie actors, the semantic web, the *World Wide Web*, the Internet (autonomous system level), and some metabolic networks [127, 128] have clustering coefficients that scale as

k^{-1} . The clustering coefficient as a function of degree (ignoring edge directions) in the Portland network exhibits similar scaling at various levels of aggregation that include, the whole network and subnetworks constructed by activity type (work, school and social/recreational activities, see Figure 5.3). We constructed subgraphs based on activity types, that is, those subgraphs constructed from all the directed edges of a specific activity type (i.e work, school, social) during a typical day in the city of Portland. The clustering coefficient of the subnetworks generated from work, school, and social/recreational activities are: 0.0571, 0.0557, and 0.0575, respectively. The largest clustering coefficient and closest to the overall clustering coefficient ($C = 0.0584$) corresponds to the subnetwork constructed from social/recreational activities. It seems that the whole network, as well as the selected activity subnetworks, support a hierarchical structure albeit the nature of such structure (if we choose to characterize by the power law exponent) is not universal. This agrees with relevant theory [128].

Understanding the temporal properties of networks is critical to the study of superimposed dynamics such as the spread of epidemics on networks. Most studies of superimposed processes on networks assumes that the contact structure is fixed (see for example [141, 142, 143, 144, 145, 146, 147, 148, 149]). Here, we take a look at the time evolution of the largest connected component of the location-based network of the city of Portland (Figure 5.4). We have observed that a sharp transition occurs at about 6 a.m. In fact, by 7 a.m. the size of the largest component includes approximately 60% of the locations (nodes). Table 3 shows the size of the largest component just before and after the sharp transition occurs.

Let $X_m(t)$ be the number of components of size m at time t . Then $X(t) = \sum_{m \geq 1} X_m(t)$ is the total number of components at time t (Figure 5.5(a)). Fur-

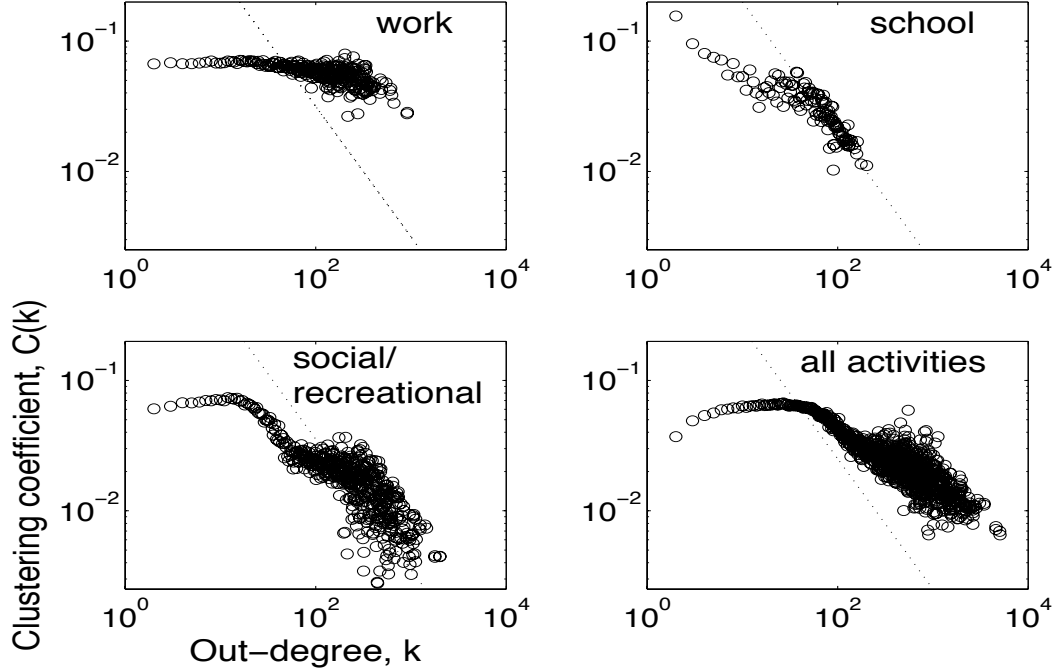


Figure 5.3: Log-log plots of the clustering coefficient as a function of the out-degree for subnetworks constructed from work activities, school activities, social activities, and all the activities. The dotted line has slope -1 . Notice the scaling k^{-1} for the school and social/recreational activities. However, for the subnetwork constructed from work activities, the clustering coefficient is almost independent of the out-degree k .

thermore, the probability $P(m)$ that a randomly chosen node (location) belongs to a component of size m follows a power law that gets steeper in time as the giant component forms (Figure 5.5(b)). To identify the relevance of the temporal trends, we computed the out-degree distribution of the network for three different time intervals: The morning from 6 a.m to 12 p.m.; the workday from 6 a.m. to 6 p.m.; and the full 24 hours. In the morning phase, the out-degree distribution has a tail that decays as a power law with $\gamma \simeq 2.7$ (for the workday $\gamma \simeq 2.43$ and for the full day $\gamma \simeq 2.4$). The distribution of the out-degree data has two scaling regions: the number of locations is approximately constant for out-degree $k < 20$ and then decays as a power law for high degree nodes (Fig. 5.6). The degree distribution

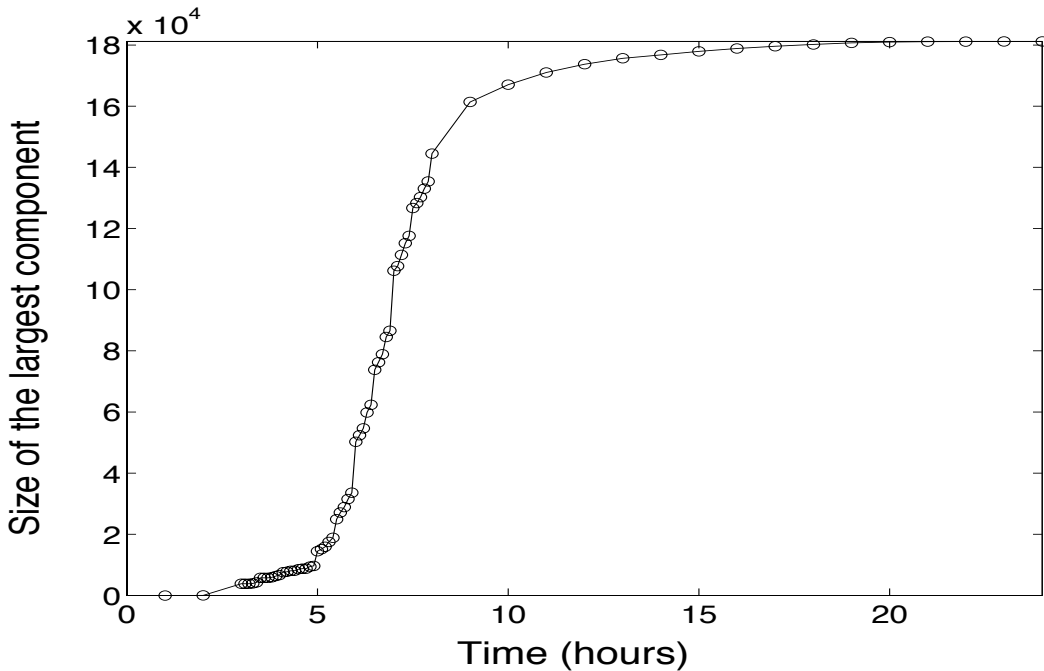


Figure 5.4: The size of the largest component (cluster) over time. A sharp transition is observed at about 6 a.m when people move from home to work or school.

for the undirected network (ignoring edge direction) displays power-law behavior, but with slightly different power-law exponents: 2.3 (morning), 2.48 (work day) and 2.51 (full day).

The strength of the connections in the location-based network is measured by the traffic (flow of individuals) between locations in a “typical” day of the city of Portland. The log-log plot of the out-traffic distributions for three different periods of time (Fig. 5.7) exhibits power law decay with exponents, $\gamma \simeq 3.56$ for the morning, $\gamma \simeq 3.74$ for the workday, and $\gamma \simeq 3.76$ for the full day. The out-traffic distribution is characterized by a power law distribution for all values of the traffic-weight matrix W . This is not the case for the out-degree distribution of the network (see Figure 5.6) where a power law fits well only for sufficiently large degree k ($k > 10$).

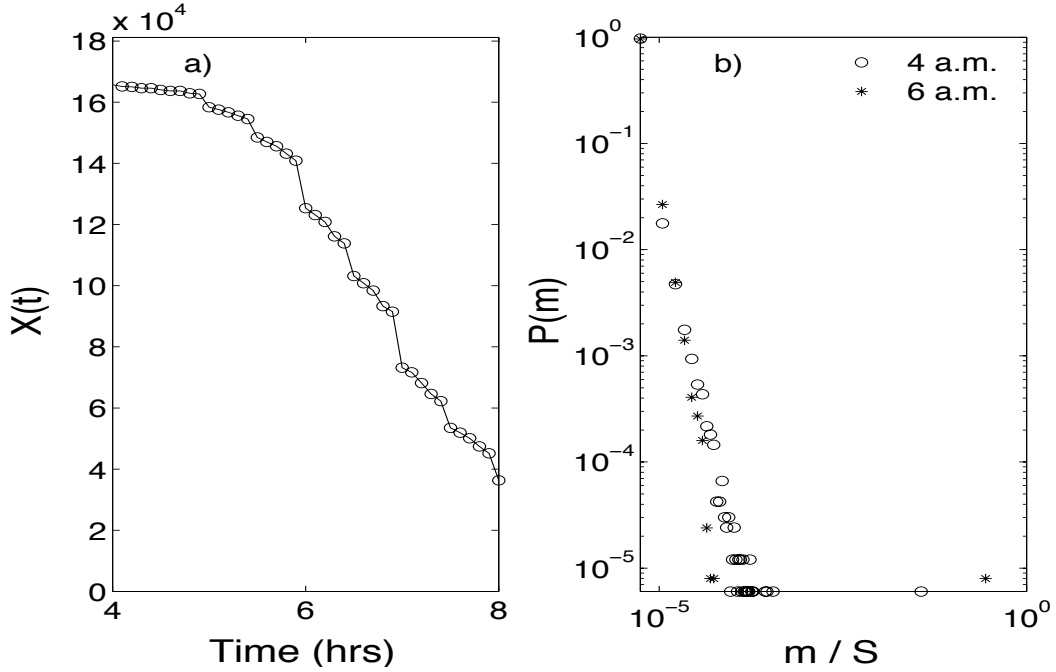


Figure 5.5: (a) The number of components $X(t)$ between 4 a.m. and 8 a.m. (b) Probability distribution $P(m)$ of the normalized component sizes at two different times of the day. The component sizes (m) have been normalized by S , the size of the largest component of the cumulative network during the whole day (Table 1).

The distribution of the total out-traffic per location, w_i 's ($w_i = \sum_j w_{i,j}$), is characterized by two scaling regions. The tail of this distribution decays as a power law with exponent $\gamma = 2.74$ (Fig. 5.8). This is almost the same decay as the out-degree distribution ($\gamma = 2.7$) because the out-degree and the total out-traffic are highly correlated (with correlation coefficient $\rho = 0.94$).

5.4 Correlation between out-degree and total out-traffic

The degree of correlation between various network properties depend on the social dynamics of the population. The systematic generation and resulting structure of these networks is important to understand dynamic processes such as epidemics that “move” on these networks. Understanding the mechanisms behind these cor-

Table 5.3: Size of the largest component just before and after 6 a.m., the time at which a sharp transition occurs. At midnight, all but 14 locations belong to the largest component (Table 2).

Time (hrs)	Size of largest component
5.6	27,132
5.8	31,511
6.0	50,242
6.2	54,670
6.4	62,346
6.6	76,290
6.8	84,516
7.0	106,160

relations will be useful in modeling fidelity networks.

In the Portland network, the out-degree k and total out-traffic v have a correlation coefficient $\rho = 0.94$ on a log-log scale with 95% of the nodes (locations) having out-degree and total out-traffic less than 100 (Fig. 5.9). That is, the density of their joint distribution $F(k, v)$ is highly concentrated near small values of the out-degree and total out-traffic distributions. The joint distribution supports a surface that decays linearly when the density is in \log_e scale (Figure 5.10).

5.5 Conclusions

Strikingly similar patterns on data from the movement of 1.6 million individuals in a “typical” day in the city of Portland have been identified at multiple temporal scales and various levels of aggregation. The analysis is based on the mapping of

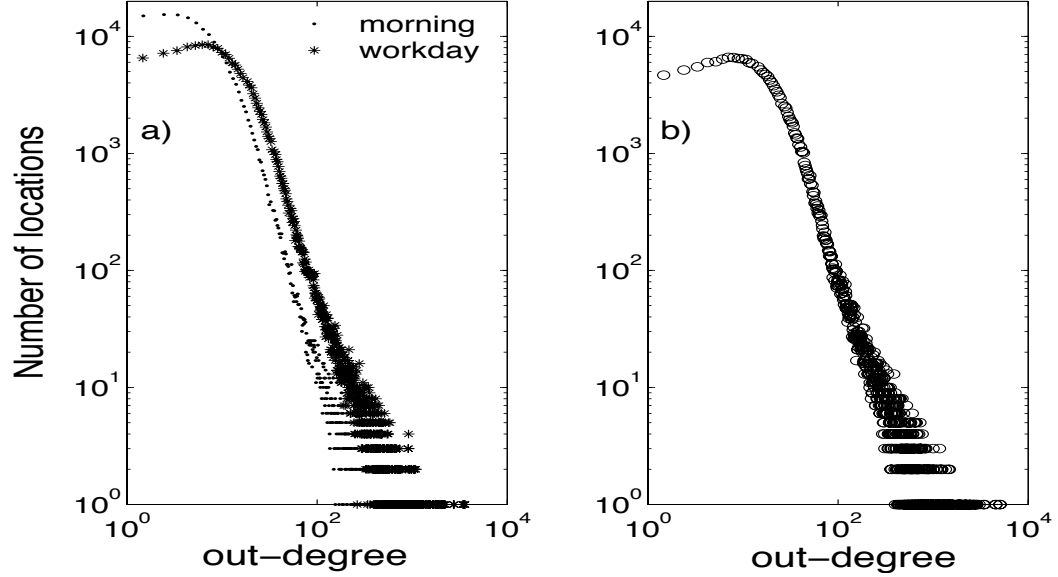


Figure 5.6: Distribution of the out-degrees of the location-based network of the city of Portland. There are approximately the same number of nodes (locations) with out-degree $k = 1, 2, \dots, 10$. For $k > 10$ the number of nodes with a given out-degree decays as a power law $P(k) \propto k^{-\gamma}$ with (a) $\gamma \simeq 2.7$ for the morning (6 a.m.-12 p.m.), $\gamma \simeq 2.43$ for the workday (6 a.m.-6 p.m.) and (b) $\gamma \simeq 2.4$ for the full day.

people's movement on a weighted directed graph where nodes correspond to physical locations and where directed edges, connecting the nodes, are weighted by the number of people moving in and out of the locations during a typical day. The clustering coefficient, measuring the local connectedness of the graph, scales as k^{-1} (k is the degree of the node) for sufficiently large k . This scaling is consistent with that obtained from models that postulate underlying hierarchical structures (few nodes get most of the action). The out-degree distribution in log-log scale is relatively constant for small k but exhibits power law decay afterwards ($P(k) \propto k^{-\gamma}$). The distribution of daily total out-traffic between nodes in log-log scale is flat for small k but exhibits power law decay afterwards. The distribution of the daily out-traffic of individuals between nodes scales as a power law for all k (degree).

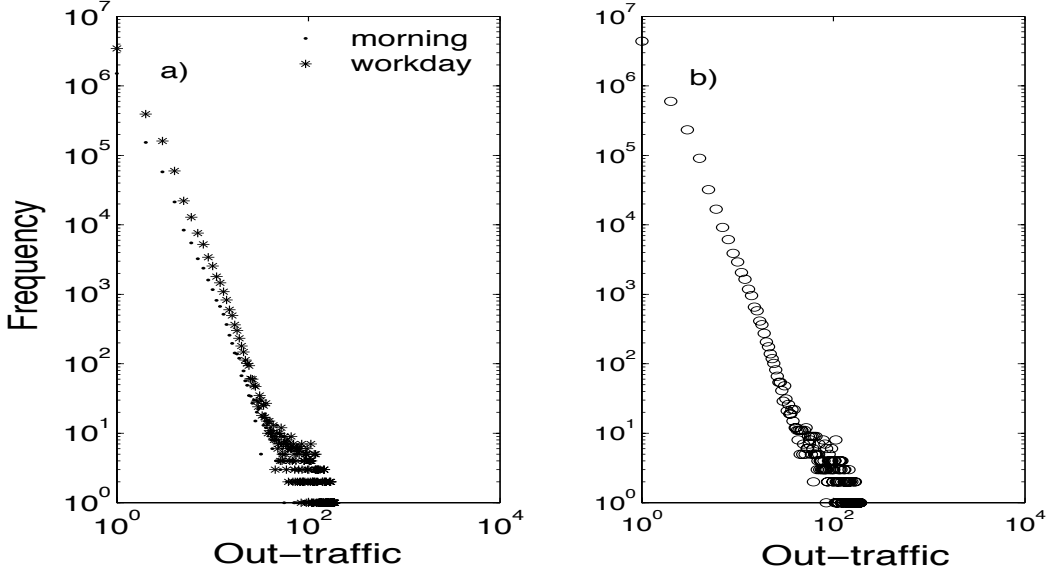


Figure 5.7: The out-traffic distribution of the location-based network of the city of Portland follows a power law ($P(k) \propto k^{-\gamma}$) with (a) $\gamma \approx 3.56$ (morning), $\gamma \approx 3.74$ (afternoon), and (b) $\gamma \approx 3.76$ (full day). Hence a few connections have high traffic but most connections have low traffic.

The observed power law distribution in the out-traffic (edge weights) is therefore, supportive of the theoretical analysis of Yook *et al.* [150] who built weighted scale-free (WSF) dynamic networks and proved that the distribution of the total weight per node (total out-traffic in our network) is a power law where the weights are exponentially distributed.

There have been limited attempts to identify at least some characteristics of the joint distributions of network properties. The fact that daily out-degree and total out-traffic data are highly correlated is consistent again with the results obtained from models that assume an underlying hierarchical structure (few nodes have most of the connections and get most of the traffic (weight)). The Portland network exhibits a strong linear correlation between out-degree and total out-traffic on a log-log scale. We use this time series data to look at the network “dynamics”. As the activity in the network increases, the size of the maximal connected compo-

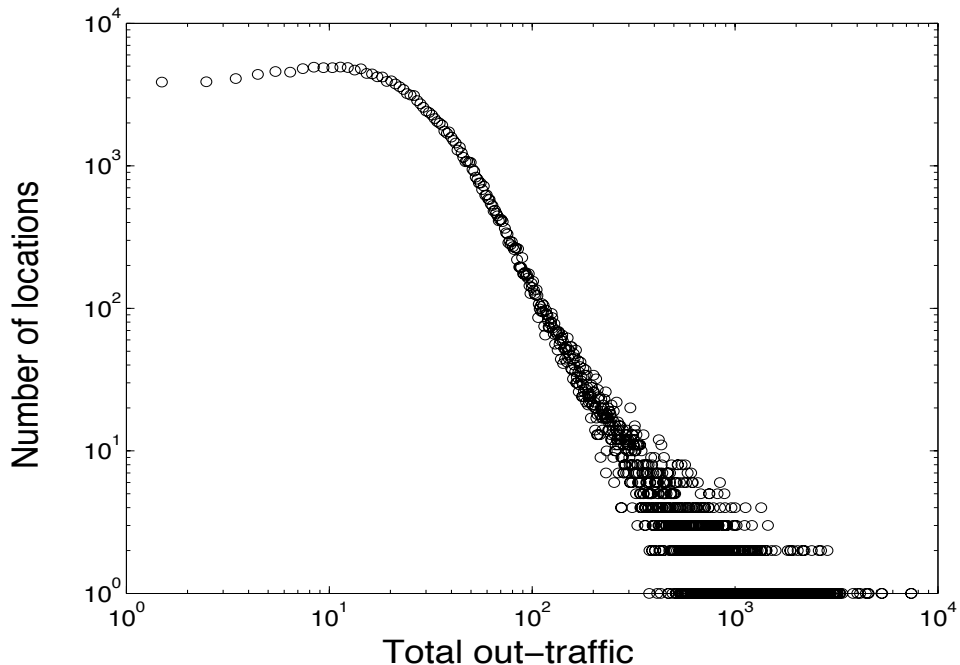


Figure 5.8: Distribution of the total out-traffic for the location-based network of the city of Portland. There are approximately the same number of locations (nodes) with small total out-traffic. The number of locations where more than 30 people (approximately) leave each day decays as a power law with $\gamma \simeq 2.74$.

net exhibits threshold behavior, that is, a “giant” connected component, suddenly emerges. The study of superimposed processes on networks such as those associated with the potential deliberate release of biological agents needs to take into account the fact that traffic is not constant. Planning, for example, for worst-case scenarios requires knowledge of edge-traffic, in order to characterize the temporal dynamics of the largest connected network components [151].

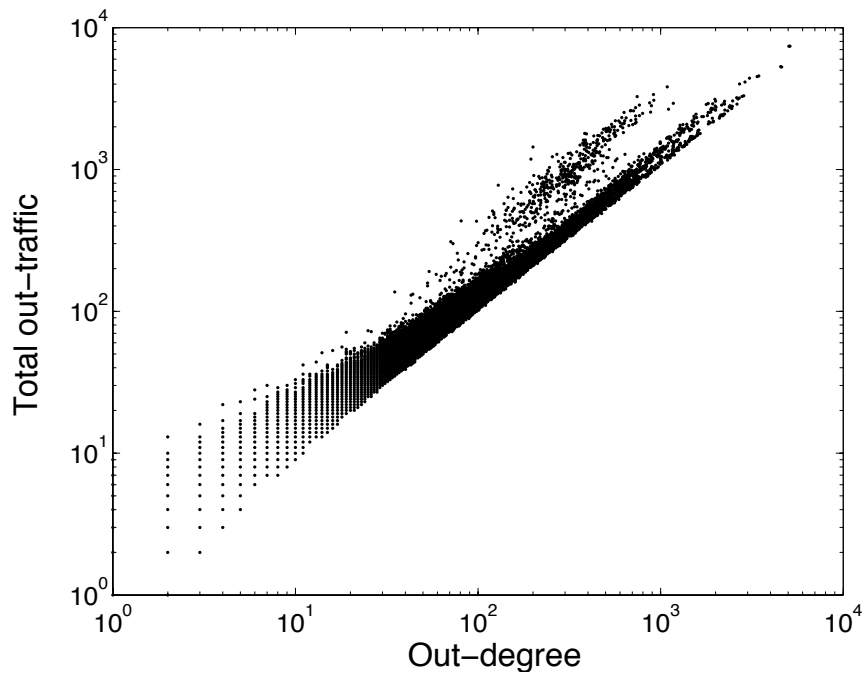


Figure 5.9: Correlation between the out-degree and the total out-traffic. The correlation coefficient is $\rho = 0.94$ on a log-log scale. Most (95%) of the locations have fewer than 100 people leaving during the day.

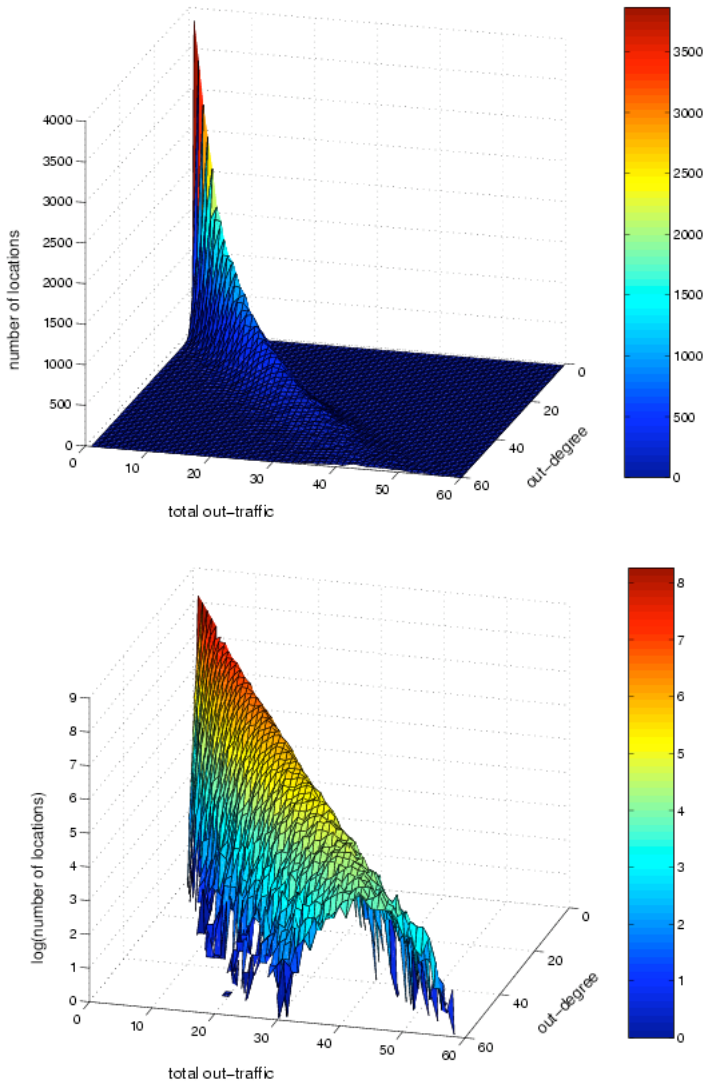


Figure 5.10: (a) Joint distribution $F(k, v)$ plot (b) \log_e density of $F(k, v)$ plot between the out-degree k and the total out-traffic v in the location-based network of the city of Portland.

BIBLIOGRAPHY

- [1] C. A. Donnelly et al., *The Lancet* **361**, 1761 (2003).
- [2] J. G. Breman *et al.*, *Proc. Int. Colloquium on Ebola Virus Inf.* (Proc. Int. Colloquium on Ebola Virus Inf., Antwerp, Belgium, 1977).
- [3] P. Piot *et al.*, *Proc. Int. Colloquium on Ebola Virus Inf.* (Proc. Int. Colloquium on Ebola Virus Inf., Antwerp, Belgium, 1977).
- [4] World Health Organization (WHO), (2003), website: <http://www.who.int/csr/sarscountry/en/>.
- [5] Health Canada, (2003), website: <http://www.hc-sc.gc.ca/pphb-dgspsp/sars-sras/eu-ae/>.
- [6] R. Kohlrausch, *Ann Phys* **72**, 393 (1897).
- [7] A. S. Khan *et al.*, *J. Inf. Dis.* **179**, S76 (1999).
- [8] World Health Organization (WHO), *Weekly Epidemiological Record* **76**, 41 (2001).
- [9] L. Ministry of Agriculture and U. Fisheries (MGAP), Montevideo, (accessed on May 01, 2001), available at: <http://www.mgap.gub.uy>.
- [10] B. Pan-American Foot-and Mouth Disease Center (PAHO), Rio de Janeiro, (accessed on June 10, 2002), available at: <http://www.panaftosa.org.br/novo>.
- [11] W. O. for Animal Health (OIE), (2002), available at: <<http://www.oie.int>>.
- [12] K. Bradsher, *The New York Times* (April 11, 2003).
- [13] D. G. McNeil and L. K. Altman., *The New York Times* (April 15, 2003).
- [14] J. W. Schoen, *MSNB news service* (April 2, 2003).
- [15] MSNBC news service, (April 15, 2003), website: <http://www.msnbc.com/news/885653.asp>.
- [16] MSNBC News Service, (April 9, 2003), website: <http://www.msnbc.com/news/897719.asp>.
- [17] C. Drosten et al., *New England J. Med.* (2003).
- [18] T. G. Ksiazek et al., *New England J. Med.* (2003).
- [19] J. L. Gerberding, *New England J. Med.* (2003).

- [20] J. Pomfret, The Washington Post (April 9, 2003).
- [21] MSNBC News Service, (2003), website: <http://www.msnbc.com/news/885653.asp>.
- [22] MSNBC News Service, (April 15, 2003).
- [23] R. Stein, The Washington Post (April 17, 2003).
- [24] Centers for Disease Control (CDC), (April 16, 2003), website: <http://www.cdc.gov/ncidod/sars/faq.htm>.
- [25] FIRE CHIEF magazine, (April 9, 2003), website: <http://www.firechief.com>.
- [26] C Health, (2003), website: <http://chealth.canoe.ca/>.
- [27] International Society for Infectious Diseases, ProMED-mail (March 25, 2003), archive Number 20030325.0744.
- [28] BBC News, (April 27, 2003), website: <http://news.bbc.co.uk/1/hi/health/2979623.stm>.
- [29] R. Stein, The Washington Post (April 2, 2003), website: <http://www.washingtonpost.com/wp-dyn/articles/A11849-2003Apr2.html>.
- [30] R. Sloan, MSNBC News Service (April 3, 2003), website: <http://www.msnbc.com/news/894251.asp>.
- [31] C. Kalb, Newsweek (April 28, 2003).
- [32] Centers for Disease Control (CDC), (April 16, 2003), website: <http://www.cdc.gov/ncidod/sars/factsheet.htm>.
- [33] K. Bradsher, The New York Times (April 8, 2003).
- [34] F. Brauer and C. Castillo-Chavez, *Mathematical Models in Population Biology and Epidemiology* (Springer Verlag, New York, 2000).
- [35] O. Diekmann1 and J. A. P. Heesterbeek, *Mathematical Epidemiology of Infectious Diseases: Model Building, Analysis and Interpretation* (Wiley, ADDRESS, 2000).
- [36] C. Castillo-Chavez *et al.*, J. Math. Biol. **27**, 233 (1989).
- [37] Hospital Staff, (April 21, 2003).
- [38] International Society for Infectious Diseases, ProMED-mail (April 16th, 2003), archive Number 20030416.0930.

- [39] J. Coomer, The Reporter. Vanderbuilt Medical Center (April 11, 2003).
- [40] J. Pomfret, The Washington Post (April 17, 2003).
- [41] Centers for Disease Control (CDC), (April 3, 2003), website: <http://www.cdc.gov/ncidod/sars/isolationquarantine.htm>.
- [42] Centers for Disease Control (CDC), (April 16, 2003), website: <http://www.cdc.gov/ncidod/sars/factsheetcc.htm>.
- [43] J. Pomfret, The Washington Post (April 25, 2003).
- [44] B. Kamps and C. Hoffmann, (2003), website: <http://www.sarsreference.com/sarsref/summary.htm> .
- [45] G. Vogel, Science **300**, 1062 (2003).
- [46] C. M. Booth et al., J. Am. Med. Asoc. **289**, 2801 (2003).
- [47] Taiwan Headlines (May 20, 2003), website: <http://www.taiwanheadlines.gov.tw/2003052020030520s1.html>.
- [48] World Health Organization (WHO), (2003), website: http://www.who.int/csr/sarsarchive/2003_04_12/en/.
- [49] M. Lipsitch et al., Science **300**, 1966 (2003).
- [50] S. Riley et al., Science **300**, 1961 (2003).
- [51] G. Chowell, P. W. Fenimore, M. A. Castillo-Garsow, and C. Castillo-Chavez, J. Theor. Biol. **24**, 1 (2003).
- [52] D. A. Brown, The Washington Post A07 (May 3, 2003).
- [53] M. A. Sanchez and S. M. Blower, Am. J. Epidemiol. **145**, 1127 (1997).
- [54] S. M. Blower and H. Dowlatabadi, Int. Stat. Rev. **2**, 229 (1994).
- [55] J. X. Velasco-Hernandez, H. B. Gershengorn, and S. M. Blower, The Lancet Inf. Dis. **2**, 487 (2002).
- [56] M. G. Kendall and A. Stuart, *The advanced theory of statistics*, 4 ed. (Macmillan Publishing Company, New York, NY, 1979).
- [57] A. Mandavilli, Nature Med. **9**, 487 (2003).
- [58] H. Caswell, *Matrix Population Models 2nd Ed.* (Sinauer Associates, Publishers, Sunderland, Massachusetts, 2001).
- [59] Centers for Disease Control (CDC), (Accessed on August 24, 2003.), <http://www.cdc.gov/ncidod/dvrd/spb/mnpages/dispages/ebola.htm>.

- [60] Centers for Disease Control (CDC), (Accessed on August 24, 2003.), <http://www.cdc.gov/ncidod/dvrd/spb/mnpages/dispages/ebotabl.htm>.
- [61] World Health Organization (WHO), (Accessed on October 17, 2003), <http://www.who.int/disease-outbreak-news/disease/A98.4.htm>.
- [62] J. G. Breman *et al.*, *J. Inf. Dis.* **179**, S139 (1999).
- [63] H. Leirs *et al.*, *J. Inf. Dis.* **179**, S155 (1999).
- [64] World Health Organization (WHO), (Accessed on August 24, 2003), <http://www.who.int/inf-fs/en/fact103.html>.
- [65] K. Birmingham and S. Cooney, *Nature Med.* **8**, 313 (2002).
- [66] R. M. Anderson and R. M. May, *Infectious Diseases of Humans* (Oxford University Press, Oxford, 1991).
- [67] E. Renshaw, *Modelling Biological Populations in Space and Time* (Cambridge University Press, Cambridge, 1991).
- [68] P. Bickel and K. A. Doksum, *Mathematical Statistics* (Holden-Day, Oakland, California, 1977).
- [69] The World Gazzetter, (Accessed on August 24, 2003), website: http://www.world-gazetteer.com/fr/fr_cd.htm.
- [70] United Nations Human Settlements Programme (UN-HABITAT), (Accessed on August 24, 2003), website: <http://www.unhabitat.org/habrdd/conditions/midafrica/zaire.html>.
- [71] U. B. of Statistics (UBOS), (Accessed on August 24, 2003), website: <http://www.ubos.org/>.
- [72] C. Castillo-Chavez, J. X. Velasco-Hernandez, and S. Fridman, in *Frontiers of Theoretical Biology, Lecture Notes in Biomathematics 100*, edited by S. Levin (Springer-Verlag, Berlin-Heidelberg-New York, 1994), pp. 454–91.
- [73] M. C. M. D. Jong, O. Diekmann, and H. Heesterbeek, in *How does transmission of infection depend on population size?*, edited by D. Mollison (Cambridge University Press, Cambridge, 1995), pp. 84–94.
- [74] P. E. Sartwell, *Am. J. Epidem.* **83**, 204 (1996).
- [75] M. Niikura, T. Ikegami, and M. Saijo, *Clin. Diagn. Lab. Immunol.* **10**, 83 (2003).
- [76] G. Chowell *et al.*, *Emerg. Inf. Dis.* (2004).

- [77] G. J. Nabel, *Nature* **4**, 373 (1999).
- [78] N. J. Sullivan *et al.*, *Nature* **424**, 681 (2003).
- [79] T. Clarke and J. Knight, *Nature* **424**, 602 (2003).
- [80] M. Enserink, *Science* **294**, 26 (2001).
- [81] T. Tsuitsui *et al.*, *Prev. Vet. Med.* **61**, 45 (2003).
- [82] M. G. Garner and M. B. Lack, *Prev. Vet. Med.* **23**, 9 (1995).
- [83] K. MJ *et al.*, *Science* **29**, 813 (2001).
- [84] N. Ferguson, C. Donnelly, and R. Anderson, *Science* **292**, 1155 (2001).
- [85] R. Kao, *Trends in microbiology* **10**, 279 (2002).
- [86] A. Rivas *et al.*, *Am. J. Vet. Res.* **64**, 1519 (2003).
- [87] A. Rivas *et al.*, *Can. J. Vet. Res.* **67**, 307 (2003).
- [88] *Supplementary materials. A movie of the 2001 Foot-and-Mouth Epidemic in Uruguay. Available online at: <http://www.bscb.cornell.edu/Homepages/gerardo/FMD/supplementary.htm>.*
- [89] J. Irvine, (Access on June 06, 2004), available online at: <<http://www.land-care.org.uk>>.
- [90] European Comission, (accessed on June 06, 2004), available online: http://europa.eu.int/comm/food/fs/inspections/vi/reports/uruguay/vi_rep_urug_3342-2001_en.pdf and http://europa.eu.int/comm/food/fs/inspections/vi/reports/uruguay/vi_rep_urug_3456-2001_en.pdf.
- [91] T. Doel, *Virus Research* **91**, 81 (2003).
- [92] S. Alexandersen *et al.*, *Journal of Comparative Pathology* **129**, 268 (2003).
- [93] R. Sanson, *Vet. J.* **42**, 41 (1994).
- [94] M. Hugh-Jones and P. Wright, *J. Hyg. Cb.* **68**, 253 (1994).
- [95] R. Seller and A. Forman, *J. Hyg. Cb.* **71**, 15 (1973).
- [96] M. Hugh-Jones and R. Tinline, *J. Hyg. Cb.* **77**, 141 (1976).
- [97] Z. Zhang *et al.*, *Journal of General Virology* **85**, 415 (2004).
- [98] G. Chowell *et al.*, *J. Theor. Biol.* **229**, 119 (2004).
- [99] R. Anderson and R. May, *Nature* **315**, 323 (1985).

- [100] I. Hanski, Nature **396**, 41 (1998).
- [101] I. Hanski and O. Ovaskainen, Nature **404**, 755 (2000).
- [102] A. Moilane and I. Hanski, Ecology **79**, 2503 (1998).
- [103] P. van den Driessche and J. Watmough, Mathematical Biosciences **180**, 29 (2002).
- [104] R. Morris *et al.*, Vet. Rec. **149**, 137 (2001).
- [105] P. Brentsen, A. Dijkhuizen, and A. Osk, Prev. Vet. Med. **12**, 229 (1992).
- [106] R. Sanson and R. Morris, The Kenya Veterinarian **18**, 186 (1994).
- [107] M. Nielsen *et al.*, Prev. Vet. Med **28**, 143 (1996).
- [108] T. Bates, M. Thurmond, and T. Carpenter, Am J. Vet. Res. **64**, 205 (2003).
- [109] T. Bates, M. Thurmond, and T. Carpenter, Am J. Vet. **62**, 1121 (2001).
- [110] E. Holmes, in *The role of space in population dynamics and interspecific interactions*, edited by D. Tilman and P. Kareiva (Princeton University Press, New Jersey, 1997), pp. 111–136.
- [111] M. Woolhouse, D. Haydon, A. Peterson, and R. Kitching, Epidemiol. Infect. **116**, 363 (1996).
- [112] M. E. J. Newman, Proc. Nat. Acad. Sci. **98**, 404 (2001).
- [113] M. E. J. Newman, Phys. Rev. E **64**, (2001).
- [114] A.-L. Barabási *et al.*, Physica A **311**, 590 (2002).
- [115] D. J. Watts and S. H. Strogatz, Nature **363**, 202 (1998).
- [116] H. Jeong *et al.*, Nature **407**, 651 (2000).
- [117] H. Jeong, S. Mason, A.-L. Barabási, and Z.-N. Oltvai, Nature **411**, 41 (2001).
- [118] R. Williams *et al.*, Proc. Nat. Acad. Sci. **99**, 12913 (2002).
- [119] M. Faloutsos, P. Faloutsos, and C. Faloutsos, SGCOMM (1999).
- [120] R. Albert, H. Jeong, and A.-L. Barabási, Nature **401**, 130 (1999).
- [121] R. Kumar *et al.*, 19th ACM SIGACT-SIGMOD-AIGART Symp. PODS (2000) (2000).
- [122] L. A. N. Amaral, A. Scala, M. Barthelemy, and H. E. Stanley, Proc. Nat. Acad. Sci. **97**, 11149 (2000).

- [123] F. Liljeros *et al.*, Nature **411**, 907 (2001).
- [124] S. Strogatz, Nature **410**, 268 (2001).
- [125] B. Bollobás, *Random Graphs* (Cambridge University Press, Cambridge, 1985).
- [126] A.-L. Barabási, R. Albert, and H. Jeong, Physica A **272**, 173 (1999).
- [127] E. Ravasz *et al.*, Science **297**, 173 (1999).
- [128] E. Ravasz and A.-L. Barabási, Phys. Rev. E **67**, (2003).
- [129] C. L. Barret *et al.*, Los Alamos Unclassified Report (2001), 1A-UR-00-1725.
- [130] , <http://www.dmampo.org/313.html>.
- [131] C. Barrett *et al.*, European Symposium on Algorithms (ESA) (2002), los Alamos Unclassified Report LA-UR-02-2427.
- [132] C. Barrett, R. Jacob, and M. Marathe, SIAM J. Computing **30**, 809 (2001).
- [133] R. Jacob, M. Marathe, and K. Nagel, ACM J. Experimental Algorithmics **4**, (1999), website: <http://www.jea.acm.org/1999/JacobRouting/>.
- [134] P. Erdos and A. Renyi, Publications of the Mathematical Institute of the Hungarian Academy of Sciences **5**, 17 (1960).
- [135] D. Peterson *et al.*, Computers in Biology and Medicine **23**, 199 (1993).
- [136] D. J. Watts, *Small Worlds: The dynamics of networks between order and randomness* (Princeton University Press, Princeton, New Jersey, 1999).
- [137] R. Sedgewick, *Algorithms* (Addison-Wesley, ADDRESS, 1988).
- [138] *m is constant for the BA model. We have used m = 16, the median out-degree of our network.*
- [139] K. Klemm and V. Eguiluz, Phys. Rev. E **65**, (2002).
- [140] P. Fronczak and J. A. Holyst, cond-mat/0306255 .
- [141] P. Grassberger, Math. Biosc. **63**, 157 (1983).
- [142] M. E. J. Newman, Phys. Rev. E **66**, (2002).
- [143] M. E. J. Newman, I. Jensen, and R. M. Ziff, Phys. Rev. E **65**, (2002).
- [144] C. Moore and M. E. J. Newman, Phys. Rev. E **61**, 5678 (2000).
- [145] R. Pastor-Satorras and A. Vespignani, Phys. Rev. E **63**, (2001).

- [146] R. Pastor-Satorras and A. Vespignani, Phys. Rev. E **65**, (2002).
- [147] R. M. May and A. L. Lloyd, Phys. Rev. E **64**, (2001).
- [148] Z. Dezso and A.-L. Barabási, Phys. Rev. E **65**, (2002).
- [149] V. M. Eguíluz and K. Klemm, Phys. Rev. Lett. **89**, (2002).
- [150] S. Yook, H. Jeong, A.-L. Barabási, and Y. Tu, Phys. Rev. Lett. **86**, (2001).
- [151] G. Chowell and C. Castillo-Chavez, in *Mathematical Modeling Applications in Homeland Security*, edited by H. T. Banks and C. Castillo-Chavez (SIAM's series Frontiers in Applied Mathematics, Philadelphia, 2003), pp. 35–53.